AD-767 180

STOL TACTICAL AIRCRAFT INVESTIGATION, EXTERNALLY BLOWN FLAP. VOLUME III. PERFORMANCE METHODS AND LANDING RULES

Dirk J. Renselaer

Rockwell International Corporation

Prepared for:

Air Force Flight Dynamics Laboratory

April 1973

AFFDL-TR-73-20
Volume III

STOL TACTICAL AIRCRAFT INVESTIGATION–
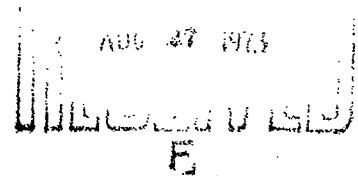# EXTERNALLY BLOWN FLAP

Volume III

Performance Methods and Takeoff and Landing Rules

D. J. RENSELAER

LOS ANGELES AIRCRAFT DIVISION
ROCKWELL INTERNATIONAL CORPORATION

TECHNICAL REPORT AFFDL-TR-73-20, VOLUME III

APRIL 1973

AUG 27 1973

E

Approved for public release; distribution unlimited.

AIR FORCE FLIGHT DYNAMICS LABORATORY
AIR FORCE SYSTEMS COMMAND
WRIGHT-PATTERSON AIR FORCE BASE, OHIO

NOTICE

When Government drawings, specifications, or other data are used for any purpose other than in connection with a definitely related Government procurement operation, the United States Government thereby incurs no responsibility nor any obligation whatsoever; and the fact that the government may have formulated, furnished, or in any way supplied the said drawings, specifications, or other data, is not to be regarded by implication or otherwise as in any manner licensing the holder or any other person or corporation, or conveying any rights or permission to manufacture, use, or sell any patented invention that may in any way be related thereto.

i

DOCUMENT CONTROL DATA - R & D

(Security classification of title, body of abstract and indexing annotation must be entered when the overall report is classified)

1. ORIGINATING ACTIVITY (Corporate author)	2a. REPORT SECURITY CLASSIFICATION
Los Angeles Aircraft Division Rockwell International Corporation Los Angeles International Airport, L. A., Calif., 90009	Unclassified
	2b. GROUP

3. REPORT TITLE

STOL Tactical Aircraft Investigation, Externally Blown Flap
Volume III Performance Methods and Takeoff and Landing Rules

4. DESCRIPTIVE NOTES *(Type of report and inclusive dates)*

Final Report (10 June 1971 to 10 December 1972)

5. AUTHOR(S) *(First name, middle initial, last name)*

Dirk J. Renselaer

6. REPORT DATE	7a. TOTAL NO. OF PAGES	7b. NO. OF REFS
April 1973	160	11

8a. CONTRACT OR GRANT NO.	9a. ORIGINATOR'S REPORT NUMBER(S)
F33615-71-C-1760	
b. PROJECT NO.	
643A - Task 0020	
c.	9b. OTHER REPORT NO(S) (Any other numbers .... may be assigned this report)
d.	AFFDL-TR-73-20 Volume III

10 DISTRIBUTION STATEMENT

Approved for public release; distribution unlimited.

11 SUPPLEMENTARY NOTES	12 SPONSORING MILITARY ACTIVITY
	Air Force Flight Dynamics Laboratory (PTA), Wright Patterson AFB, Ohio, 45433

13 ABSTRACT

The basic objective of the work reported herein was to provide a broader technology base to support the development of a medium STOL Transport (MST) airplane. This work was limited to the application of the externally blown flap (EBF) powered lift concept.

The technology of EBF STOL aircraft has been investigated through analytical studies, wind tunnel testing, flight simulator testing, and design trade studies. The results obtained include development of methods for the estimation of the aerodynamic characteristics of an EBF configuration, STOL performance estimation methods, safety margins for takeoff and landing, wind tunnel investigation of the effects of varying EBF system geometry parameters, configuration definition to meet MST requirements, trade data on performance and configuration requirement variations, flight control system mechanization trade data, handling qualities characteristics; piloting procedures, and effects of applying an air cushion landing system to the MST.

From an overall assessment of study results, it is concluded that the EBF concept provides a practical means of obtaining STOL performance for an MST with relatively low risk.

DD FORM 1473 NOV 65

14. KEY WORDS	LINK A		LINK B		LINK C	
	ROLE	WT	ROLE	WT	ROLE	WT
STOL Transport						
Externally blown flaps						
Medium STOL Transport						
Performance methods						
Take-off and Landing Criteria						

STOL TACTICAL AIRCRAFT INVESTIGATION–EXTERNALLY BLOWN FLAP

Volume III

Performance Methods and Takeoff and Landing Rules

D. J. RENSELAER

APRIL 1973
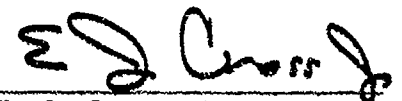
FOREWORD

This report was prepared for the Prototype Division of the Air Force Flight Dynamics Laboratory by the Los Angeles Aircraft Division, Rockwell International. The work was performed as part of the STOL tactical aircraft investigation program under USAF contract F33615-71-C-1760, project 643A0020. Daniel E. Fraga, AFFDL/PTA, was the Air Force program manager, and Garland S. Oates, Jr., AFFDL/PTA, was the Air Force technical manager. Marshall H. Roe was the program manager for Rockwell.

This investigation was conducted during the period from 10 June 1971 through 9 December 1972. This final report is published in six volumes and was originally published as Rockwell report NA-72-868. This report was submitted for approval on 9 December 1972.

This technical report has been reviewed and is approved.

E. J. Cross, Jr.
Lt Col, USAF
Chief, Prototype Division

ABSTRACT

The basic objective of the work reported herein was to provide a broader technology base to support the development of a medium STOL Transport (MST) airplane. This work was limited to the application of the externally blown flap (EBF) powered lift concept.

The technology of EBF STOL aircraft has been investigated through analytical studies, wind tunnel testing, flight simulator testing, and design trade studies. The results obtained include development of methods for the estimation of the aerodynamic characteristics of an EBF configuration, STOL performance estimation methods, safety margins for takeoff and landing, wind tunnel investigation of the effects of varying EBF system geometry parameters, configuration definition to meet MST requirements, trade data on performance and configuration requirement variations, flight control system mechanization trade data, handling qualities characteristics, piloting procedures, and effects of applying an air cushion landing system to the MST.

From an overall assessment of study results, it is concluded that the EBF concept provides a practical means of obtaining STOL performance for an MST with relatively low risk. Some improvement in EBF performance could be achieved with further development - primarily wind tunnel testing. Further work should be done on optimization of flight controls, definition of flying qualities requirements, and development of piloting procedures. Considerable work must be done in the area of structural design criteria relative to the effects of engine exhaust impingement on the wing and flap structure.

This report is arranged in six volumes:

Volume I   - Configuration Definition

Volume II - Design Compendium

Volume III - Performance Methods and Takeoff and Landing Rules

Volume IV - Analysis of Wind Tunnel Data

Volume V   - Flight Control Technology

    Part I   - Control System Mechanization Trade Studies
    Part II - Simulation Studies/Flight Control System Validation
    Part III - Stability and Control Derivative Accuracy
            Requirements and Effects of Augmentation System Design

Volume VI - Air Cushion Landing System Trade Study

The present document represents Volume III and is generated to provide a technical basis for a STOL supplement of MIL-C-5011A, "Military Specification; Charts, Standard Aircraft Characteristics and Performance, Piloted Aircraft," dated 5 November 1951. This supplement is intended to provide takeoff and landing performance criteria for STOL aircraft. The present volume also presents methods for the computation of the field performance on the basis of such new criteria.

The performance criteria are suggested in terms of safe speed margins, maneuver capabilities, engine failure considerations and angle of attack margins to accommodate gusts for a typical medium sized STOL transport. Nomograms for the determination of the takeoff and landing distance are presented along with their derivation. Sample aerodynamic data are used to show how the best STOL performance can be obtained under the constraints of such new STOL performance ground rules.

The criteria and the performance methods were generated with the externally blown flap lift/propulsion system as the technical background; however, both, the criteria and the performance methods are sufficiently general to be applicable for many other lift/propulsion concepts.

TABLE OF CONTENTS

LIST OF ILLUSTRATIONS

LIST OF SYMBOLS

A	Aspect ratio of wing
AEO	All engines operating
Ai_{pE}	Intake area inside the inlet, per engine, ft^2
b	Wing span, feet
B	Engine bypass ratio
BLC	Boundary layer control
CEF	Critical engine failed
C_D	Drag coefficient, D/qS
C_L	Lift coefficient, L/qS
C_μ	Engine blowing coefficient, T/qS
D	Total drag (with power effects in power-on cases), pounds
D_i	Intake momentum drag, pounds
DLC	Direct lift control
D_{pE}	Diameter of the inlet throat of each engine, feet
F	Average accelerating/decelerating force, pounds
h or H	Height above ground (altitude), feet
I	Moment of inertia, pounds $ft\text{-}sec^2$
IGE	In ground effect
K	Factor with respect to the intake momentum drag for given engine/aircraft layout
KEAS	Knots equivalent airspeed
KTAS	Knots true airspeed
L	Total lift, pounds

LIST OF SYMBOLS - Cont.

$\mathcal{L}$ Rolling moment, feet pounds

ℓ Distance between two gust vortices, feet

ℓ_N Length between aircraft nose gear and main gear, feet

m Mass of aircraft, slugs

n Normal acceleration, ft/sec^2

N Number of engines operating

OGE   Out of ground effect

q Freesteam dynamic pressure, $1/2 \, V^2 \rho$, pounds/ft^2

R Radius of turn during flight, feet

R_g Taxi radius to the outer gear, feet

s Ground distance, feet

S Wing reference area, ft^2

T Total nozzle exhaust static thrust, pounds, length of gust in time, seconds

t Time, seconds

V Freestream velocity, knots or ft/sec.

V_F Aircraft velocity at which engine fails, knots

V_g Gust velocity, ft/sec

V_{mc} Minimum control velocity, knots

V_{mtd} Minimum touch down velocity, knots

V_S Stall velocity, knots

V_z Sink rate, ft/sec

W Weight of aircraft, pounds

X Horizontal displacement, feet

LIST OF SYMBOLS - Concluded

X_R Rolling distance, feet

Z Vertical displacement, feet

α Angle of attack, degrees or radians

β Angle of sideslip, positive nose left, degrees

γ Flight path angle, positive in climb direction, degrees

γ_c Takeoff climb flight path angle, degrees

δ_F Flap deflection angle, degrees

δ_n Deflection angle of engine exhaust deflector, positive for downward deflections, degrees

ζ Damping ratio

θ Pitch-attitude angle, positive nose-up, degrees

μ Friction coefficient of front and main landing gear on ground

ρ Atmospheric density, slugs/ft^3

ρ_0 Atmospheric density at sea level in standard atmosphere, slugs/ft^3

ϕ Bank angle, degrees

ω Damped frequency, rad/sec

ω_n Undamped natural frequency of aircraft, rad/sec

ω_{nd} Undamped natural frequency of aircraft of the dutch roll mode, rad/sec

SUBSCRIPTS

a	Approach
Aero	Aerodynamics excluding engine exhaust forces
AV	Average
α	Due to angle of attack
B	Braking
C.O.	Climbout
F	Failure of one engine
L.O.	Lift off
Max	Maximum
N	Nozzle
PE	Per engine
P.O.	Power off
R	Reversal of engines
3	3-engine operation
4	4-engine operation

Section I

INTRODUCTION

In the past, flight safety rules for landing and takeoff were related to a definition of the stall speed in which power effects were ignored. This definition was introduced several decades ago when the level of engine power was relatively low and the effect of power on the minimum speed was relatively insignificant. However, with elapse of time, the power installed in the airplanes grew in connection with increasing cruise speed, and thus the potential of using power for the decrease of the stall speed became stronger.

Recently, interest was focused on using aircraft with short takeoff and landing (STOL) capability to increase mobility and decrease traffic congestion, for example by using a number of small airfields instead of fewer large airports. Also, important military logistic benefits can be derived from such a capability. As a result, short takeoff and landing aircraft studies have been made where power effects were used to reduce the stall speed, and a variety of lift/propulsion concepts have been found suitable to achieve this. In order to make use of this reduced speed new takeoff and landing ground rules or criteria have to be established to assure flight safety, taking into account typical STOL aircraft characteristics. Such characteristics are associated with these power effects such as aircraft motion after engine failure, and are associated with sensitivity to gusts because of the low forward speed. Furthermore, new ground rules may be established associated with the steeper flight path angles during approach and takeoff which are used to shorten the field length even further, beyond what can be achieved with a mere speed decrease.

At the present time an attempt is made to develop a basis on which such new ground rules can be established. However, unlike conventional aircraft, flight experience with STOL aircraft with propulsion concepts other than with propellers is inadequate. Yet a number of different propulsion concepts are possible, many with their own characteristics. Therefore, in the present report it is attempted to generate ground rules on a basis of deductions wherever flight information or simulator information is not available. These deductions are made on the basis of the impact that engine failure and gust may have on aircraft response, and on the basis of maneuver requirements.

The ground rules or criteria are generated here using a typical medium size transport having externally blown flaps as the lift/propulsion concept. These criteria are suggested for use in a future supplement

to the military specification, MIL-C-5011A (Reference 1).

Similar deduction may also be used for other lift/propulsion concepts. A comparison of the impact of STOL safety criteria for the various different concepts can then be made provided that consistent gust models, engine failure thrust decay rates, and maneuver requirements are used. This could enhance the selection of a particular lift/propulsion concept for STOL operation from airports with particular field lengths.

Because it has been found that the determination of the takeoff and landing speed and therefore the STOL field performance is surprisingly complex, the present report also presents a methods development showing how such STOL safety criteria are applied. Additionally a number of nomograms are presented for speeding up the determination of the field performance. The nomograms are derived for four-engine aircraft using the externally blown flap lift/propulsion concept, but can easily be modified to other concepts and a different number of engines.

Section II

TAKEOFF AND LANDING RULES

2.1 IDENTIFICATION OF CRITICAL STOL SAFETY ASPECTS

2.1.1 ENGINE FAILURE

(a) Bank Angle Control

One of the most stringent roll control requirements for a STOL aircraft equipped with externally blown flaps pertains to the control of the bank angle in the case of an engine failure during a landing approach. In this section it is attempted to identify a minimum speed at which adequate roll control is available so that this speed can be used on which to base a minimum safe margin for the aircraft speed.

Computed time histories of aircraft bank angle transients following engine failure and subsequent pilot corrective action are presented in Figure 1 for an approach flap setting of 50°. Herein, it is assumed that no automatic rolling moment compensation exists. A realistic engine thrust decay is used, and the pilot initiates corrective action approximately one second after the engine failure. A control system lag of 0.1 second is assumed, and full roll control is reached 0.4 second after the pilot initiates the control. Two different approach speeds are chosen, i.e., 70 and 85 knots equivalent airspeed, so that the effect of speed can be shown in the speed regime of interest. Both these speeds are higher than the engine-out stall speed.

A criterion for the severity of the effect of engine failure in the roll mode is the maximum bank angle reached. However, it is seen from the above figure that speed has very little effect on the maximum bank angle, both bank angles being approximately six degrees. This may be due to the fact that increase of speed not only results in an increased rolling moment due to engine failure but also results in an increase of the roll control moment.

Similarly, also only a small bank angle difference was found from time histories where an infinite rate of thrust decay was used approximating an engine disintegration or nacelle detachment, except that the maximum bank angle excursions were approximately twice as large.

Thus it may be expected that no speed safety margin on the basis of bank angle excursions after engine malfunction can be established for present day transports employing the externally blown flaps lift/propulsion concept. However care must be taken that the aircraft speed

3
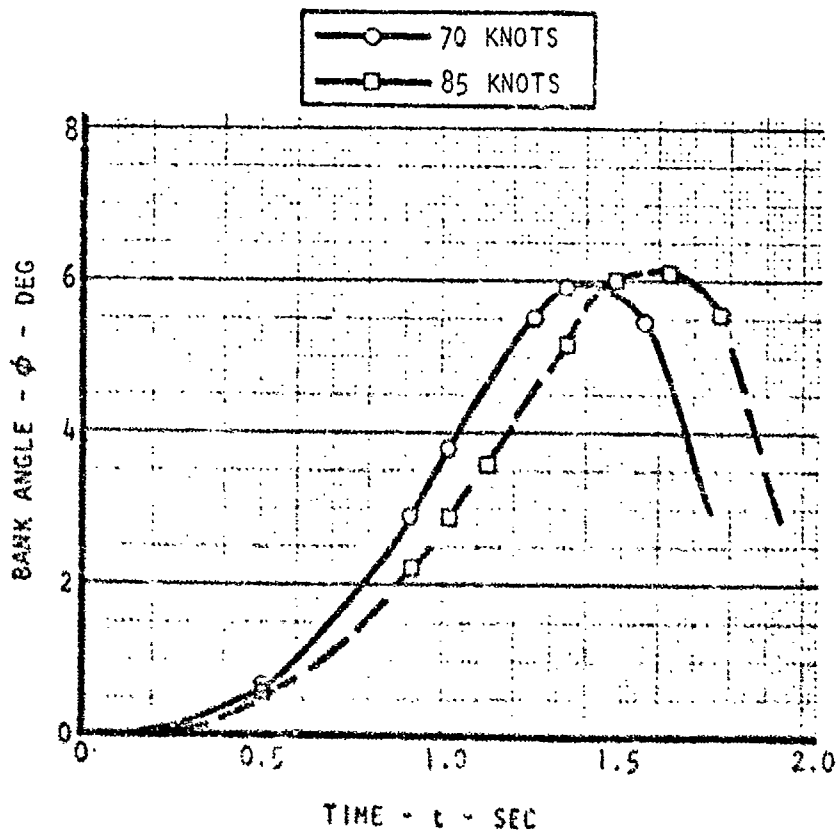
Figure 1. Bank Angle Response After Engine Failure

4

is greater than the stall speed or minimum controllable speed with the critical engine failed.

In the subsequent portion of this section, additional details are given with regard to data used in the above time histories, such as engine thrust decay, time of pilot's control initiation, and rolling moments involved. The rate of thrust decay used in the above transients pertains to an instantaneous fuel loss and is shown in Figure 2, top. The decay depends on the engine bypass ratio and the engine polar moment of inertia, and is estimated here for a bypass ratio 6 and an engine diameter of 6 feet. These values are typical for the STOL transport considered in this study.

The rolling moment increases as a function of this decay, and it is also a function of the aircraft speed, see Figure 2, bottom. The speed enters because the lift augmentation due to external blowing is a function of speed. The rolling moment is presented by the symbol $\mathcal{L}$ in this figure, and is divided by the moment of inertia, I. This gives an impression of the rather substantial rolling accelerations involved in the system if the damping were ignored:

$$I\ddot{\phi} = \mathcal{L}$$

$$\ddot{\phi} = \frac{\mathcal{L}}{I} \left(\frac{\text{lbs ft}}{\text{lbs ft sec}^2} \quad \text{or} \quad \frac{\text{rad}}{\text{sec}^2} \right)$$

Values of $\mathcal{L}/I$ shown represent a failure of an outboard engine for an airplane weighing 160,000 pounds, having an inertia of 1.36×10^6 pounds ft sec^2, a span of 142 feet and having the outboard engine located at 40 percent wing span.

With regard to the time at which the pilot initiates corrective bank angle control, it is assumed that no automatic rolling moment compensation exists in the aircraft that may alleviate his response. Various cues are available to the pilot on the basis of which he may react. These may be roll acceleration cues, yaw acceleration cues, or visual bank angle cues. In the present analysis it is assumed that the pilot will use the visual cue, being close to the runway during STOL operation. Further, it is assumed that the pilot reacts at a time when the bank angle has reached three degrees. This angle is chosen arbitrarily, except that a low angle of one degree is not expected to induce him to act, and a larger angle such as five degrees probably gives reason for considerable concern while operating near the ground. The 3-degree
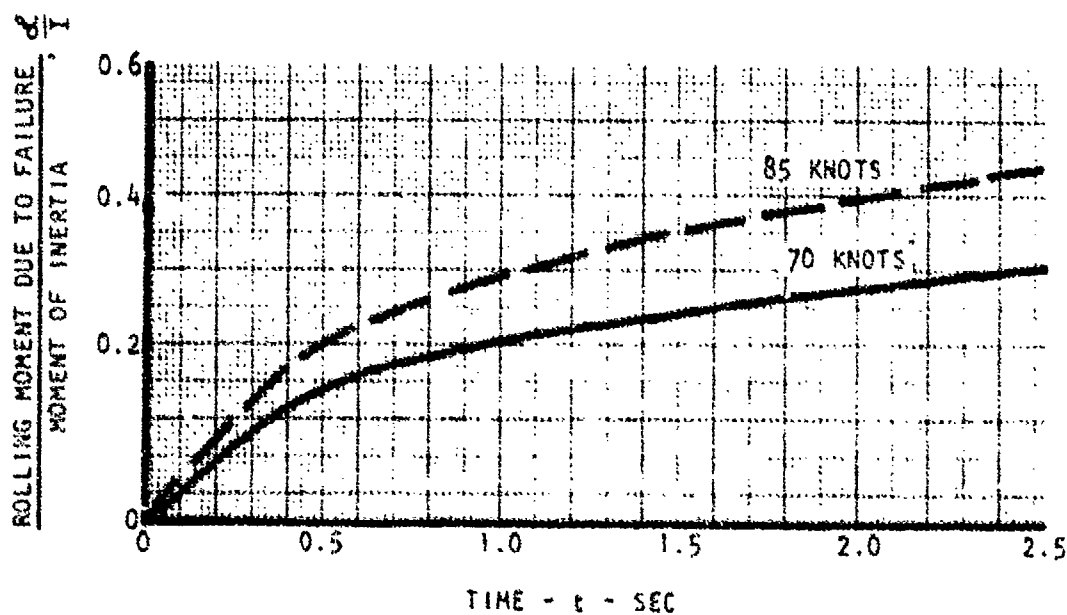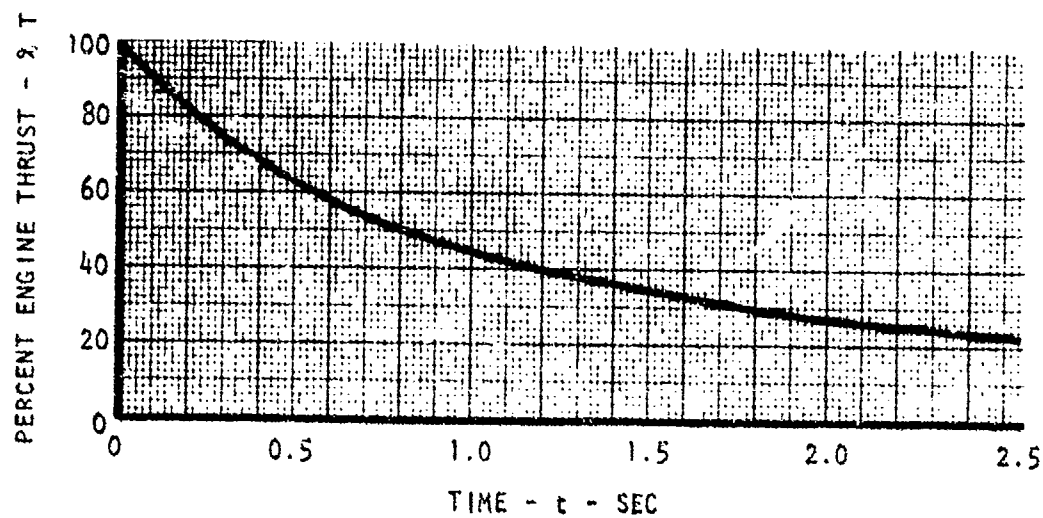
Figure 2. Engine Thrust Decay and Rolling Moment After Engine Failure

criterion, used here consistently, is adequate for the purpose of possibly identifying the effect of the aircraft speed on the maximum bank angle excursion.

The time at which a bank angle of 3 degrees is reached is 1.03 seconds when the speed is 70 knots, and .93 second when the speed is 85 knots equivalent airspeed. At these times, which are found from Figure 1, it is assumed that the pilot starts to use the maximum roll control available. Consistent with NASA TND 5594 (Reference 2), a control system lag of 0.1 second is applied, and the maximum control is reached 0.4 second after the start of the pilot's input. The resulting rolling moment due to pilot action is shown in Figure 3.

The maximum levels of roll control are $\ddot{\phi} = \mathcal{L}/I = 1.01$ rad/sec^2 for 70 knots, and $\ddot{\phi} \sim 1.37$ rad/sec^2 for 85 knots. Both values are greater than the minimum absolute values to satisfy the roll acceleration criteria of MIL-F-83300 (Reference 3) in normal operations (not shown here).

The total rolling moment forcing function is now found by the superposition of the rolling moment due to the engine failure, and the rolling moment due to the control input. This forcing function, divided again by I, is presented in Figure 4, top. Also, the remaining values of $\mathcal{L}/I$ with full control input satisfy level 3 roll acceleration criteria of MIL-F-83300.

To complete the comparison between the two speeds the damping also needs to be considered. The greater the forward speed not only the values of the forcing function are greater, but also of the damping:

V	70	80
$\dfrac{d\mathcal{L}/I}{d\dot{\phi}}$	0.654	$0.80 \left(\dfrac{1}{\text{sec.}}\right)$

Dividing the forcing functions by the respective dampings results in the curves shown in Figure 4, bottom. It is seen that these two functions are very similar in magnitude and shape, which leads to the expectation that the maximum bank angles are of similar magnitudes for the two speeds.

Figure 3. Rolling Moment Due to Pilot Control Input

8
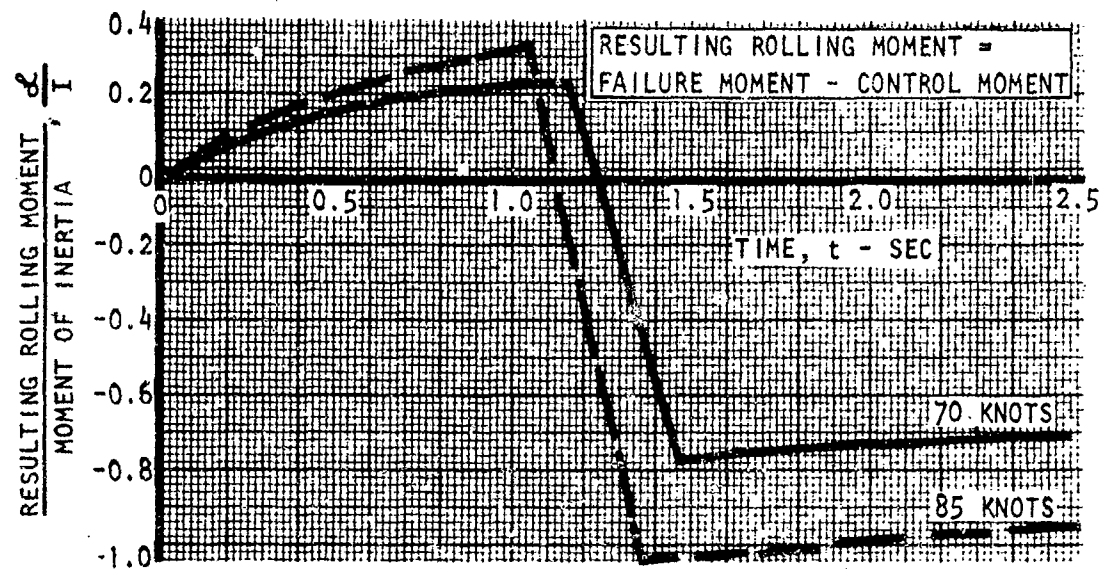
Figure 4. Rolling Moment Characteristics After Engine Failure

9

(b) Flight Path Correction

This subsection pertains to the requirement that the pilot be able to control and maintain the flight path during final approach almost immediately after an engine failure.

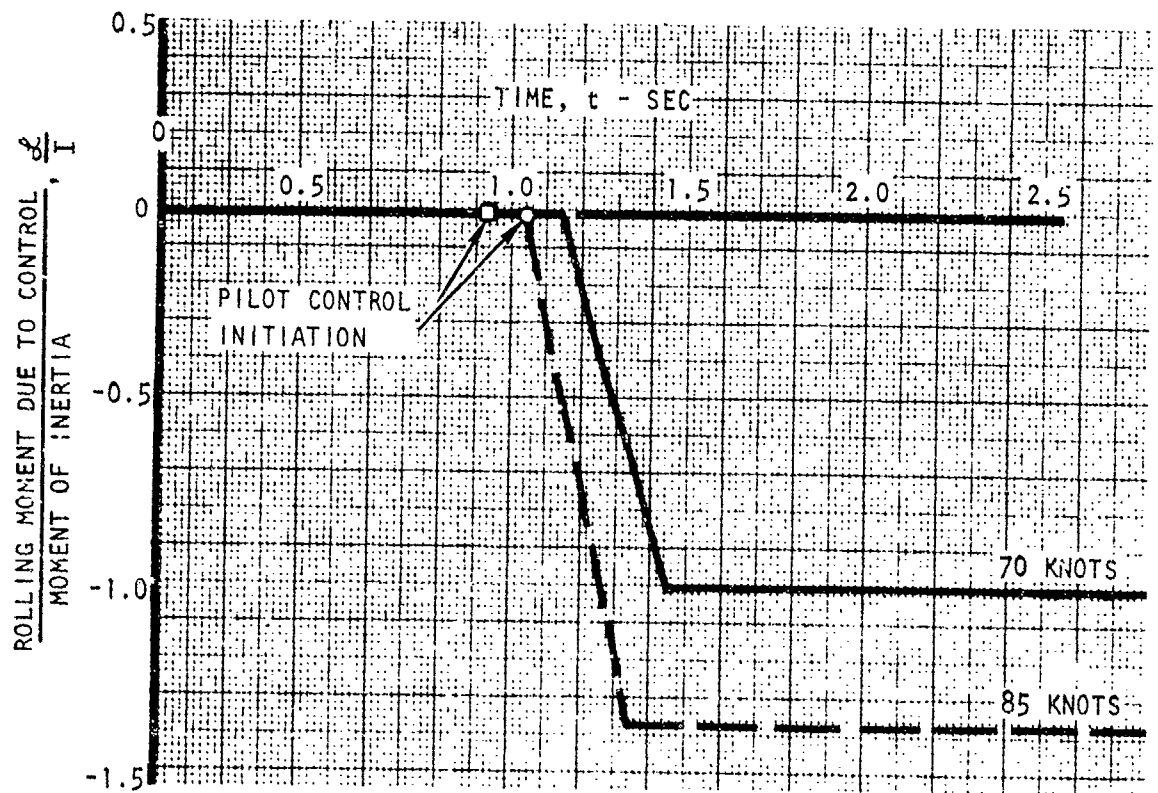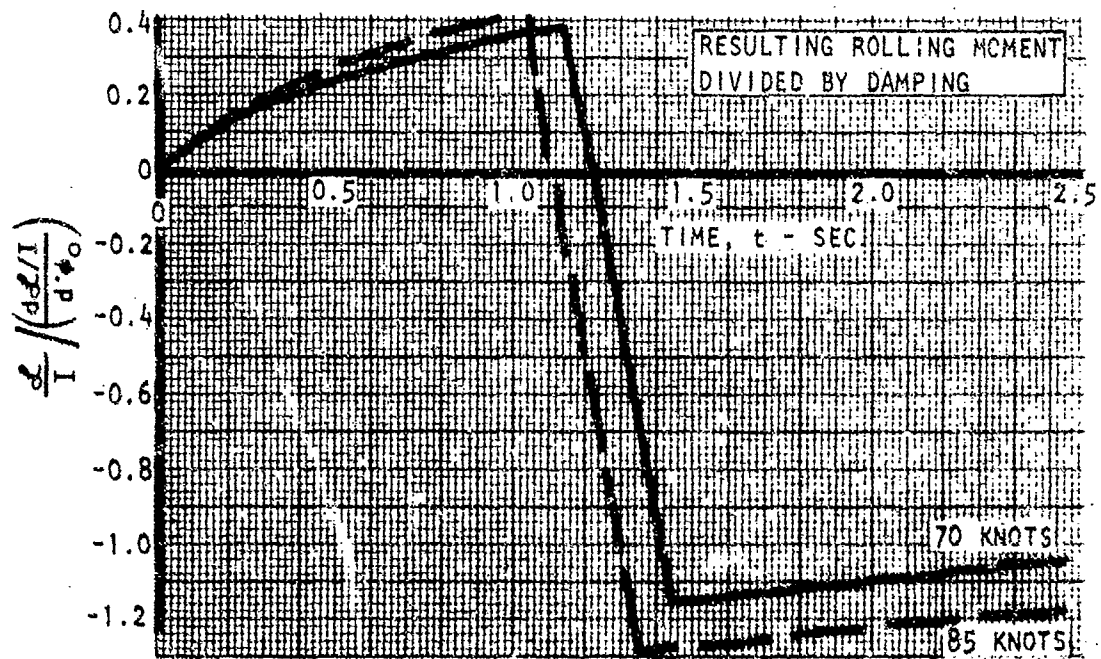The need for such a control action may be illustrated by presenting the undershoot distance below the touch down point and by the increased sink rate in the event that the pilot does not react and in the event that the engine fails when the aircraft is at a critical height above the threshold. Figure 5 shows the definition of the undershoot distance schematically.

Assuming a height above the threshold of 50 feet, Figure 6 shows that the magnitude of this undershoot distance ranges from 125 feet to 210 feet depending on aircraft speed, power settings, and flap settings existing just before the failure. The speeds, flaps, and power settings are chosen arbitrarily except that the values chosen bracket the area of interest. The thrust levels chosen may not necessarily be those associated with a 10 ft/second descent rate but they are expected to encompass those needed for the descent. The figure also shows that the increase in sink velocities ranges from 5.5 to 8.5 ft/second for these conditions. The lift loss from the engine as a function of time is approximated here by a ramp shape with a ramp time of two seconds, which is roughly equivalent to the thrust decay curve shown in Figure 2 as far as such downstream effects such as undershoot distances are concerned.

It is seen that the magnitude of undershoot and especially the increase of sink rate require positive pilot action or automatic compensation. However, it is difficult to assess how the pilot will react to the engine failure without test data based on flight or simulations.

However, such an assessment is nevertheless attempted here, primarily to show what the requirements possibly could be, and also to describe a frame of aircraft characteristics within which the pilot operates.

Computed results of time histories with pilot reaction are shown in Figure 7 for speeds of 70 knots and 85 knots. The worst case in terms of thrust setting and flap angle is used, i.e., 100 percent thrust and 75 degrees flap angle. In each case the full lift loss due to engine failure is assumed to have developed in two seconds, and a pilot delay of 1.2 seconds has been used after the start of the engine failure. This time is an average at which a bank angle of three degrees is encountered, similar to the analysis of the bank angle control after engine failure.

10

Figure 5. Illustration of Effect of Engine Failure on Undershoot Distance Without Pilot Lift Control
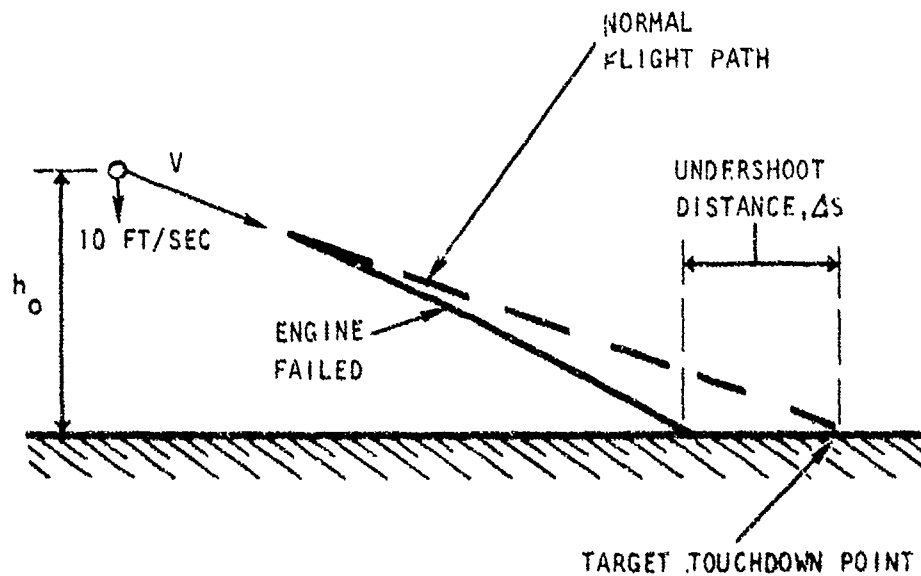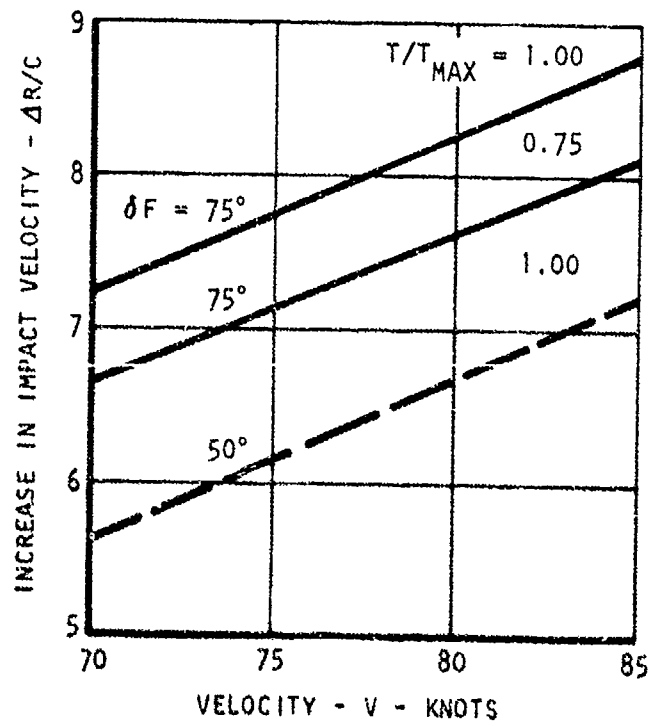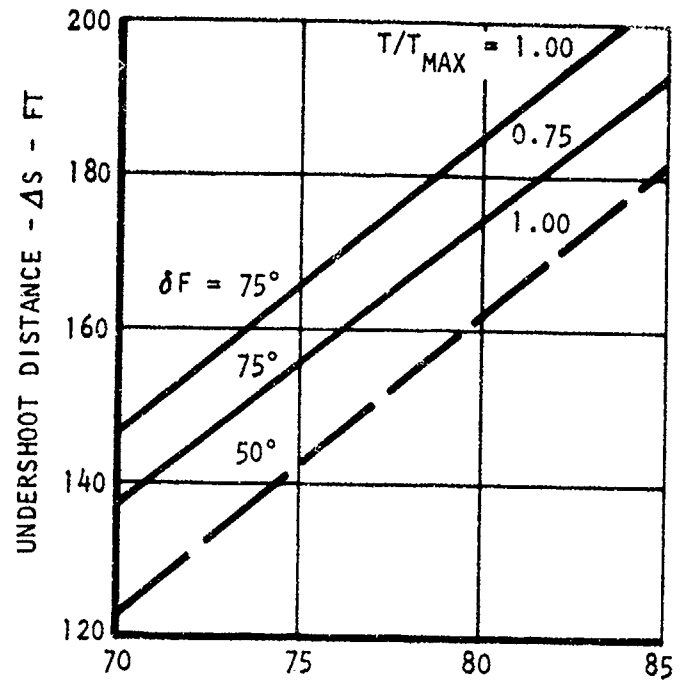
11

Figure 6. Effect of Engine Failure on Landing Impact Without Pilot Corrective Action
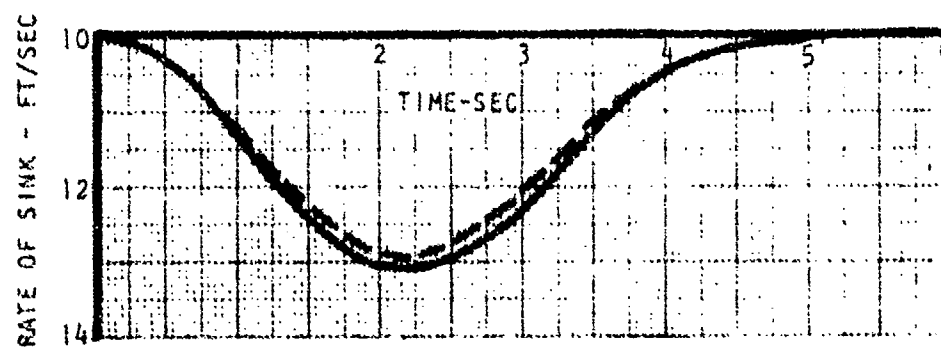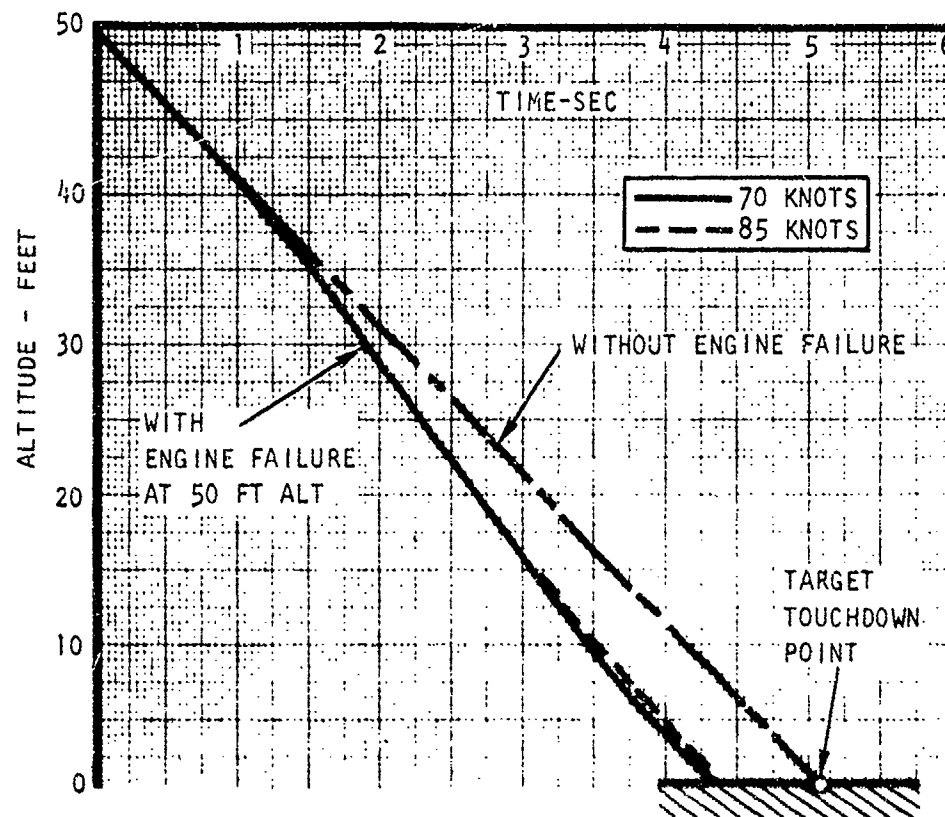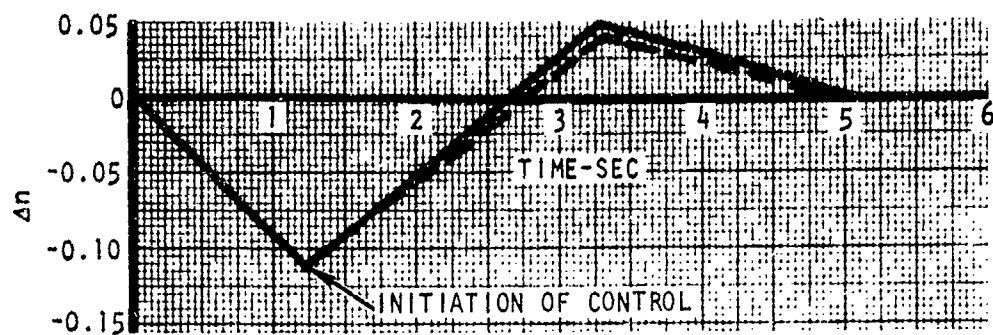
Figure 7. Longitudinal Motion After Engine Failure

13

Various ways to control the airplane in lift may be available to the pilot. He can increase the pitch angle of the aircraft, or he may increase thrust, or lift from DLC if that is available, or a combination thereof. It is assumed here, that he will use an angle of attack increase and either DLC or thrust. The reason for this is the fact that the lift loss due to engine failure is large, and thus the lift increase desired by the pilot not only must overcome the loss due to the failure, but should also provide an excess normal acceleration to reduce the buildup of the sink rate. For example the lift change due to engine failure used in the present analysis for 85 knots can be -18 percent, and if a normal acceleration of $\Delta n = 0.10$ were required a total lift increase of 28 percent would be needed. This amount of lift increase is difficult to obtain quickly with an angle of attack change only. This is especially true for STOL aircraft with high wing loadings such as is considered in the present study where the wing area and the landing dynamic pressure are small, and large lift changes require excessive angle of attack changes. Thus adding either lift due to DLC or thrust increase (or both) is expected to be necessary for a successful recovery from engine failure.

Whichever method is used, the maximum positive normal acceleration is taken here to be two seconds after the pilot's initiation of the lift control, assuming that it will require this much time for high bypass ratio engines to reach maximum thrust. This will place the maximum positive normal acceleration at 3.2 seconds past the threshold, see above Figure 7.

It is further assumed that the rate of sink above the threshold was 10 ft/second, and that the rate of sink shall not be larger at the instant of touch down. Moreover this shall be achieved with a gradual decrease of normal acceleration to $n \approx 1.0$ at touch down as indicated in Figure 7. This decrease to $n = 1$ is imposed so that a remaining normal acceleration capability is reserved for the pilot to maintain some control over the sink rate and to counteract the ground effect.

These assumptions now reduce the determination of the required control capability to an assessment of how much positive normal acceleration is required at the peak value two seconds after pilot control initiation. This peak value is determined without ground effect, being still approximately 15 to 20 feet above the ground. Some ground effect already exists at that height but it becomes much more significant at a closer ground proximity, i.e., downstream of this peak. In this way it is hoped to separate effects of engine failure from effects of ground proximity, at least for the present theoretical computations.

14

Results of time histories in the above Figure 7 show that the normal accelerations required with these assumptions are in the order of Δn = 0.04 to 0.05. Also, it is seen that the maximum increase in sink rate is approximately 3 ft/second. The time history shows a vertical displacement of the flight path of approximately 7 feet. The associated undershoot distance can be shown to be 93 feet for V = 70 knots, and 98 feet for 85 knots. These results are also presented in Figure 8, top.

These undershoot distances are still considerable. For this reason, similar computations have been made to determine the maximum normal acceleration required to touch down at the same point on the runway as the targeted impact before engine failure and no flare. Again, the peak acceleration is assumed to occur two seconds after pilot control initiation, and again the pullup is phased out thereafter to Δn = 0 at a time five seconds after the engine failure. Results in Figure 8, bottom, show that the required peak acceleration is Δn = 0.12 to 0.13. It is surmised that this acceleration capability should be provided for better control of the touch down point, rather than the lesser amount needed for control of just the sink rate.

Furthermore, the pilot may not pullup exactly at the time indicated in the above time history. In case pullup is delayed somewhat, it is suggested to provide the normal acceleration not only out of ground effect but also in ground effect, and to round it off at a nominal value of Δn = 0.15. It must be emphasized though, that a successful touch down after engine failure in the longitudinal sense requires a fast acting lift control, and the required value of Δn most likely depends on it.

(c) Yaw Angle Control

In the present document the required speed margin for satisfactory directional control during flight after engine failure is not established, because such a speed margin enters only into the sizing of the vertical tail and the rudder, and is not a primary input in the determination of safety margins for use in general STOL performance criteria; performance criteria determine the size of the tail for the design condition, not vice versa in general.

15

OUT OF GROUND EFFECT

APPROACH SINK RATE 10 FT/SEC

ENGINE FAILURE AT 50 FT ALT

SL STANDARD CONDITIONS
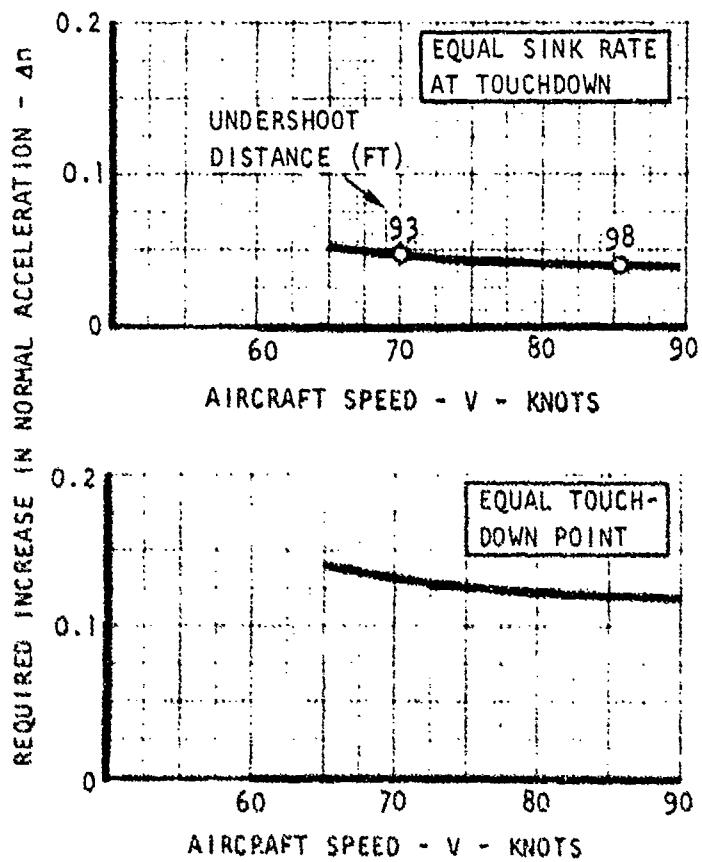
Figure 8. Normal Acceleration Required for Flight Path Control After Engine Failure

2.1.2 MANEUVER CAPABILITY WITH ONE ENGINE FAILED

(a) Turning Maneuver During Approach

After engine failure the airplane must have a maneuver capability
suitable for turns and sidesteps. For example it may be needed to follow
a prescribed landing pattern of a STOL port. The aircraft may be in a
turning maneuver according to this landing pattern when an engine failure
occurs. Surrounding structures or adjacent landing patterns for other
aircraft may commit the aircraft to continue this landing pattern with
the engine failed at least partially until the pilot can safely abort
the landing, or continues the pattern until the landing is completed.
Examples of such landing patterns are presented in Figures 9 and 10, which
are taken from References (4), (5), (6), and (7).

It is seen that a turning radius of 1500 feet is considered feasible
for STOL patterns, at least on the basis of some of these references.
The normal acceleration needed for this turning radius is approximately
$n = 1.03$ for 70 knots true airspeed and $n = 1.09$ for 85 knots as shown
in Figure 11.

These normal acceleration capabilities must be provided, as well
as an additional margin for flight path corrections, control of gust
response, and prevention of stall under these circumstances, assuming
that all engine failure transients have disappeared.

However, if the airplane is subjected to a severe gust while in the
turning maneuver it is likely that the pilot is distracted from the turn-
ing maneuver and will put most of his attention to the control of the
gust response. If he is distracted during a nominal period of time of
3 to 4 seconds, he will not follow the curved flight path over a distance
of about 500 feet. In order to catch up with the intended curved flight
pattern, he must then be able to perform a curved path with a radius of
1000 feet, see Figure 12. The normal acceleration required for this
radius is shown in Figure 13. If a radius of 1000 feet is to be flown at
an approach speed of approximately 95 knots, a normal acceleration of
$\Delta n = 0.30$ is required, if a speed of 80 knots is flown, Δn needs to
be only 0.15.

17

TOUCHDOWN
WP7

WP6

LIFTOFF
WP1

WP5
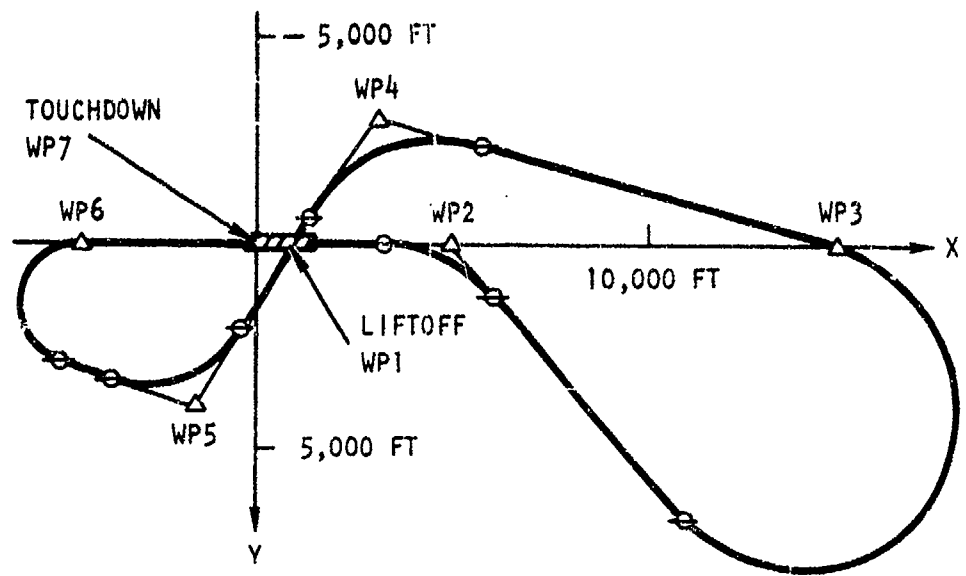
WP = WAYPOINT

NUMBERS REFER TO
DISTANCE ON
GROUND SURFACE
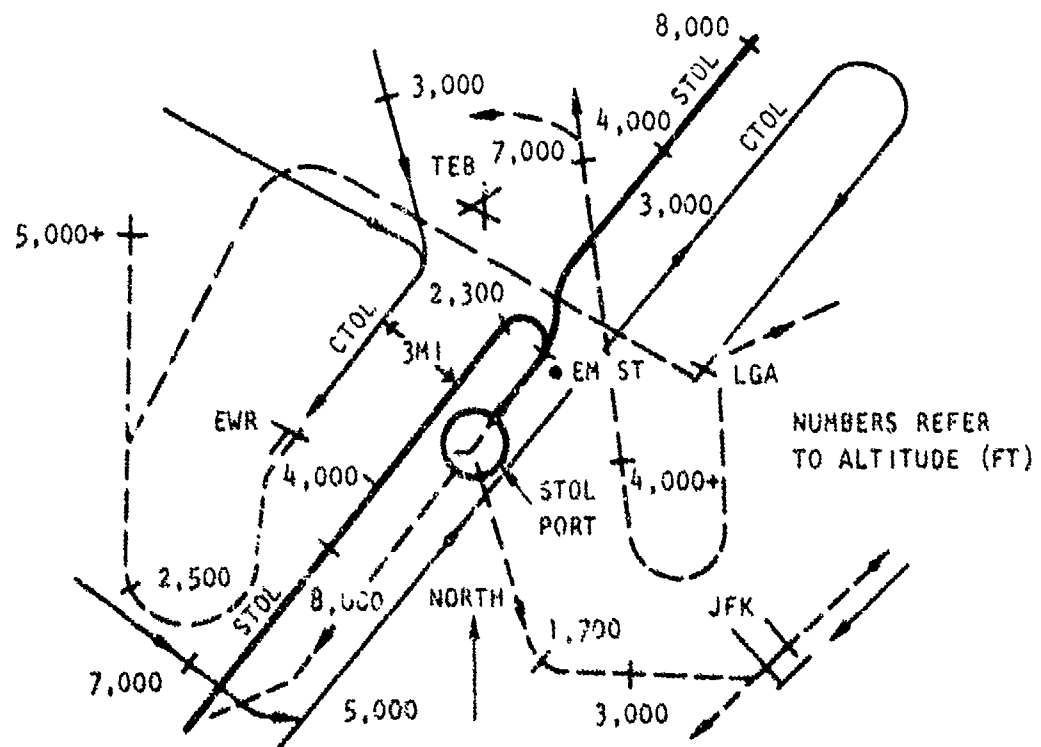
Figure 9. Sample Approach Flight Patterns

18
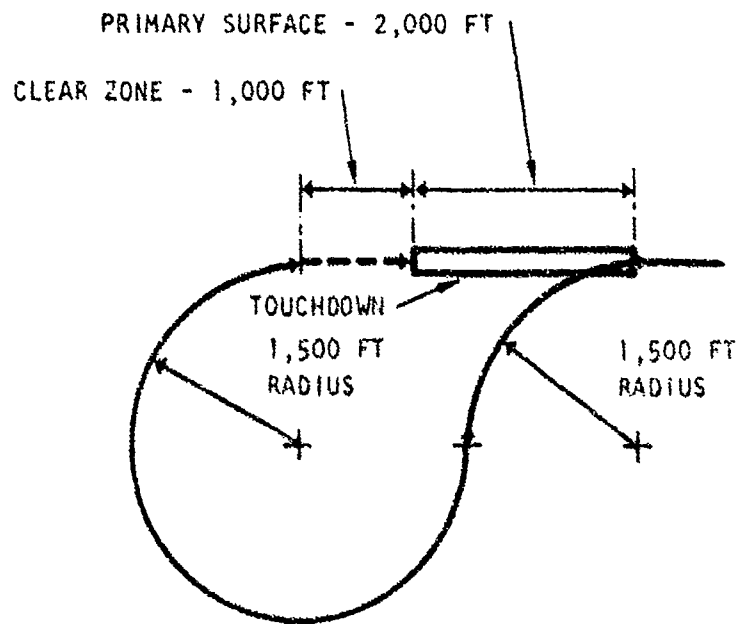
Figure 10. Typical Approach Flight Pattern

$$R = \frac{V^2}{g\sqrt{n^2-i}}$$
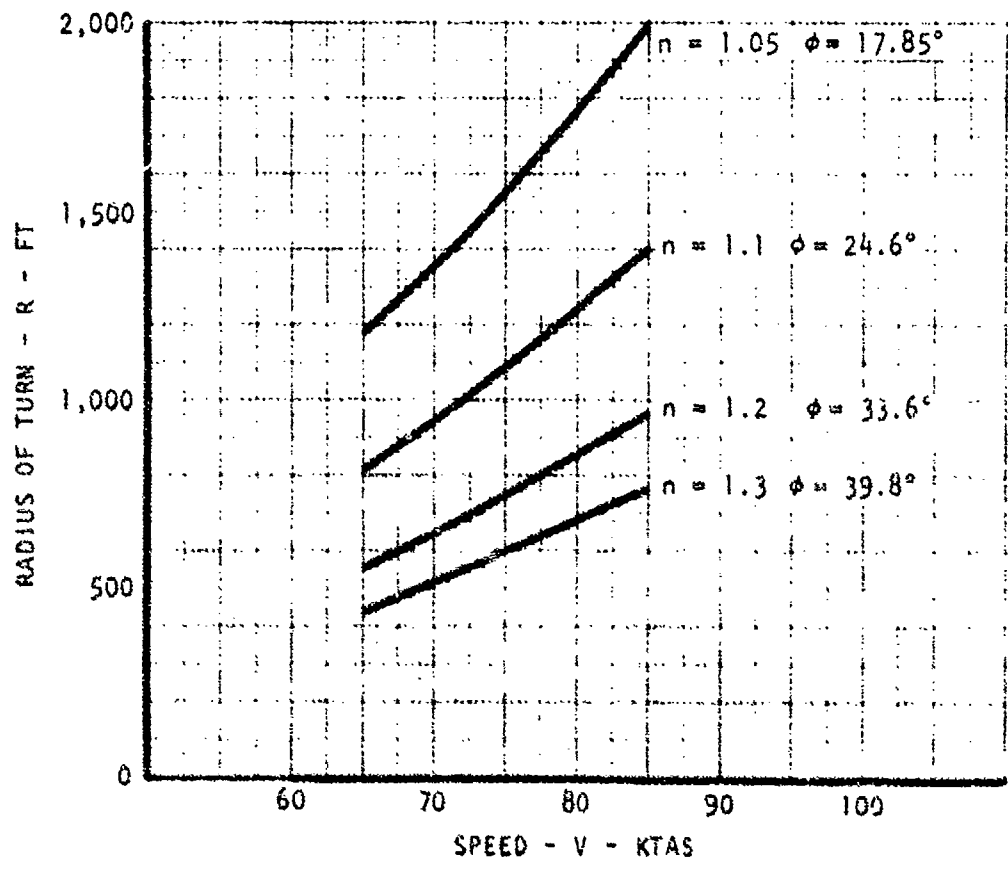
Figure 11. Radius of Turn as a Function of Speed and Normal Acceleration

20
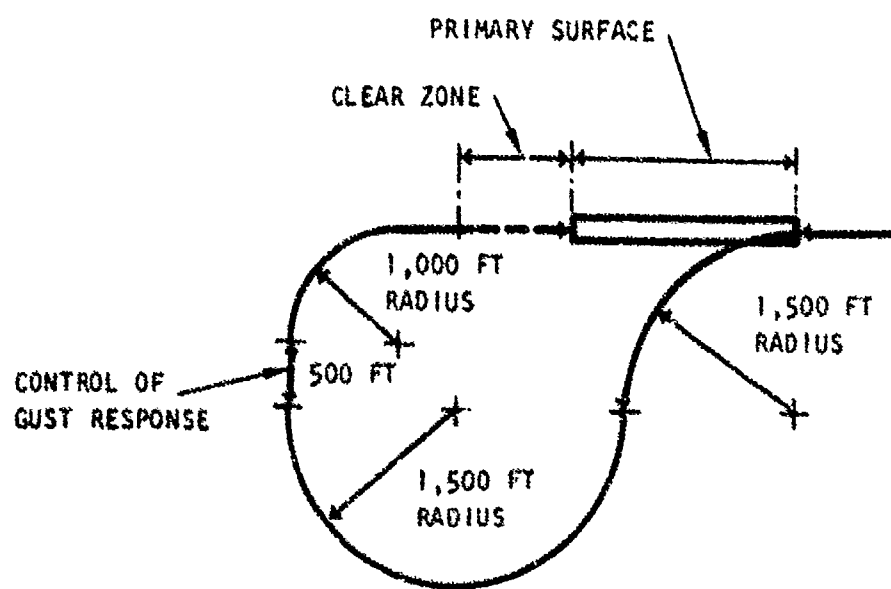
Figure 12. Interrupted Turning Maneuver

21
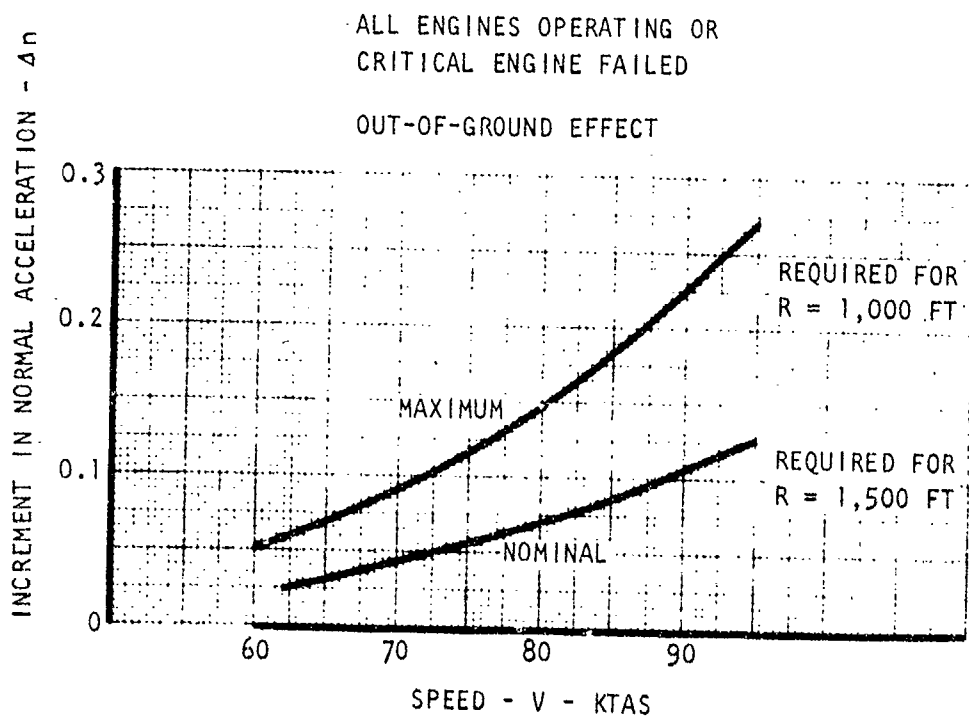
Figure 13. Recommended Turning Acceleration

22

(b) Sidestep Maneuver During Approach

Sidestep maneuvers are primarily a criterion for the required roll control power rather than for the normal acceleration capability. A computed time history of the bank angle variation that yields a lateral displacement of the airplane of 200 feet is shown in Figure 14. Herein the roll acceleration capability specified in MIL-F-83300 for Class II aircraft is used pertaining to the engine failure case (Level 3). The total time to complete this maneuver is about 10 seconds, during which time the altitude is reduced by 100 feet using a sink rate of 10 ft/second.

If it is desired to compensate for the loss in normal acceleration at each point of this time history, a normal acceleration capability of only $n = 1.04$ needs to be provided regardless of speed. It is not a function of speed because the roll acceleration requirement is independent of speed.

(c) Landing Touch Down

The normal acceleration required just prior to touch down is assessed here, assuming that the initial approach sink rate is equal to the design value, and that the pullup just prior to the touch down is delayed as long as possible within certain constraints. It is further assumed that one engine has failed and that the failure transients have disappeared.

Constraints should be based on flight or simulator test data; however, in the absence of adequate test data the following is suggested:

> The pilot anticipates a lift loss due to full roll control over a time period of two seconds just prior to touch down. Because of this and because of the possibility of engine failure, the pilot will routinely decrease the rate of sink just prior to touch down, using a minimum time of two seconds to accomplish this.

Lift characteristics for full roll control with one engine failed in ground effect depends on the roll control system used. Assuming an average 5 percent

23
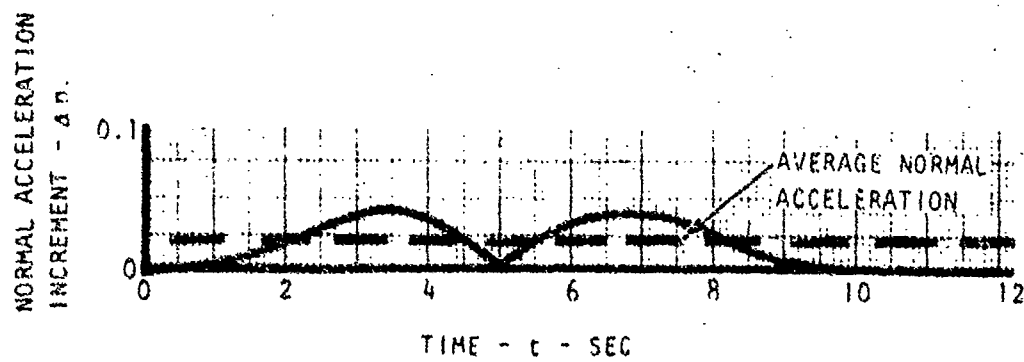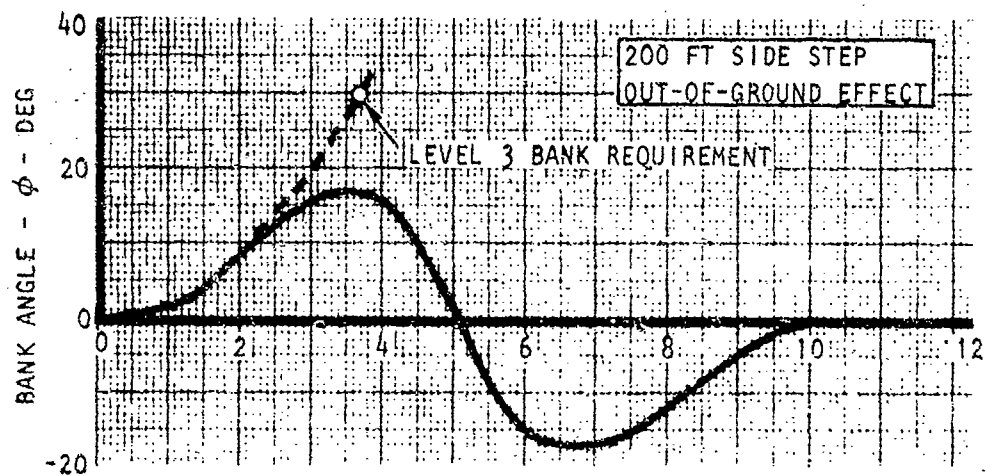
Figure 14. Side-Step Maneuver Characteristics

24

lift loss during a time period of $\Delta t = 2$ seconds results in a sink speed increase of

$$\Delta V_Z = (\Delta n\ g)\ \Delta t = (0.05)(32.2)2 = 3.22\ \text{ft/second}.$$

In Figure 14 it is seen that the bank angle may change only 9 degrees during this time, and only about half as much is expected when the bank angle is to be increased as well as stopped in this time. If the pilot descends with a design rate of 10 ft/second without intention to pullup, such a sudden roll control maneuver will increase the sink rate to a value in excess of 13 ft/second. This increase in sink rate is excessive in comparison to a design sink rate of 10 ft/second. In order to avoid this increase in sink rate, the pilot probably desires to pullup before touch down so that the rate of sink at touch down is in average 6 to 7 ft/second, thus leaving a 3 ft/second margin for the maximum roll control input.

A similar philosophy is applied to the buildup of rate of sink in case an engine fails just prior to touch down. This yields a similar constraint as above. Figure 7 shows that the sink rate increases also approximately 3 ft/second before adequate pilot action can be applied. The pilot is expected to attempt this pullup routinely or automatically, thus also in the present case where one engine has already failed.

The last two seconds before the touch down is thus considered the latest opportunity for the pilot to reduce the sink rate. In order to reduce the sink rate from 10 ft/second to 7 ft/second within the two seconds, a normal acceleration capability is required in ground effect amounting to:

$$\Delta n = \Delta \ddot{z}/g = \Delta V_{\dot z}/\Delta t/g = \tfrac{3}{2}/32.2 = 0.0465 \approx 0.05$$

This acceleration requirement is independent of forward speed. However, the increased distance traveled before touch down does depend on speed, see Figure 15. It is seen, that during the 0.35 second involved in the touch down delay, a distance is travelled of 41 feet for $V = 70$ knots, and 50 feet for 85 knots. Effectively this means that the height above the threshold with flare must be 45 to 46 feet to yield the same air distance as a height of 50 feet without flare, also shown in Figure 15.

It should be mentioned that it is assumed that this maneuver capability can be generated quickly. The necessary lift increase must not

INITIAL SINK SPEED 10 FT/SEC
PULLUP IN GROUND EFFECT
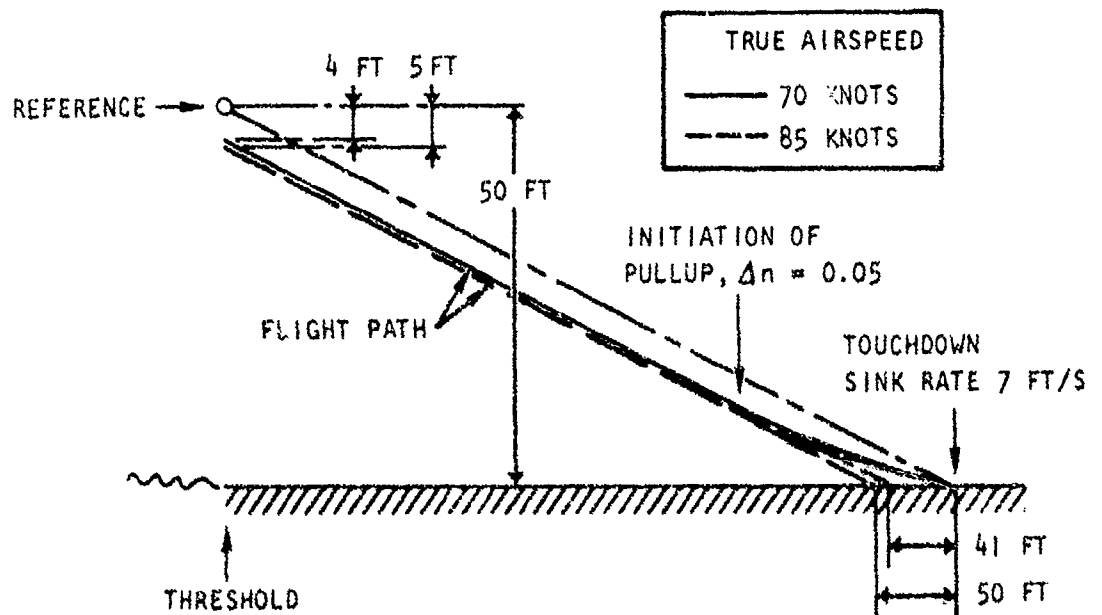
Figure 15. Approach Profile for a High Approach

26

only generate the normal acceleration for pullup, but must also overcome the negative ground effect that builds up very fast at low heights above the ground. An example of test data showing how the landing dispersion is affected by the rapidness with which the lift can be changed is presented in Figure 16. This figure is taken from Reference (8). In this figure lift control is derived from pitch attitude control, but it should be realized that direct lift control (DLC) through spoiler retraction can provide a quicker lift increase.

Additional test data, especially with DLC, should be obtained to corroborate the above acceleration requirements and to define the best type of control. In particular, the normal acceleration requirements to control a descent immediately after a rebounce should be established from flight tests with ground effects and with a suitable lift control system.

Another consideration in the control of the aircraft in touch down is the sensitivity of the lift control with airspeed. Assuming that the aircraft approaches with a forward speed that is 10 percent lower than the normal touch down speed due to pilot error, for example, from a misinterpretation of the aircraft weight, it should be at least possible to continue the flight path into the ground effect without increase of the sink rate, i.e., with $\Delta n = 0$. This is the minimum touch down speed, V_{mtd} Essentially, this means that the normal approach speed should be

$$V_a \geq 1.10 \, V_{mtd} \quad (IGE, CEF, \Delta n = \cos \gamma - 1 \approx 0)$$

(d) Waveoff Capability

An aircraft has adequate waveoff capability when it satisfies various criteria. These are:

1. Adequate climb capability must exist after waveoff is completed

2. Adequate maneuver capability must be available to clear the runway

3. Adequate maneuver capability must exist to clear an obstacle at the far end of the runway, and to obtain a flight path angle equal to the climb path.
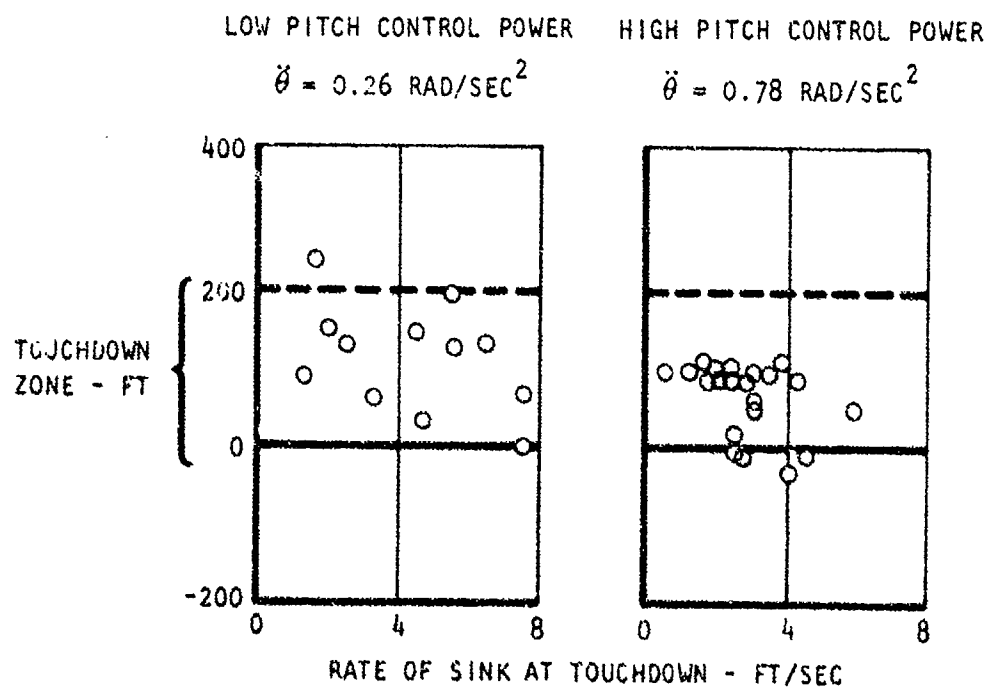
Figure 16. Touchdown Dispersion

28

The climb capability after waveoff is either provided by a thrust increase, or by a drag decrease such as a reduction in flap angle, or both.

The maneuver capability needed to prevent physical ground contact(item 2) can be found from

$$\Delta n = \frac{1}{2} V_z^2 / (\Delta h)(g)$$

where V_Z is the initial sink rate, and Δh is the height of the aircraft above the ground where the full normal acceleration is first achieved. Assuming a sink rate of $V_Z = 10$ ft/second, and assuming that it requires 0.5 second to generate this normal acceleration fully, the decision height becomes then

$$H = \Delta h + 5 \text{ Ft.}$$

With these assumptions, the normal acceleration required is shown in Figure 17 as a function of the height, H. It is seen that for a nominal height of H = 35 feet, the required acceleration is, regardless of flight speed:

$$\Delta n = 0.05$$

Because a portion of the flight path is in ground effect, and the remainder is out of ground effect, this capability should exist with and without ground proximity.

If the maneuver capability equation above is extended to clear an obstacle at the other end of the runway and to provide a positive flight path angle or climb path angle at that obstacle, it can be shown that

$$\Delta n = (\gamma_c \cdot \gamma_A) V^2 / (g \cdot l)$$

where γ_c is the climb path angle in radians at the far end of the runway, γ_A is the flight path during approach when the aircraft is above the threshold (γ_A is negative) and l is the runway length, see Figure 18.

The top portion of this figure shows the required capability when $\gamma_c = -.75 \gamma_A$. This is typical for the aircraft presently under study, where $\gamma_A \approx -4°$ and $\gamma_c = +3°$. No obstacle exists at the end of the runway in this case. If an obstacle does exist at the end of the runway,

29

IN GROUND EFFECT AND
OUT OF GROUND EFFECT

DECISION
HEIGHT

SINK RATE 10 FT/SEC

INCREMENTAL NORMAL
ACCELERATION - Δn

0.2

0.1

0

0   20   40   60

DECISION HEIGHT - H - FT
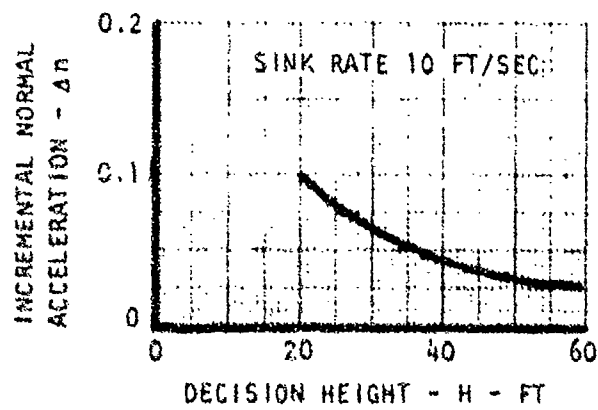
Figure 17. Minimum Normal Acceleration for Waveoff Required to
Clear Ground

30

IN GROUND EFFECT AND
OUT OF GROUND EFFECT

SINK RATE 10 FT/SEC
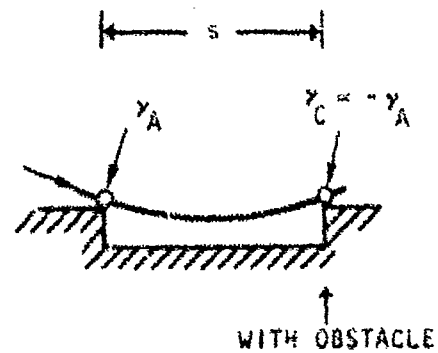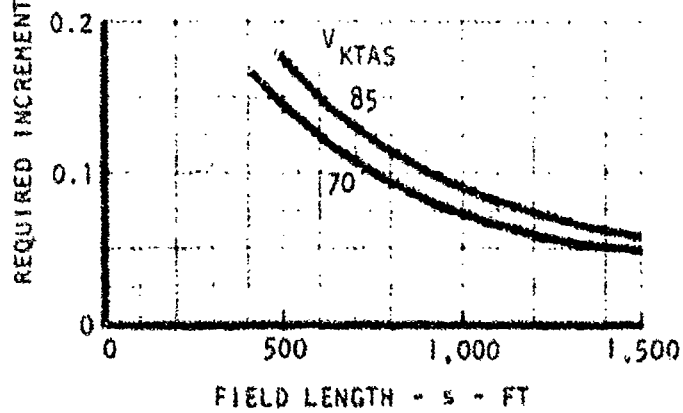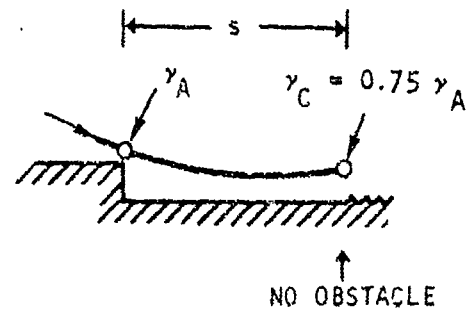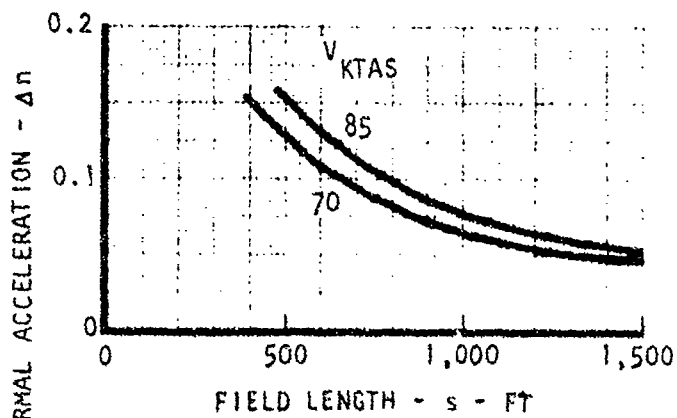
Figure 18. Normal Acceleration for Waveoff

31

and if it is equally as high as an obstacle at the beginning of the runway, then the approach angle and the climb angle are equal in absolute magnitudes in this simplified equation. Also, it is assumed that the speed is approximately constant. Results for this case are shown in Figure 18, bottom. It is seen that for field lengths of 1500 to 2000 feet a normal acceleration of $\Delta n = 0.05$ to 0.06 is adequate.

If the approach speed is lower than the speed needed to obtain the desired climb angle in the waveoff, the aircraft should have the capability to increase the speed during the pullup maneuver. For the moderate pullups involved this is possible by thrust increase or rapid but limited flap angle decrease.

2.1.3 GUST

(a) Upward Gust

In this subsection the angle of attack response of the airplane is given following various different gust frequencies and velocities of a discrete gust. The angle of attack excursions of these gusts is used to establish the angle of attack margin the airplane should have in order to prevent airplane stall. The excursions are computed from

$$\ddot{\alpha} + 2\omega_n \dot{\alpha} + \omega_n^2 \Delta\alpha = -\omega_n^2 \left(\frac{V_g}{V}\right) - C_{L_\alpha} \frac{qS}{mV} \cdot \frac{\frac{d(V_g/V)}{dt}}{\cdot + (C_{L_{\dot\alpha}}) \frac{qS}{mV}}$$

the derivation of which is found in the Appendix and is valid for $\zeta = 1.0$. This damping is a reasonable average for STOL aircraft. Also a typical value is used for the undamped natural frequency ($\omega_{nd} = 1$ rad/second). Gust frequencies used were equal to 1/2, 1.0, and 2.0 times the undamped natural frequency of the airplane, as shown in Figure 19. The maximum gust levels are obtained from MIL-F-8785B(ASG), "Military Specification, Flying Qualities of Piloted Airplanes," dated 1 August 1969 (Reference 9).

Gust response characteristics without pilot control input for these conditions are presented in Figure 20. The shortest gust shown is probably not significant from a standpoint of wing stall, because the flow probably attaches again so rapidly after a possible stall that no significant aircraft response is caused in angle of attack. The gust with the

32
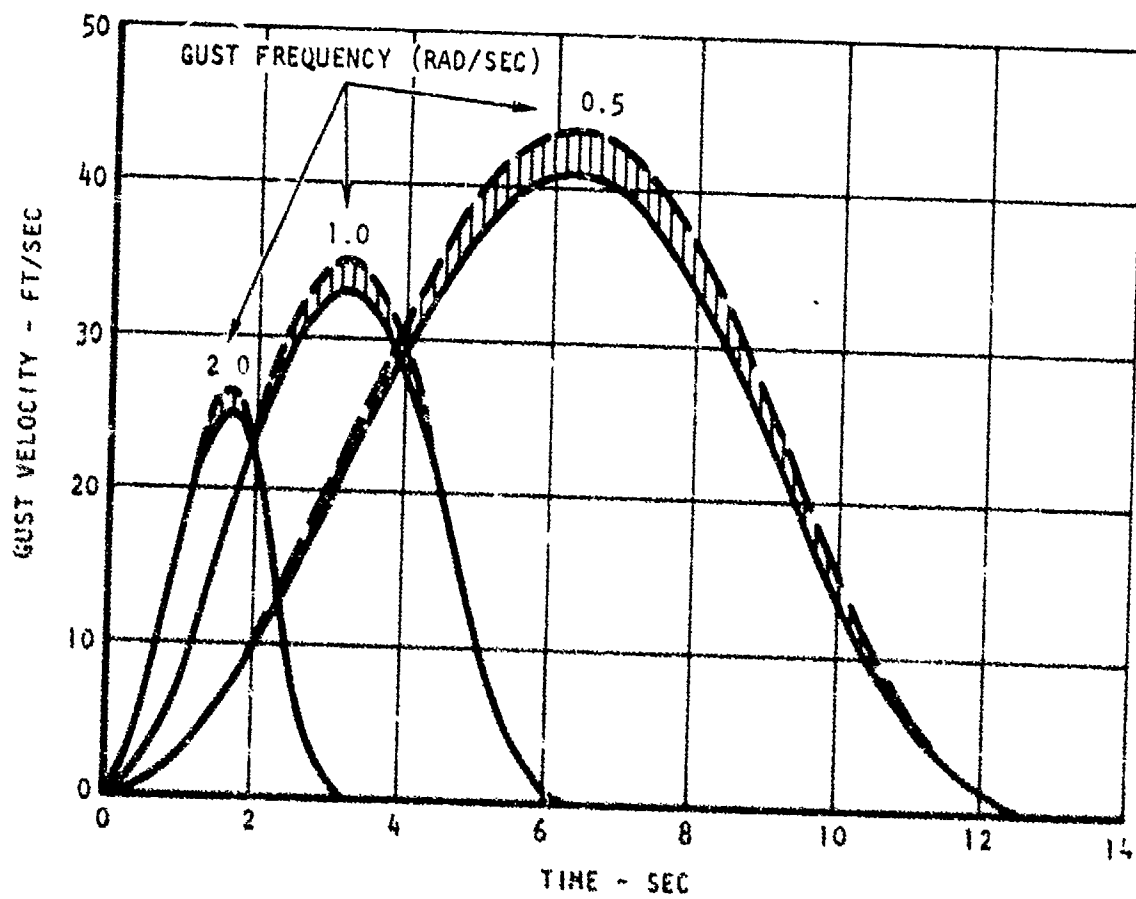
Figure 19. Gust Velocities Considered for Aircraft Speeds 70 to 85 Knots

33
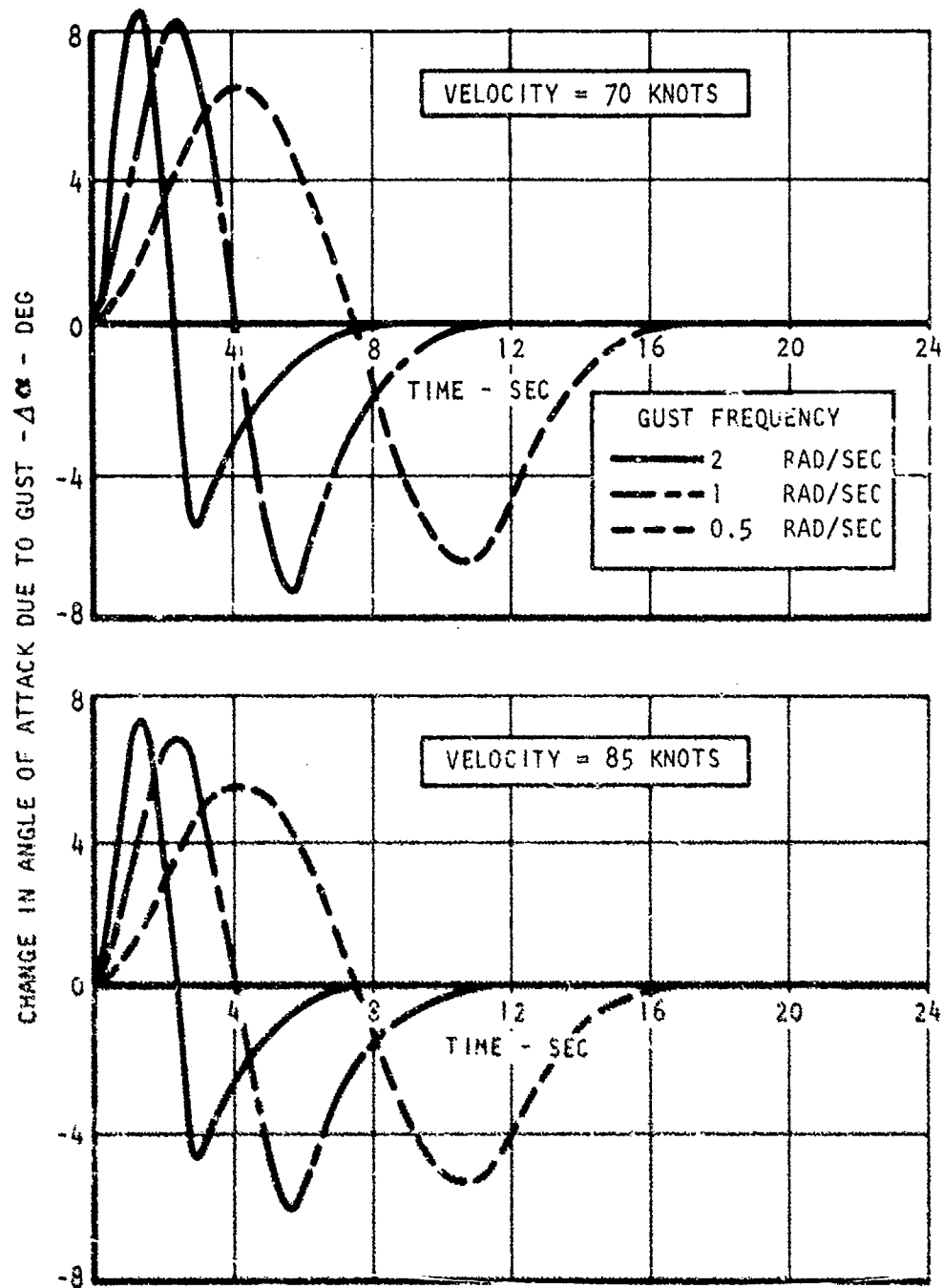
Figure 20. Effect of Gust on α-Response for ω_{nd} = 1 Rad/Sec and ζ = 1.0

34

longest duration probably induces the pilot to smoothen the motion so that the time history shown for this case without the pilot control is also only of limited interest. However, the medium gust shown is considered to be too short for the pilot to react upon, and possibly long enough to produce a condition dangerously close to stall or to produce a significant response after stall.

It is seen that angle of attack increases occur in the order of 8.2 degrees for 70 knots, and 7.0 degrees for 85 knots for the medium gust frequency. To prevent aircraft stall, an angle of attack margin of this magnitude should be provided. Figure 21 shows that the required magnitude can be approximated by the equation

$$\Delta\alpha_{STALL} = 10 \text{ KTS} / V_{KTAS}$$

It is assumed that the vertical gust of the above magnitude exists without ground effect, applicable in the approach condition for landing and during the climbout away from the ground.

The gust response results described above can also be used to assess the magnitude of the vertical displacement of the aircraft following the gust, which is of particular interest during landing approach. Vertical displacements without pilot control are computed on the basis of

$$m\ddot{z} = \Delta\alpha C_{L_\alpha} qS$$

or

$$\frac{\ddot{z}}{g} = \Delta\alpha C_{L_\alpha} / C_L$$

where $\Delta\alpha$ is taken from the gust response in Figure 20.

Estimated results are shown in Figure 22 for various gust frequencies, using $C_{L_\alpha}/C_L = 0.03$ per degree as a typical value.

It is seen that vertical displacement of rather large magnitudes can occur if no corrective action is taken. Assuming that the pilot will have recovered control in approximately 3 to 4 seconds, vertical displacement of 8 to 14 feet can be expected. Using a nominal 10 feet displacement, an average and a high flight path over the threshold may be defined as illustrated in Figure 23.

35
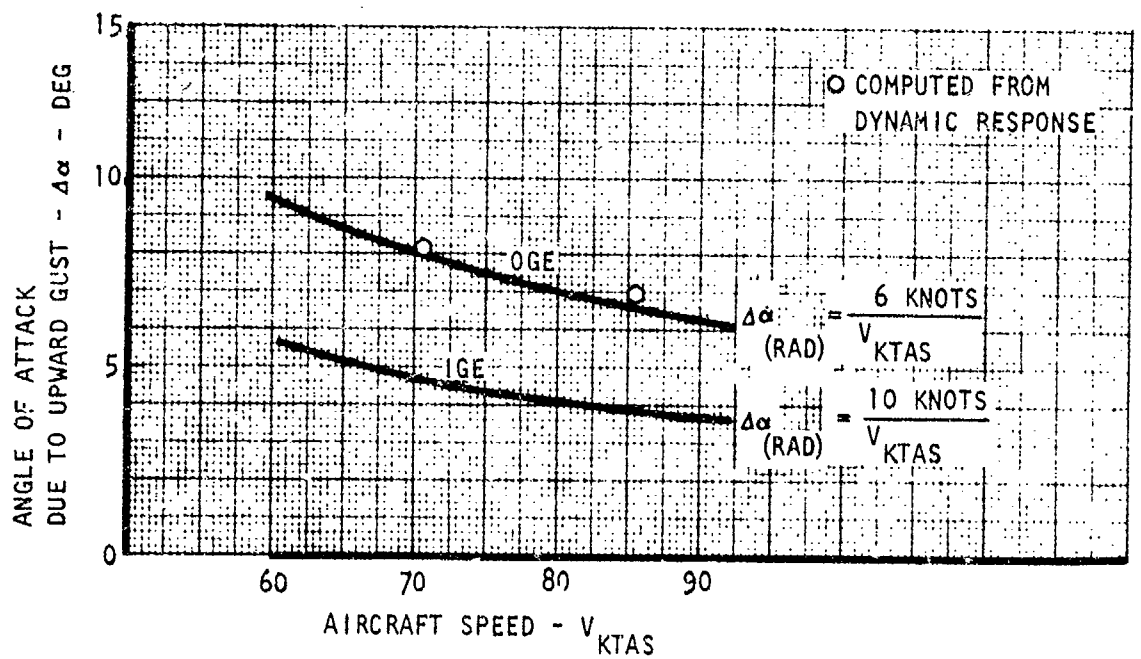
Figure 21. Angle-of-Attack Margin for Upward Gust

36

NO PILOT INPUT
OUT OF GROUND EFFECT

$$\frac{C_{L_\alpha}}{C_L} = 0.03 \ DEG^{-1}$$
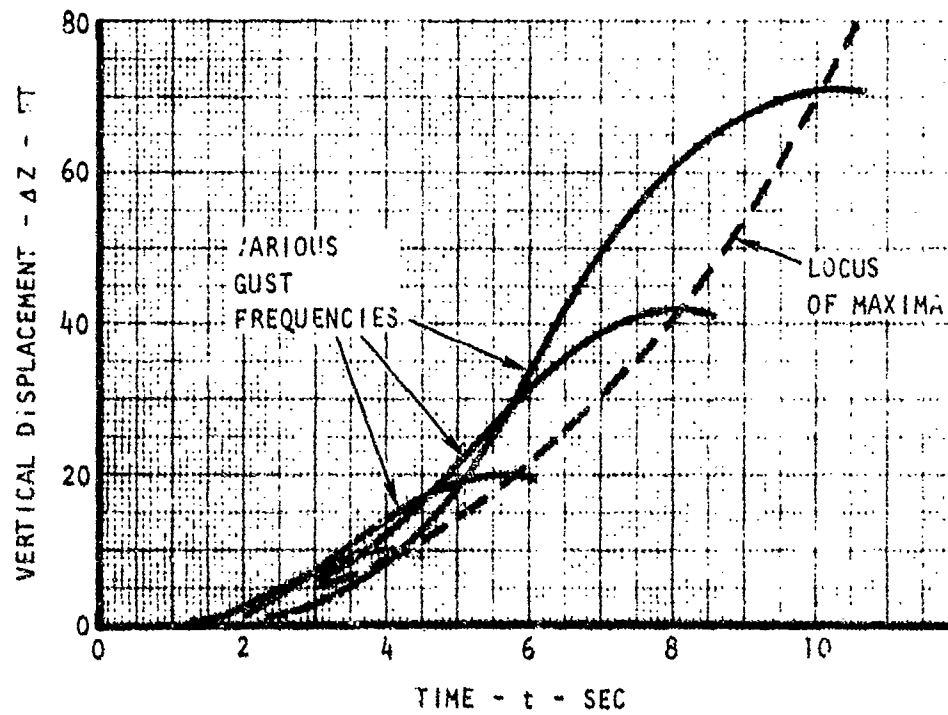
Figure 22. Vertical Displacement Due to Upward Gust

INITIAL APPROACH SINK RATE 10 FT/SEC

50 FT REFERENCE

10 FT

HIGH APPROACH

10 FT

AVERAGE

35 FT

LOW

THRESHOLD

AIM
POINT

TOUCHDOWN
ZONE
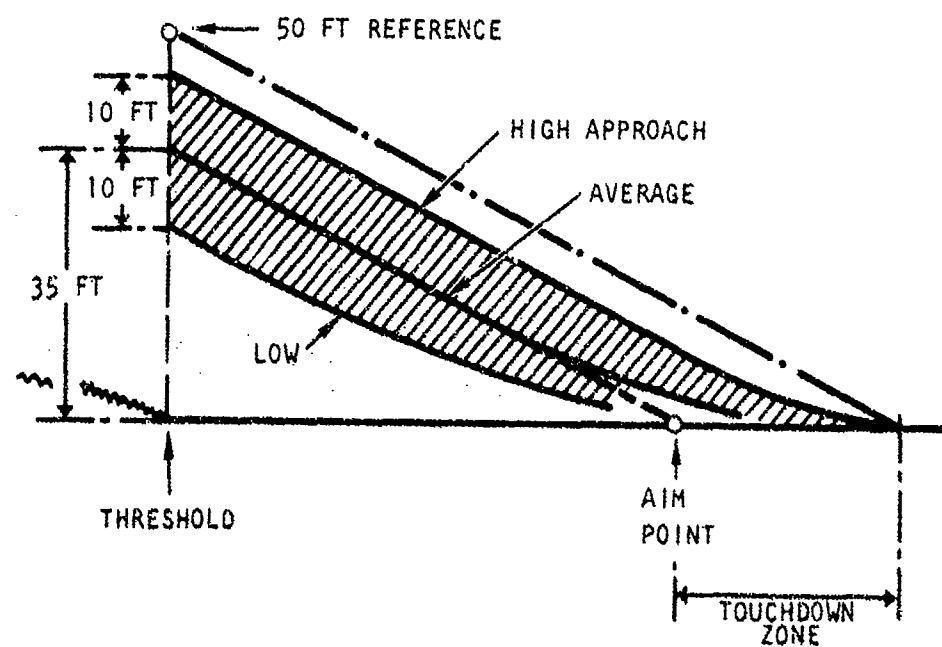
177 FT FOR V = 70 KTAS
215 FT FOR V = 85 KTAS

Figure 23. Height of Approach Flight Path

Upward gusts in ground effect are also of particular importance during the initial takeoff maneuvers. Shortest takeoffs over obstacles are obtained by rotating the aircraft to the highest safe angle of attack immediately after liftoff. The highest angle should have a safety margin with respect to wing stall, and should not cause the aircraft to decrease speed. Only after this highest angle is reached will the angle of attack be bled off to maintain approximately constant speed while increasing the flight path angle until a steady state value is reached. To avoid stall during the initial maximum rotation, an assessment of the upward gust near the ground is needed, as one criterion to determine the magnitude of the margin.

This poses a dilemma because probably no data are published about upward gust in ground effect. In order to obtain a general idea of what the ground effect might be on the magnitude of gust, a simplified theoretical model of a discrete gust is developed here for use in ground effect.

It is assumed that the vertical gust can be represented by two parallel vortices of infinite length, each moving upward with a speed of $1/2\, V_{gmax}$, see Figure 24. Of interest is the speed that is induced at a point A in this figure located in a plane in the middle between the two vortices. At the time the vortices are at the same vertical location as point A, the velocity induced is by definition V_{gmax}. At vertical locations above or below point A the vertical velocities induced at that point are less and will depend on the time that is consumed for the vortices to travel upward. It can be shown that the variation of V_g with time can be expressed by

$$\frac{V_g}{V_{gmax}} = \frac{1}{1 + \left(\frac{V_{gmax} \cdot t}{l}\right)^2}$$

Defining T as the lengths of the gust in time (see Figure 24), and using

$$l = V_{gmax} \cdot \frac{T}{4}$$

the relation follows closely the greatest part of the discrete gust model from MIL-F-8785 (Reference 9). The agreement between the two gust models is illustrated also in Figure 24.

Using $T = 2\pi$, which belongs to a gust frequency of $\omega_A = 1$ rad/second and $V_{gmax} = 34$ feet/second the distance between the two vortices becomes $l = 53.2$ feet.

39
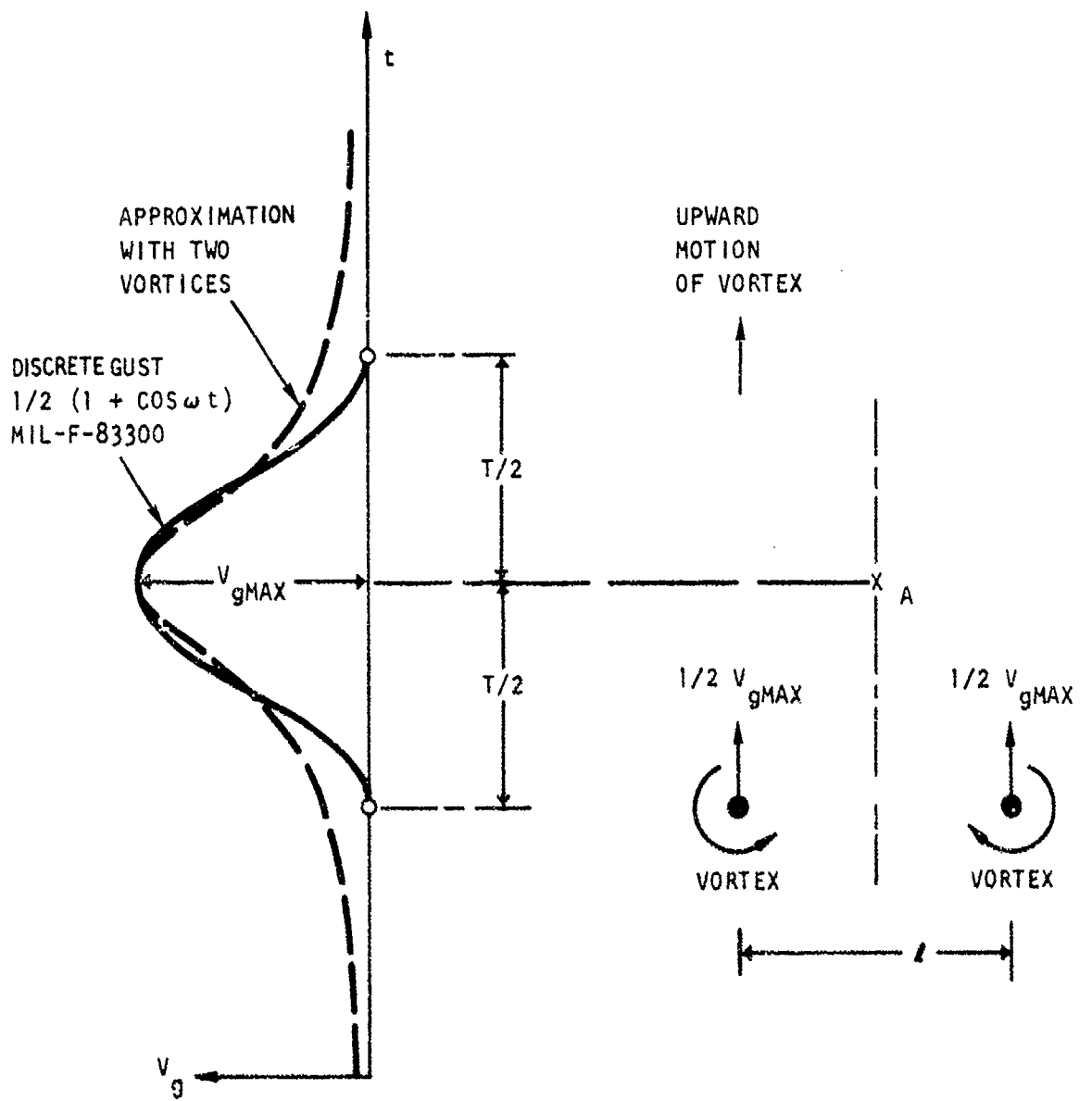
Figure 24. Representation of a Discrete Gust by a Twin Vortex

40

Given the magnitude of this distance, and the height h of the vortices above the ground, image vortices can be placed underneath the ground and the reduction of the maximum gust velocity can be computed. The equation becomes:

$$\frac{V_{g\,max\,IGE}}{V_{g\,max\,OGE}} \approx 1 - \frac{1}{\sqrt{1 + \left(\frac{4h}{\ell}\right)^2}}$$

The variation of this maximum gust velocity ratio with h/ℓ is presented in Figure 25. Assuming that the pilot rotates the aircraft to a maximum tolerable angle of attack at a wing altitude of 30 feet or less, a gust margin should then be in existence consistent with

$$h/\ell = 30/53.2 = .56$$

This yields

$$\frac{V_{g\,max\,IGE}}{V_{g\,max\,OGE}} \approx .60$$

so that the angle of attack margin at that condition should be

$$\tan(\Delta\alpha) = 6\,KTS / V_{KTAS}$$

This amounts to a margin of 4.85 degrees at 70 knots and 3.95 degrees at 85 knots, see Figure 21.

It may be of interest to compare this margin with the 10 percent margin in lift, or $\Delta n = 0.1$, often used in conventional aircraft. Using an aspect ratio of $A = 4$, and a $C_{L_{max}}$ of 2.0, the 10 percent margin yields

$$\Delta\alpha = \frac{\Delta C_L}{C_{L_\alpha}} = \frac{C_{L\,max}/10}{(2\pi/57.3)(A/2 + \sqrt{A^2 + 4})} = 2.95°$$

It is seen that the margin is not incompatible with the margin derived here based on ground effect, noting that for STOL aircraft $C_{L_{max}}$ is higher, thus also is $\Delta\alpha$. It is suggested to use the gust margin derived here for $\Delta\alpha$ rather than using Δn because it relates more to the physical model involved and can take into account a rounded lift curve. However, it should be emphasized that additional work is required to define

41
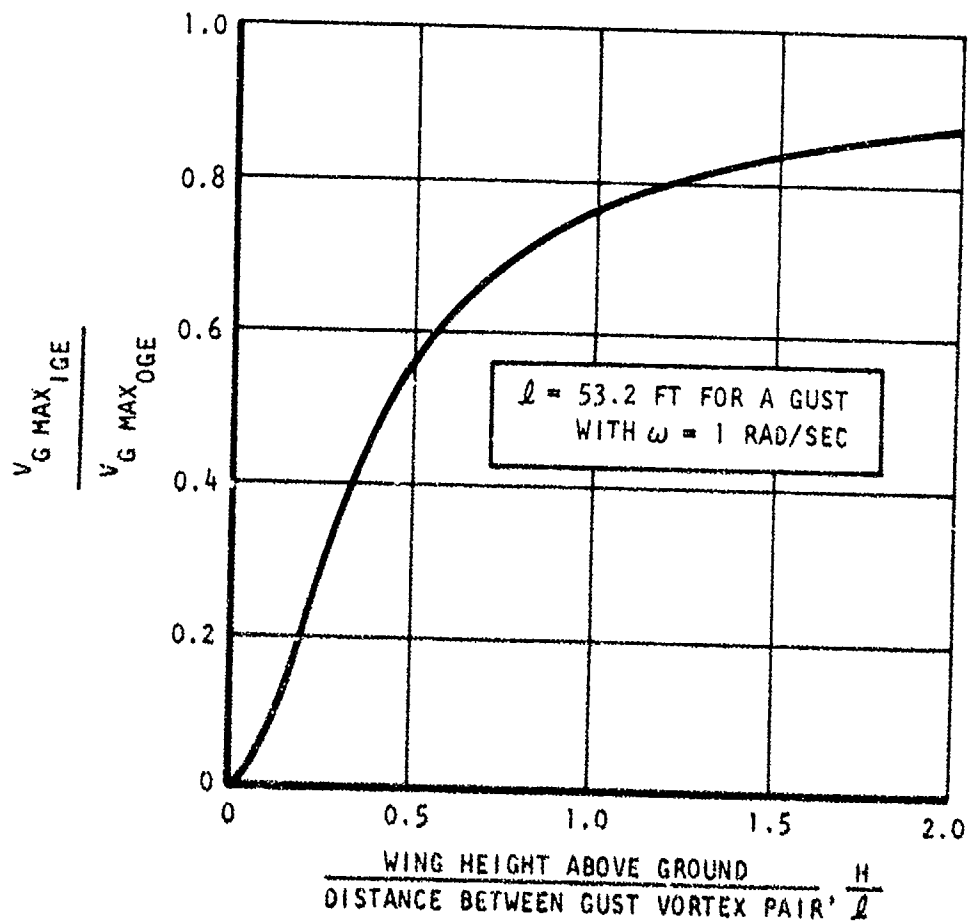
Figure 25.   Ground Effect on Maximum Gust Velocity

42

the gust in ground effect more closely. The present derivation should be considered as an investigation that was needed to point out where additional research should be made.

Based on Figure 25 the ground effect has essentially disappeared at an altitude of $h = 2\ell \approx 100$ feet above the runway. It is suggested to use full velocities above this altitude.

(b) Down Draft

Figure 23 of the previous section yields an estimated downward displacement of 10 feet, similar to the upward displacement from the upward gust.

Figures 26 and 27 illustrate the effect of a down draft for respectively a landing and takeoff flight trajectory for an airport with obstacles. The down draft will displace the aircraft vertically requiring an allowance of an undershoot distance with an additional margin and similarly an overshoot distance with a margin for the total takeoff distance over the obstacle. These figures relate the margins with respect to the obstacles.

However, it is not known how successful the pilot will be to counteract this gust. It is suggested to determine this from simulator data or flight tests.

Because the down draft appears to have rather significant effects on the runway margins, it is suggested that down draft magnitudes be defined in the vicinity of airport obstacles at heights from a multiple of the obstacle height to near the ground.
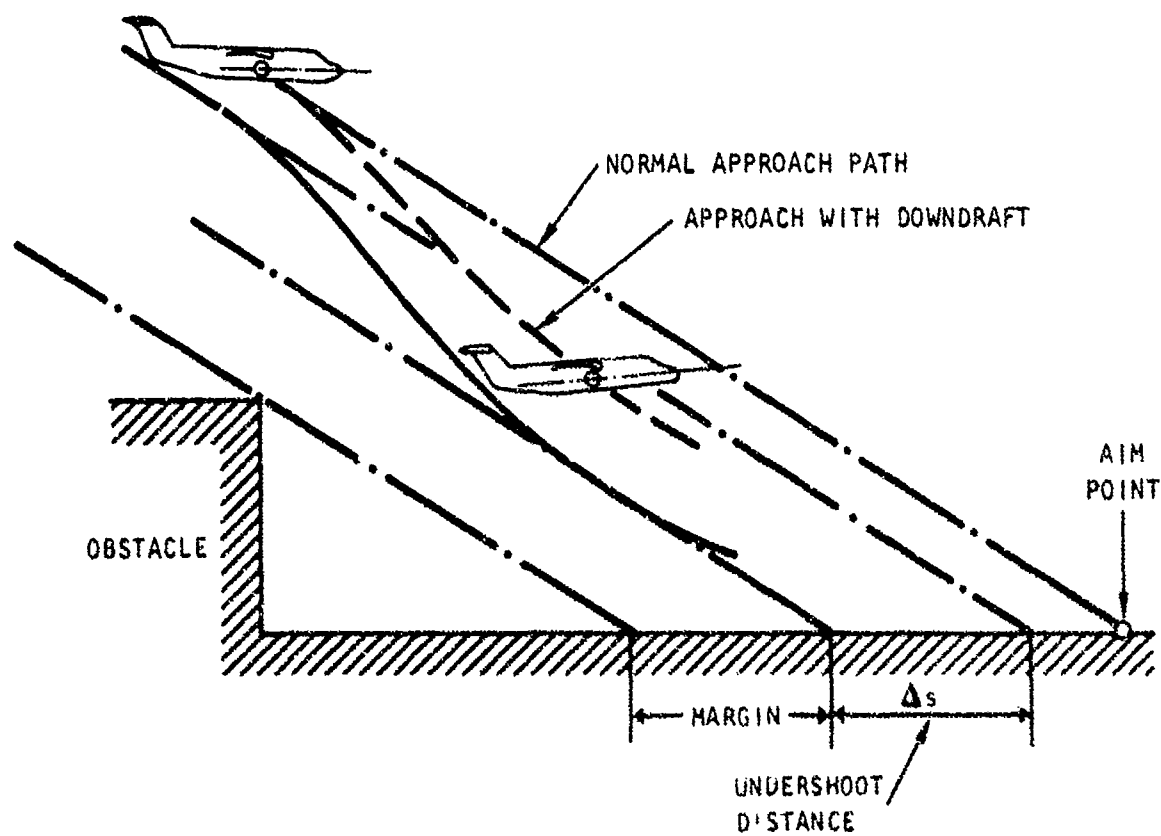
Figure 26. Illustration of Effect of Downdraft on Landing Undershoot Distance
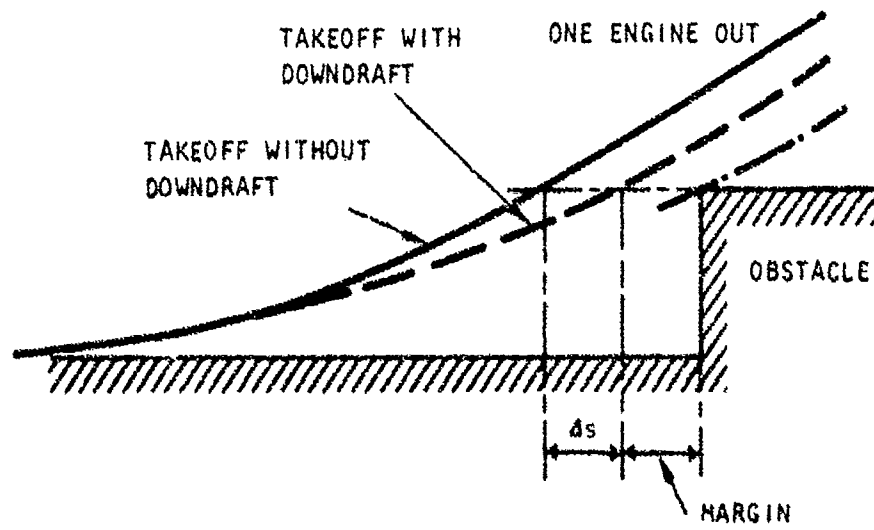
Figure 27. Illustration of Downdraft Effect on Takeoff Overshoot

(c) Headwind Fluctuations

An airplane that encounters a gust head-on will sense an increase in aerodynamic pressure and accordingly will generate an increase of lift and drag.

The aircraft drag will decrease the speed somewhat, however, the safety margin in speed will usually not be reduced significantly. The aircraft lift will displace the aircraft vertically similar to an updraft or upward gust. This has the effect of introducing an overshoot distance during landing approach as illustrated in Figure 28. This overshoot distance will have to enter as a margin for the ground roll distance while determining the runway length. Some of this margin is accounted in Figure 23 by using a 50-foot height above the threshold instead of an average height of 35 feet.

The magnitude of the lift change can be somewhat larger than that resulting from an upward gust, if no pilot reaction is considered for both types of gusts. Figure 29 shows the determination of the effect of the headwind gust on the aircraft lift increment. This increment is 29 percent as compared to 23 percent increase due to an angle of attack change of eight degrees from the vertical gust.

It is presently not known how to present the pilot reaction to the gust in a form suitable for computation of overshoot distances. For this reason it is again suggested to determine this distance from simulator studies and to correlate these with flight data for corroboration. However, for the present time, it is assumed that the maximum upward displacement will be approximately equal to that of an updraft, i.e., 10 feet, see Figure 23. Prerequisite is, again, that immediate control manipulation is performed, and that the lift change can be carried out quickly.

(d) Tail Wind Fluctuations

When the airplane encounters a sudden tail wind, and when the airplane motion has not yet reacted to this wind, then only the effective dynamic pressures changes and no angle of attack change has as yet developed. However, a lift loss has developed from the dynamic pressure loss which, in the event of a gust of the magnitude specified in 'HL-F-8785 is large at STOL speeds. This lift loss is sketched in Figure 30, point B. The airplane will start to sink with respect to its original flight path and the pilot will attempt to arrest this sink by increasing angle of attack.

It is not known how much angle of attack increase the pilot desires for flight path correction; however, it is known how much angle of attack increase is needed to at least maintain the aircraft lift on a steady

46
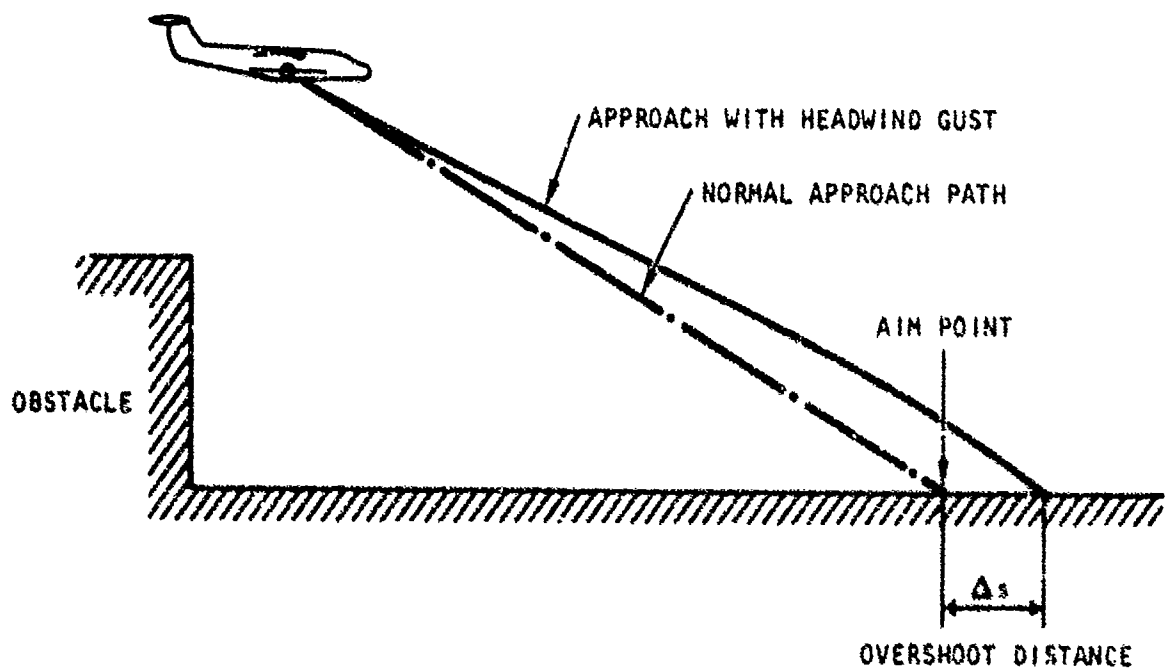
Figure 28. Illustration of Effect of Headwind Gust on Landing Overshoot Distance

47
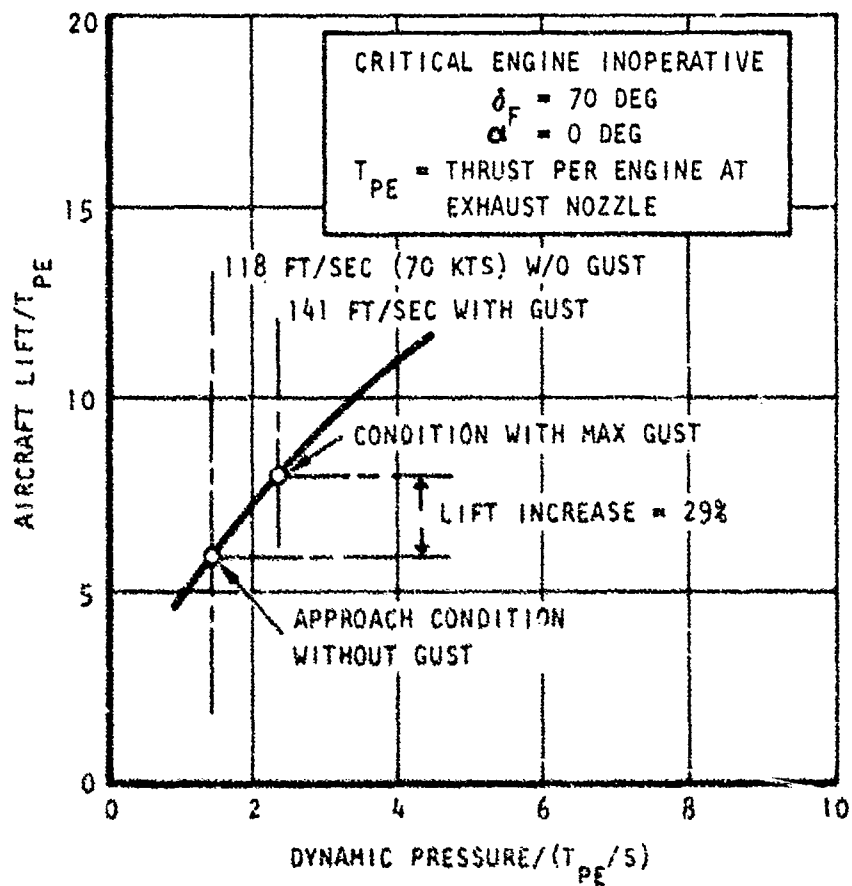
Figure 29. Determination of Lift Increment Due to Head Wind Fluctuation
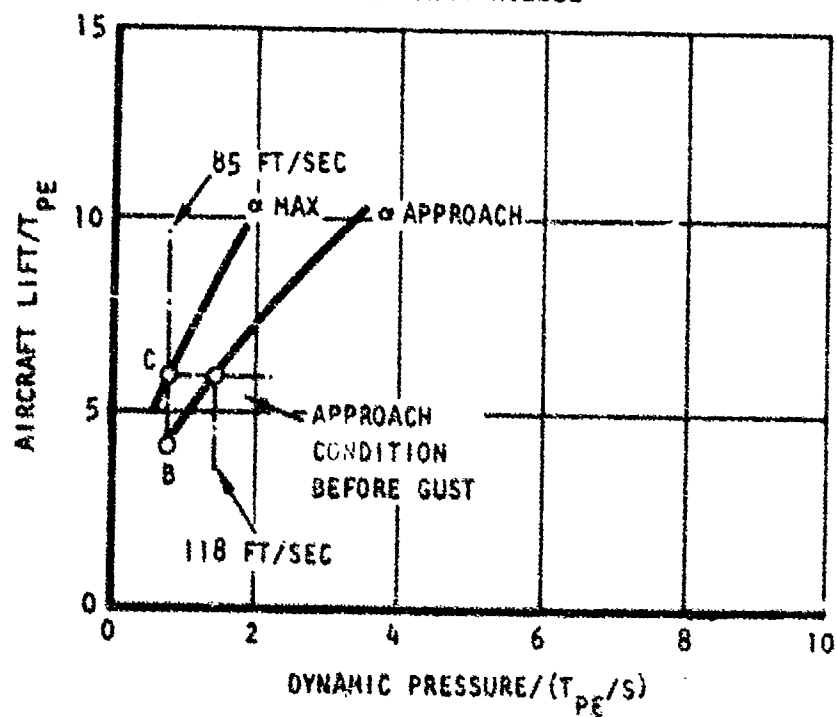
Figure 30. Determination of Speed Margin Due to Tail Wind Fluctuation

state basis. This is also illustrated in Figure 30, point C. To allow just that much capability coincides with allowing the aircraft to reach $C_{L_{max}}$ at the peak of the gust. This, in turn, determines the stall speed of the aircraft as illustrated, again, in this figure.

From this, a relation between V/V_S and the peak gust velocity V_{gmax} can be derived as follows.

At point C, the velocity is $V = V_S$, and at point A it is:

$$V = V_S + V_{gmax}$$

Thus:

$$\frac{V}{V_S} = \frac{V}{V - V_{g\,max}} = \frac{1}{1 - \frac{V_{g\,max}}{V}}$$

Using $V_{gmax} = 34$ ft/second or 20 knots associated with a frequency of one rad/second, the required speed ratios are shown in Figure 31. They range from $1.4\ V_S$ at 70 knots to $1.3\ V_S$ at 85 knots.

It should be noted that frequently a circular landing approach pattern is flown. Even though the landing is made predominantly with head wind, at a portion of the circular pattern the gust velocity may appear as a tail wind fluctuation. This circular pattern is followed at an appreciable ground distance, so that the curve in the above Figure 31 does not apply in ground effect.

It also should be noted that the stall speed V_S pertains to the maximum lift and it is assumed that the pilot can generate this lift quickly, including pitch angle, thrust increase, and possibly DLC. Flight experience is needed to determine whether the thrust increase can actually be used for the control of the response from this gust.

50

OUT OF GROUND EFFECT
PEAK TAIL WIND 34 FT/SEC TRUE
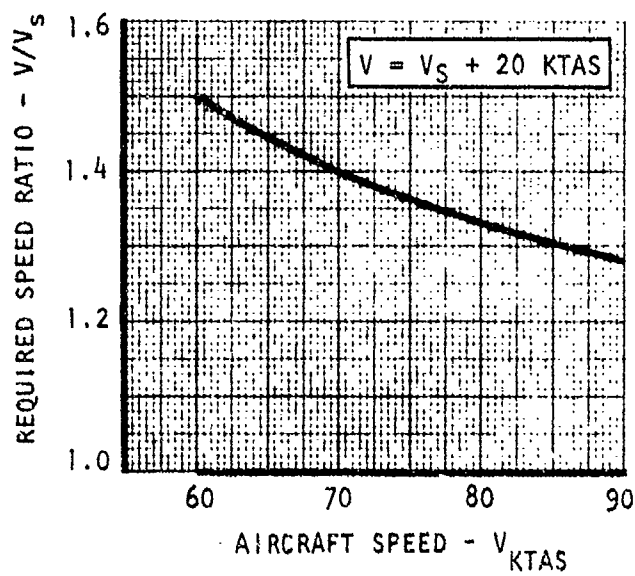
Figure 31. Required Speed Margin for Gust with Aircraft in Approach Pattern

51

(e) Side Gust

The effects of side gusts on sideslip excursions were analyzed on
the basis of one dimensional equations of motion. Results are intended
for first order assessments only.

A maximum gust velocity was used equal to 34 ft/second, a gust dura-
tion of 6.28 seconds, and an aircraft speed of 70 knots. Frequencies and
dampings used are those along the border of level 1 flying qualities
indicated by point no. 1 through 9 in Figure 32. The frequencies and
dampings are also listed in the following table:

Point No.	ω_{nd}	ζ
1	2.00	1.00
2	1.00	1.00
3	.50	1.00
4	.25	1.00
5	.25	.50
6	.25	.08
7	.50	.08
8	1.00	.08
9	2.00	.08

Time histories of the gust response in terms of sideslip angle are
presented in Figures 33 and 34. It is seen that the maximum sideslip
angle is in the order of 23.5 degrees or much less. the angle of 23.5
degrees is the required steady state sideslip capability associated with
a steady sidewind of 30 knots at a flight speed of 70 knots. Thus, it
appears that the side gust is generally not more critical than the
required steady state sideslip, and at the present time, no speed margin
requirements are derived from the side gust. However, it should be noted
that steady state sideslips of this magnitude are difficult or impossible
to obtain and this steady state requirement may have to be reviewed along
with the side gust requirements.

52
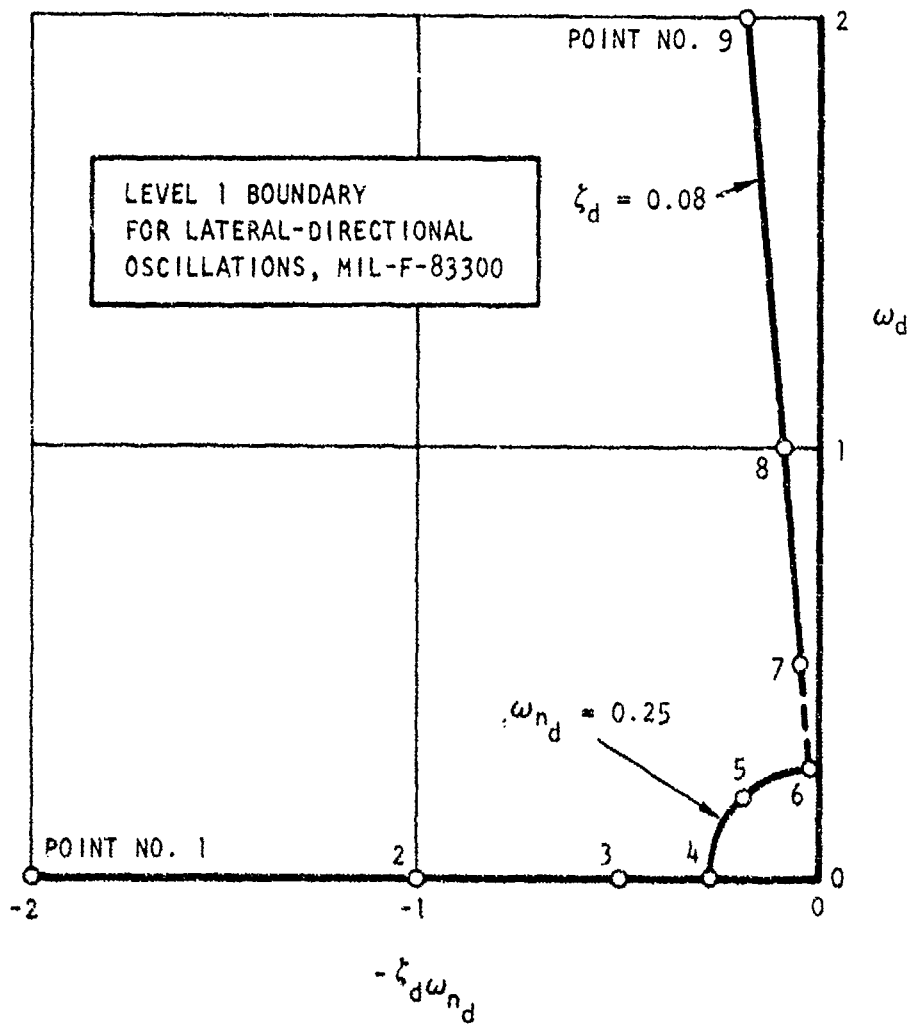
Figure 32. Conditions Used for Side Gust Analyses
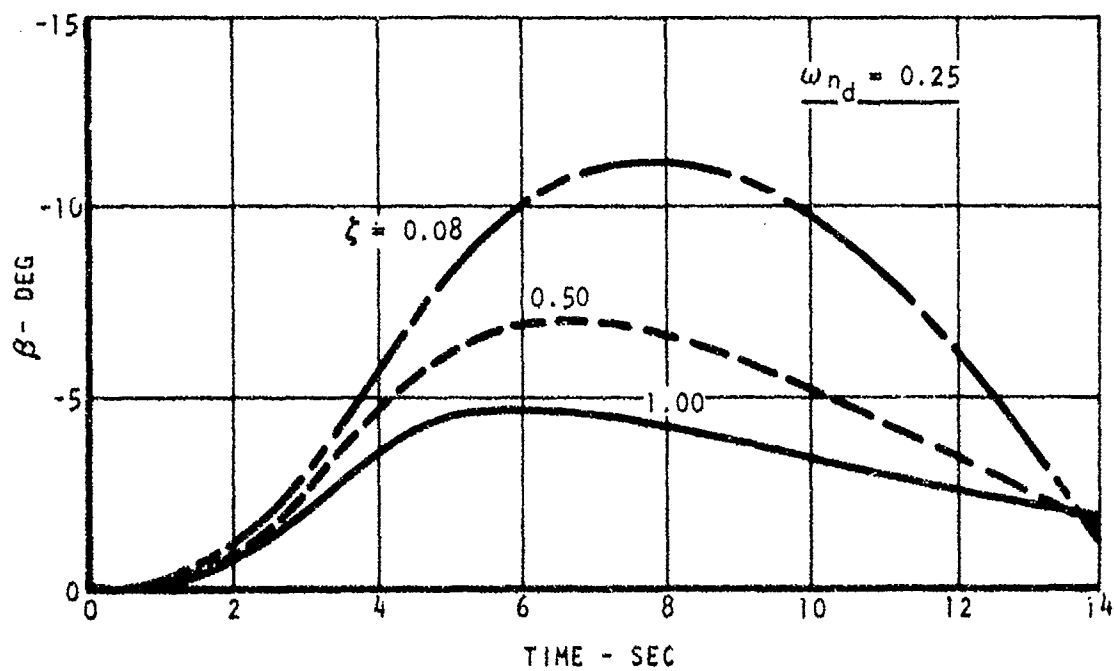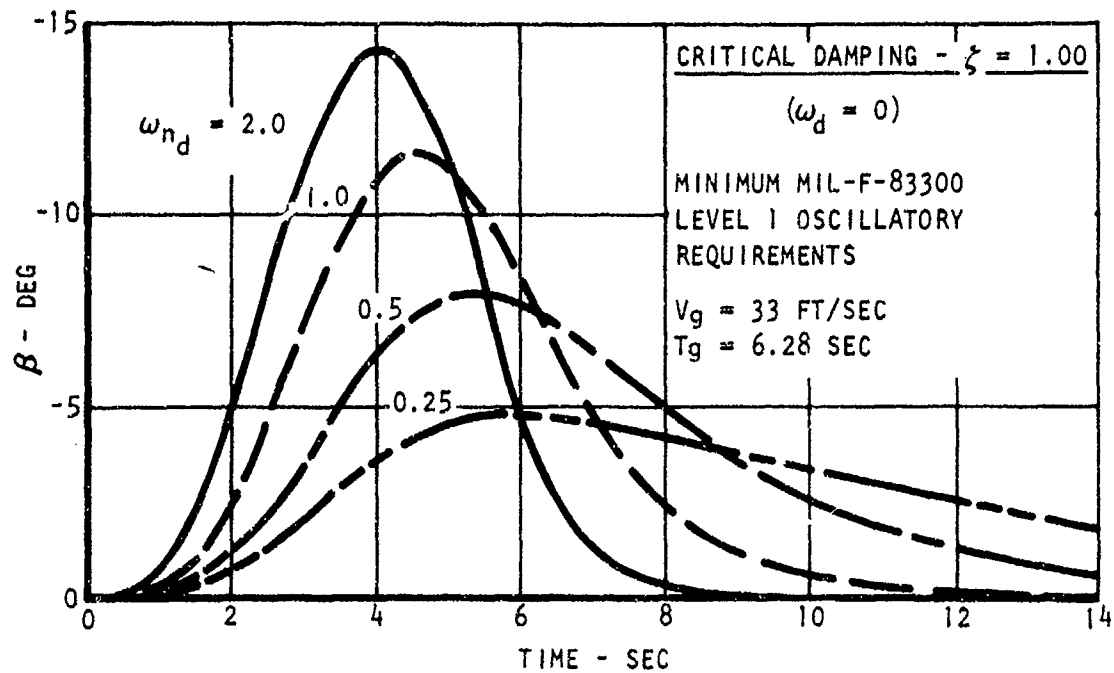
Figure 33. Response to Side Gust at a Damping Ratio of 1.00 or Frequency of 0.25

54
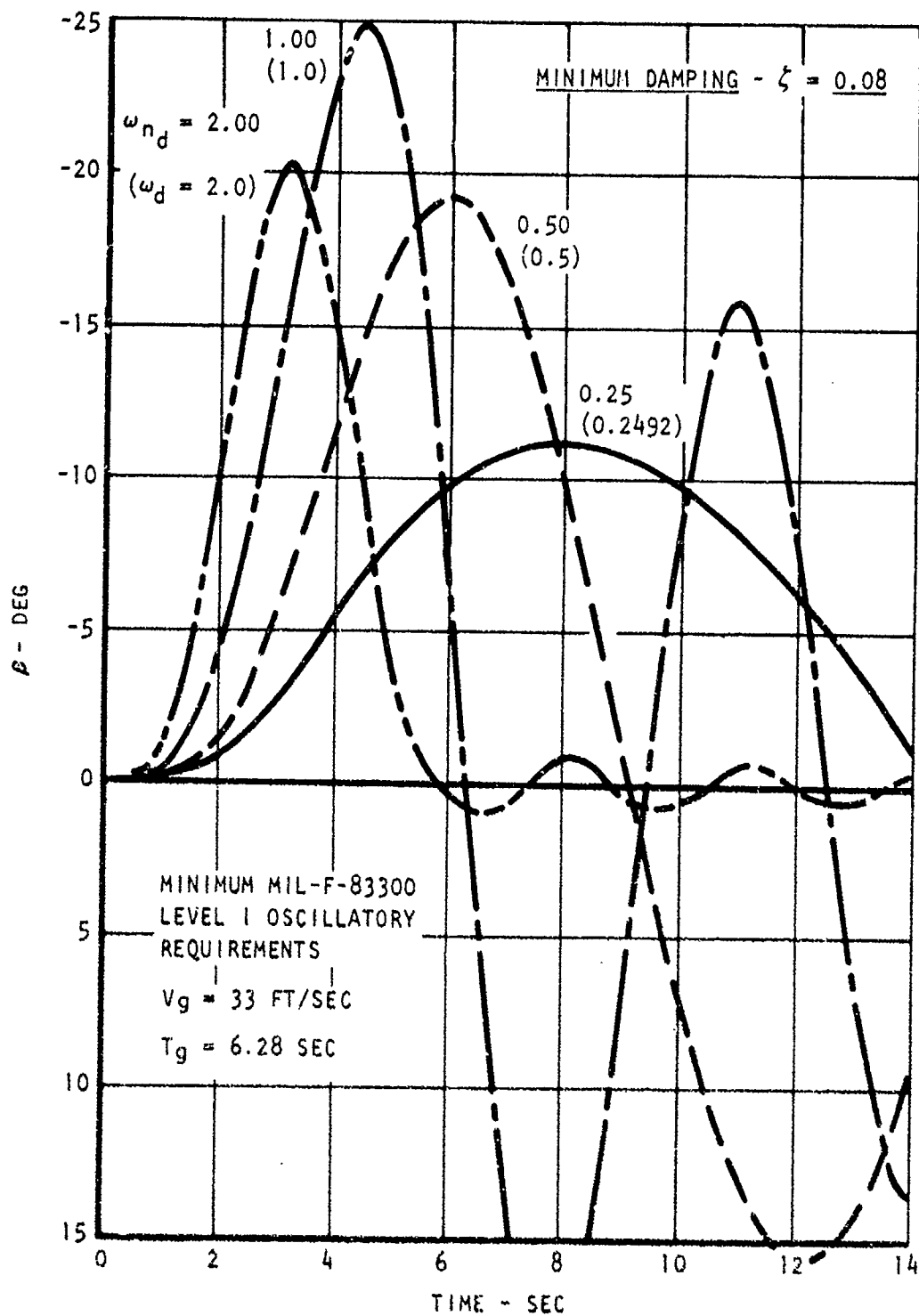
Figure 34. Response to Side Gust at a Damping Ratio of 0.08

55

2.2 RECOMMENDED GROUND RULES

2.2.1 TAKEOFF

In this section takeoff ground rules are proposed based on the previous
sections as well as on some additional considerations described here.
They are proposed for use as a supplement to MIL-C-5011A and MIL-M-7700A
to cover STOL aircraft.

Although most margins described previously pertain to approach and
landing, some pertain to takeoff. These are related to vertical gust and
will be used here. In addition, a margin is added here against pilot
error in the speed to weight relationship. To cover this error a 5
percent speed margin with respect to stall is used so that positive
liftoff is assured at takeoff rotation.

Also, a differentiation is made between normal military or commercial
operation and assault operation. The normal takeoffs are based on
safety with one engine failed, whereas assault takeoffs are performed
without engine failure consideration.

The ground rules recommended here pertain to takeoff and landing
strips with cleared perimeters such that obstacles do not impose addi-
tional restrictions. Emphasis is placed on ground rules for the flight
phase and no safety margins for the ground roll portion are given here.
Also not included are normal acceleration capabilities for evasive man-
euvers such as the avoidance of small arms fire after takeoff during
military operations.

(a) Normal Operation

1. The takeoff shall be made using the accelerate and stop concept.
   The minimum failure speed to be used for the determination of
   the takeoff distance is the speed for which the accelerate and
   stop distance is equal (balanced) to the runway distance needed
   to continue the takeoff to the liftoff point after the critical
   engine fails at the most critical moment. The point of lift-
   off is defined as the condition where the normal liftoff speed
   is reached.

2. The normal liftoff speed shall not be less than 1.05 V_S where V_S is the minimum flyable speed with the critical engine failed in ground effect or out of ground effect, whichever is more critical.

3. At no point along the takeoff flight path may the aircraft have a lower speed than at any previous point along the flight path. This pertains to takeoffs with all engines operating as well as with the critical engine failed.

4. The flight path angle during climbout at a speed equal to the minimum climbout speed, and for conditions out of ground effect and the critical engine failed, shall not be less than a minimum value to be specified by the procuring agency. The minimum climbout speed is obtained when liftoff is made at the normal liftoff speed and the subsequent speed increase is held to a minimum within safety constraints while all but the critical engine perform at the maximum tolerated thrust.

5. At the rotation of the aircraft to the maximum angle of attack after liftoff, an angle of attack margin $\Delta\alpha$ with respect to the stall condition in ground effect with one engine failed shall exist according to $\Delta\alpha_{rad} = 6 \text{ knots}/V_{K_{TAS}}$.

6. At altitudes higher than 100 feet above the ground the minimum angle of attack margin with respect to the stall with one engine failed shall not be less than the value given by $\Delta\alpha_{rad} = 10 \text{ knots}/V_{K_{TAS}}$.

(b) Assault Operation

1. The ground run to the liftoff speed shall be made assuming no engine failure.

2. The liftoff speed shall not be less than 1.05 V_S where V_S is the minimum flyable speed in ground effect with all engines operating.

3. At no point along the takeoff flight path may the aircraft have a lower speed than at any previous point along the flight path.

4. At the rotation of the aircraft to the maximum angle of attack after liftoff, an angle of attack margin $\Delta\alpha$ with respect to the stall condition in ground effect with all engines operating shall exist according to $\Delta\alpha_{rad} = 6$ knots/$V_{K_{TAS}}$.

5. At altitudes higher than 100 feet above the ground, the minimum angle of attack margin $\Delta\alpha$ with respect to the stall with all engines operating shall not be less than the value given by $\Delta\alpha_{rad} = 10$ knots/$V_{K_{TAS}}$.

(c) Comments

A few comments may be made with regard to these ground rules. In the present study, the climb path angle of item 4 for normal operation is taken equal to $\gamma = 3°$. This climb path angle is considered to clear the terrain following the liftoff, and to clear obstacles at a greater distance. If obstacles are present in critical locations, down draft effects have to be considered for altitude margins.

With regard to item 5 for normal operation (or item 4 for assault operation) it should be understood that the quickest gain in altitude is obtained when the maximum tolerable vertical acceleration is achieved at the earliest possible time after liftoff. This will put a maximum of energy into potential energy, and a minimum into kinetic energy as required for maximum obstacle clearances. In order to achieve this, the aircraft is quickly rotated to the angle of attack with the specified margin, or to the angle at which a negative aircraft acceleration along the flight path is just prevented (item 5), whichever is reached first. Thereafter the angle of attack is bled off to satisfy item 3 while the flight path angle increases with time.

2.2.2 APPROACH AND LANDING

Almost all safety margins derived in previous sections for engine failure conditions and gust are applicable for the approach or landing phase. The required margins are summarized in the following table.

Critical Case	Ground Effect	Eng. Fail. Cond.	Type of Margin	Margin At Speed(KEAS)		
				75	85	95
Turning Maneuver(R=1000 ft)	OGE	CEF	$\Delta n =$	0.09	0.185	0.30
Rear Gust ($\Delta V = -20$ KTAS)	OGE	CEF	$V/V_s =$	1.40	1.30	1.27
Upward Gust ($\tan\Delta\alpha = V/10$KTAS)	OGE	CEF	$\Delta\alpha =$	8.0°	6.7°	6.0°
Sidestep Maneuver	OGE	CEF	$\Delta n =$	0.04	0.04	0.04
Engine Failure at 50 feet	OGE		$\Delta n =$	0.13	0.12	
Arrest of Sink Rate for TD	IGE	CEF	$\Delta n =$	0.05	0.05	
T.D. at V_{mtd}	IGE	CEF	$\Delta n =$	0	0	
Engine Failure at 50 feet	IGE	CEF	$\Delta n =$	0.13	0.12	
Waveoff Altitude (35 feet)	IGE	CEF	$\Delta n =$	0.05	0.05	
Waveoff Distance (1500 feet)	IGE	CEF	$\Delta n =$	0.05	0.06	

In addition, it must be possible to accelerate the airplane during the waveoff maneuver from the approach speed to the climbout speed.

The margins out of ground effect are of various different types ($\Delta n, \Delta\alpha , \Delta V$). Figure 35 is included in this report showing a comparison of the effect of the various types of margins on the useable lift of the aircraft.

It is seen that the speed margin is most restrictive, and the angle of attack margin of 8° is about as severe as a maneuver margin of $\Delta n = .2$ to .15 but both are not even half as restrictive as the speed margin. However, comparison of this lowest useable lift with the lowest useable lift in ground effect in Figure 36 shows compatible values.

Based on the above, and with cognizance that different relations exist between $\Delta n, \Delta\alpha ,$ and ΔV for different lift/propulsion systems than the externally blown flap concept analyzed in the present report, the recommended ground rules for approach and landing are as follows.

T_{PE} = THRUST OF ONE ENGINE AT EXHAUST NOZZLE
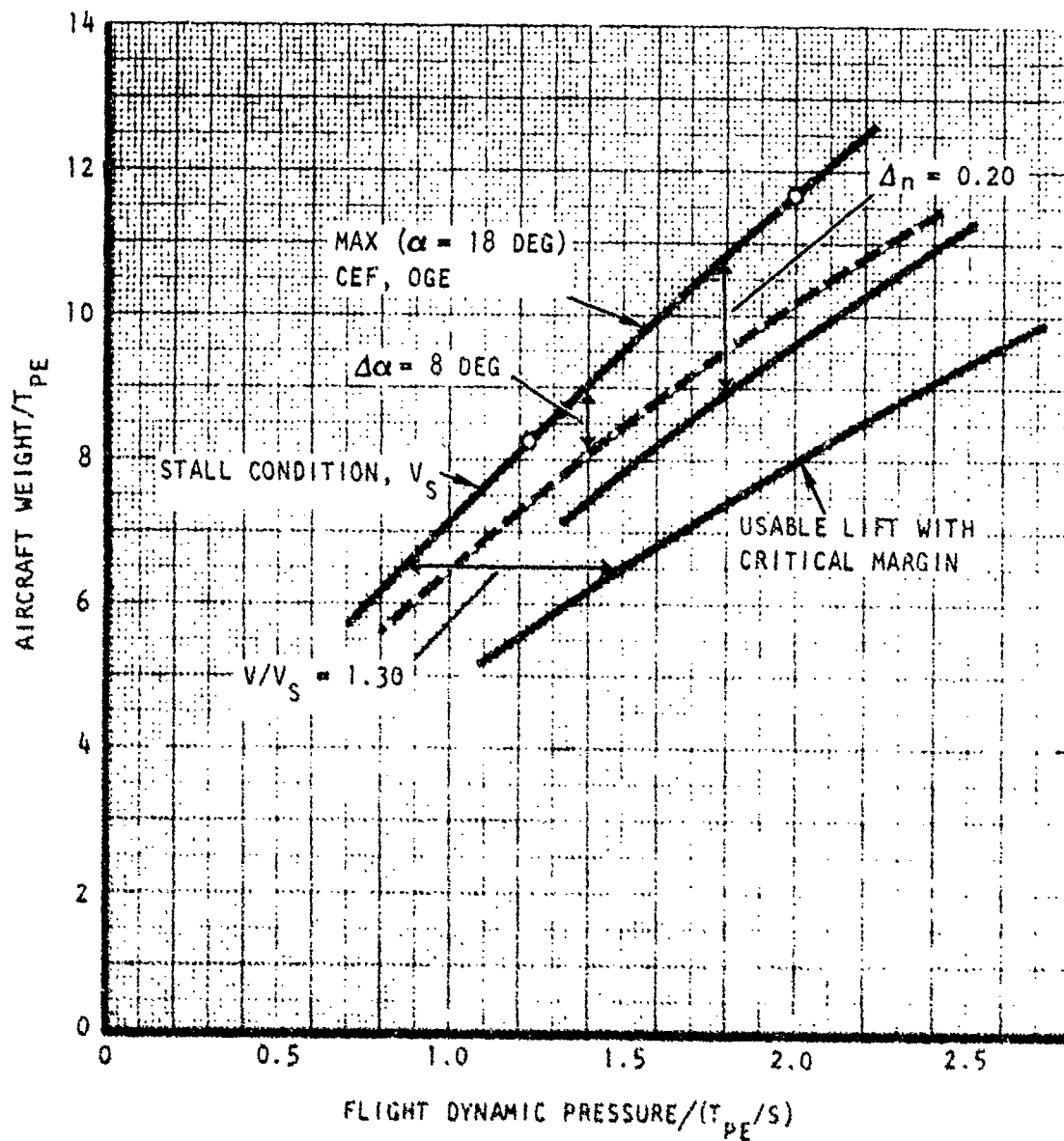
FLAP ANGLE 70 DEG

Figure 35. Comparison of Safety Margins in Approach Out of Ground Effect

60

T_{PE} = THRUST OF ONE ENGINE
AT EXHAUST NOZZLE

FLAP ANGLE 70 DEG
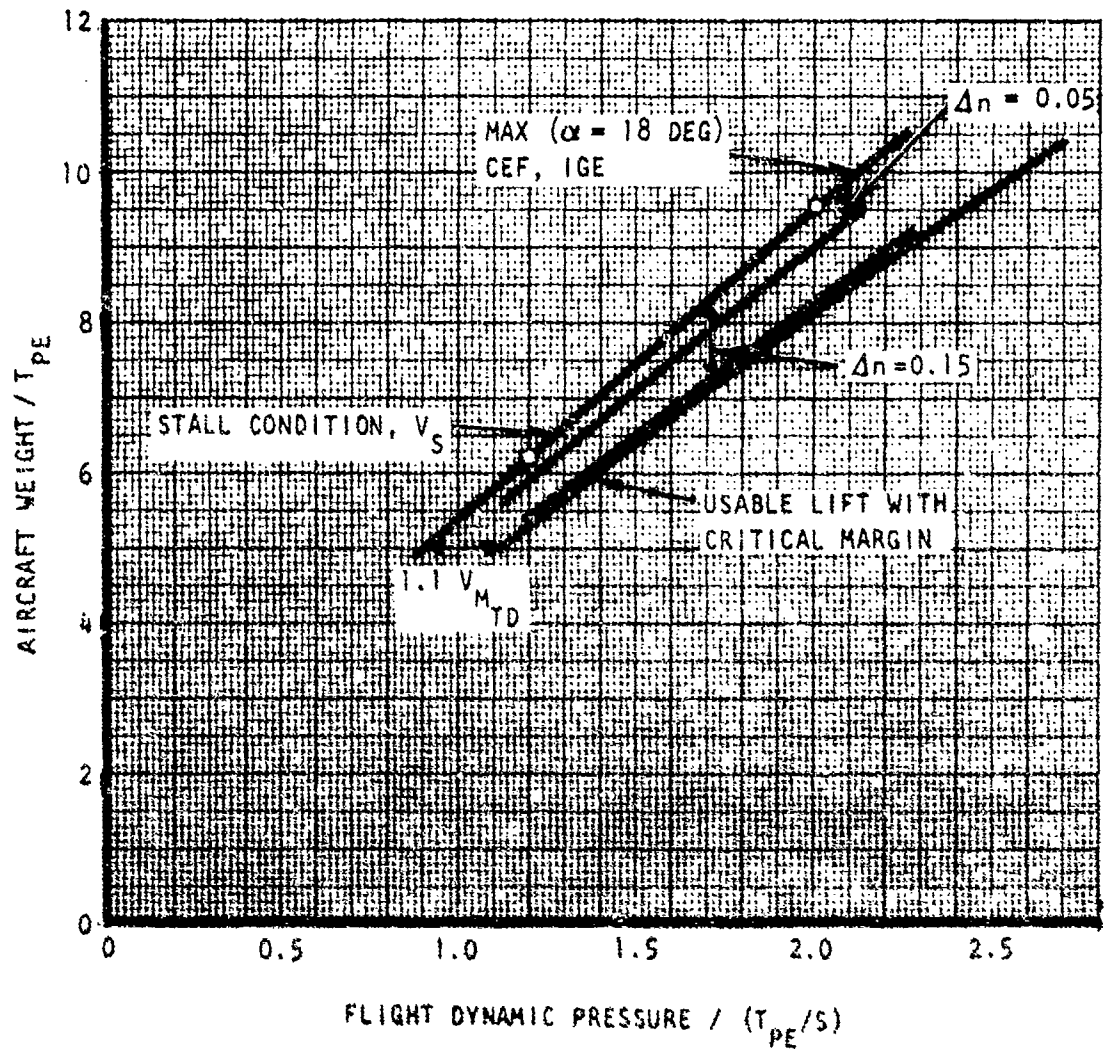
Figure 36. Comparison of Safety Margins in Approach In Ground Effect

61

(a) Normal Operation

1. Landing distances for landings without obstacles are to be determined on the basis of a flight path height of 50 feet above the threshold. The rate of sink above the threshold will be specified by the procuring agency.

2. The final turning maneuver in the approach shall be made with a minimum speed margin of 20 knots true airspeed with respect to the stall speed with the critical engine failed and out of ground effect.

3. The normal acceleration margin during approach out of ground effect and with the critical engine inoperative shall not be less than $\Delta n = .15$ or the acceleration required to perform a turn with a radius of 1,000 feet, whichever is critical.

4. The angle of attack margin during approach at altitudes greater than 100 feet above the runway and with the critical engine failed shall be **equal** to or greater than a value given by $\Delta\alpha_{rad} = 10/V_{K_{TAS}}$.

5. The normal acceleration capability in ground effect, with the critical engine inoperative, and at the normal touch down speed with $V \geq 1.1 V_{mtd}$ shall be at least $\Delta n = 0.15$

6. The normal acceleration capability in ground effect, with the critical engine failed, and at a speed 10 percent less than the normal touch down speed, shall be at least $\Delta n = 0$. The minimum speed in the condition where $\Delta n = 0$ is defined as V_{mtd}.

7. It shall be possible to perform a waveoff from an altitude of 100 feet above the runway with the critical engine failed. During the waveoff the angle of attack margin out of ground effect at 100 feet above the runway shall be at least a value given by $\Delta\alpha_{rad} = 10 \text{ kts}/V_{K_{TAS}}$ and in maximum ground effect at least a value according to $\Delta\alpha_{rad} = 6 \text{ kts}/V_{K_{TAS}}$. The waveoff shall be considered completed above the end of the runway, and the aircraft speed at that point shall be at least equal to the minimum climbout speed defined for takeoff. To achieve this, flap angle reduction is permitted.

(b) Assault Operation

In this report, no separate ground rules for approach and landing in assault operation are given.

(c) Comments

Comments with regard to the approach and landing ground rules are offered here with regard to the normal operation as well as assault operation. Similar to the takeoff ground rules, also here no obstacle is assumed to exist. If an obstacle does exist, it probably should be cleared by the flight path by a nominal margin of 35 feet to account for down drafts and engine failure.

The rate of sink assumed to exist above the threshold is taken in this report equal to 10 feet/second. This yields a flight path angle above the threshold of approximately $\gamma = -4°$. At the position of the approach prior to the threshold the descent angle may be greater.

Also the flight velocity above the threshold may be lower than during the last turn in the approach pattern (item 2), depending on the deceleration capability of the aircraft and the length of the straight portion of the flight path just prior to touch down.

With regard to item 5, the normal acceleration assumed here for control of the sink rate during touch down after engine failure is $\Delta n = 0.15$. However, the adequacy of this value depends on the amount of ground effect and the quickness of control application in lift (DLC) and it may be necessary to specify a minimum response time in lift together with this normal acceleration. Research is needed to define the normal acceleration margin to a better degree.

Assault ground rules for approach and landing are not developed in the present report because some very important operational considerations must be taken into account that are of military nature rather than the domain of aerodynamic flight safety, and therefore go beyond the scope of the present analysis. For example, operational considerations should include the consequences to the military operation around the landing strip when an engine fails on approach and the aircraft crash lands

somewhere near the middle of the landing strip, making all further flight operation impossible. This problem does not exist during takeoff. If an engine fails during an assault takeoff the landing strip will probably be left clear except for the very end of it, or the airplane will come to rest on a clear way. Also, considered should be assault flight training aspects. Assault type landings without critical engine-out safety can only be trained with a high risk to the aircraft and the crew. Assault takeoffs, however, can be trained with a small risk at very low altitude as long as the runway used for training is large enough, or may be simulated at high altitudes.

It should be noted that removal of the engine failure safety improves the takeoff performance considerably, however the improvement in the landing performance may not be compatible. Possibly a better way to improve the landing performance in the assault mission is to decrease the height above the threshold rather than the removal of the engine-out safety. Along with it could go a lesser flare, and thrust reversal on four engines rather than two, while taking the risk of overshoot into the clearway.

In addi   to make full use of a minimum landing distance capability with all engines operating, the fuselage upsweep needs to be increased for ground angle clearance. This penalizes the aircraft weight and cruise performance.

Section III

PERFORMANCE METHODS

In this section, the critical safety margins of the previous section are used, and methods for the determination of the field length derived. In addition, other criteria are also considered to facilitate direct comparison with other aircraft studies.

3.1 STOL PERFORMANCE

3.1.1 LIFTOFF SPEED

(a) A Nomogram for Liftoff Speed

In general, takeoff speeds can be determined rapidly from nomograms. An example of such a nomogram is presented in Figure 37. This particular nomogram pertains to optimum aerodynamic data for aircraft employing the externally blown flap lift/propulsion concept.

The nomogram makes use of the thrust to weight ratio, T/W, and the ratio of thrust to wing area, T/S, as independent variables. The latter ratio is obtained from

$$\frac{T}{S} = \frac{T}{W} \cdot \frac{W}{S}$$

Herein, both factors on the right hand side are basic design parameters entering into sizing exercises during preliminary design stages.

(b) Ground Rules Used

The above nomogram is based on various performance constraints and assumptions. Constraints considered pertain to the following safety margins:

$V_{LO} \geq 1.05\ V_{mc}$ (CEF, IGE)

$V_{co} \geq 1.10\ V_{mc}$ (CEF, OGE)

at V_{LO}: $n \geq 1.1$ (CEF, IGE)

at V_{co}: $n \geq 1.3$ (AEO, OGE)

65
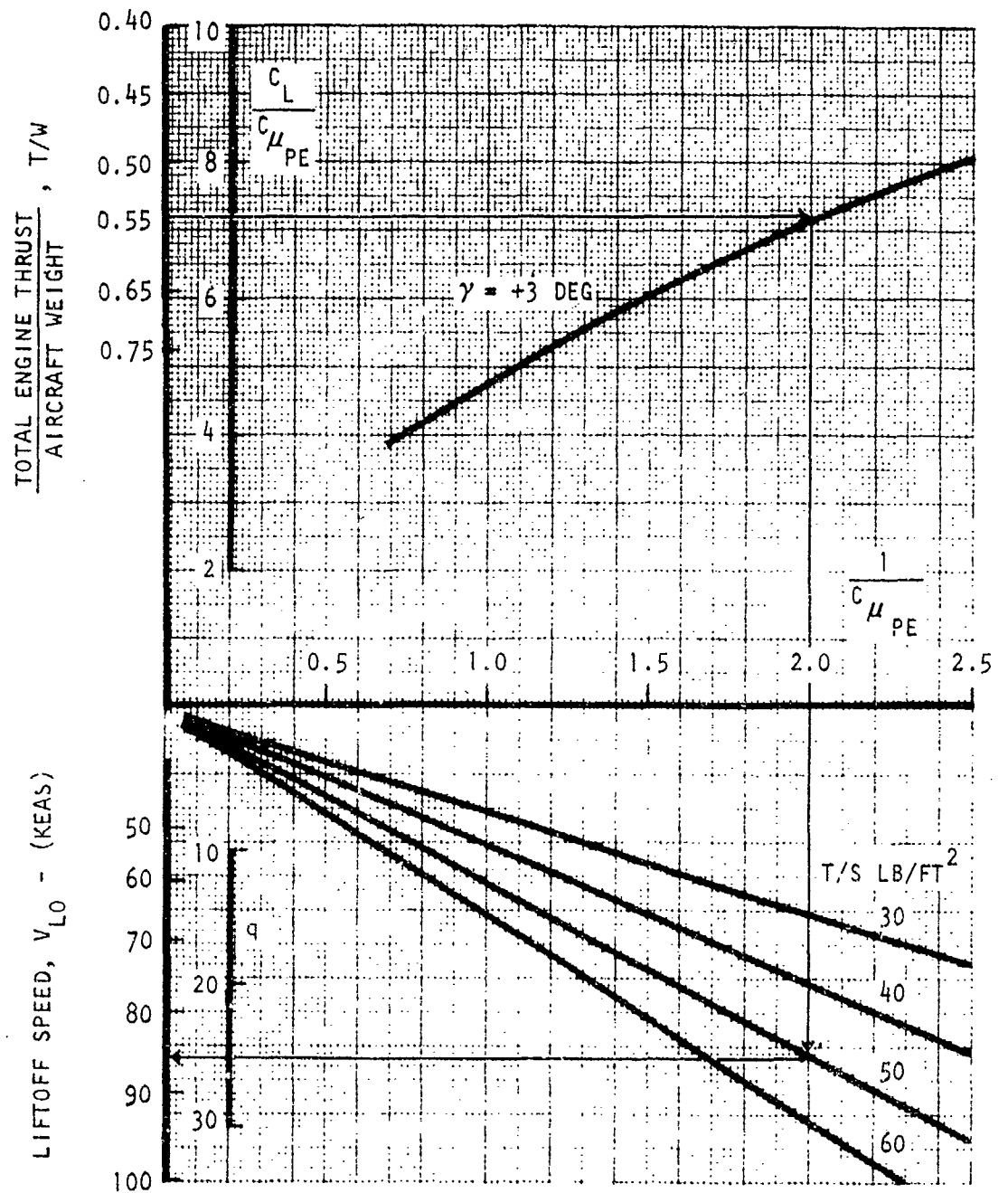
Figure 37. Nomogram For Liftoff Speed

66

Herein, V_{mc} is the minimum flyable speed or stall speed of the air-
craft. Assumptions are that a minimum control speed existing during the
ground roll portion of the takeoff is not critical for the determination
of the liftoff speed, and that the climbout speed is a given percentage
greater than the liftoff speed. The actual percentage value is not
determined in this report since it depends on aircraft dynamic characteris-
tics and pilot technique. Especially, the latter must still be established.
Another assumption used is that the aircraft is required to climb at
a three-degree angle at the climbout speed with the critical engine inopera-
tive.

(c) Aerodynamic Limitations

In order to illustrate how the various constraints and assumptions
enter into the construction of the nomogram the derivation of it will be
described hereafter in detail.

The basic aerodynamic data for maximum lift used in the nomogram are
presented in Figure 38. These are untrimmed data with all engines
operating as obtained from wind tunnel data. The maximum is defined to
exist at an angle of attack where the rolling moment is not becoming too
large in case of an engine failure. In the present document an angle of
18 degrees is used as the limitation. This angle is essentially the same
as the stall angle of attack in the power-off condition.

After trimming the aircraft in pitch these data yield the maximum
useable lift with all engines operating. This maximum lift is indicated
by the uppermost lines in Figures 39 and 40. The two figures show
similar data but for different blowing coefficients, $C_{\mu_{PE}}$.

The above data pertain to conditions out of ground effect. Only one
type of safety margin (i.e., $n = 1.3$, AEO) is based on such a condition,
but all other takeoff safety margins are based on conditions with ground
effect as well as with a critical engine failed (CEF). The ground effect
is estimated in two steps, the first step being an estimate of the change
of the stall angle of attack, and the seco | step being an estimate of
the change of lift at that new stall angle of attack. The maximum angle

67
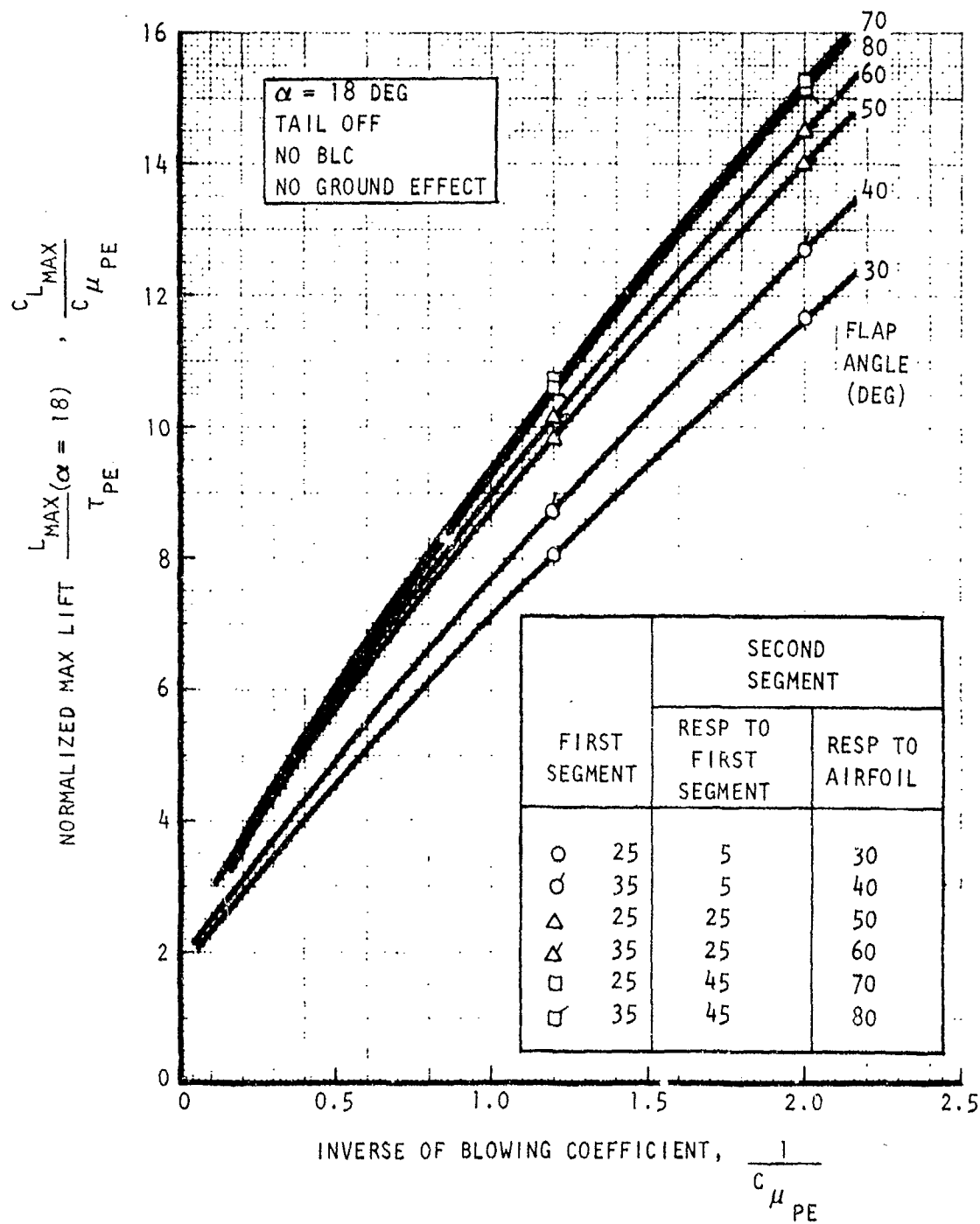
Figure 38. Maximum Untrimmed Lift for Double-Slotted Flaps and All Engines Operating

68

NO BLC - DOUBLE-SLOTTED FLAPS

$$C_{\mu_{PE}} = 0.825$$

TRIMMED CONDITIONS (25% MAC).
NO SPOILER DEFLECTIONS FOR DLC
FIRST FLAP SEGMENT 25 DEG
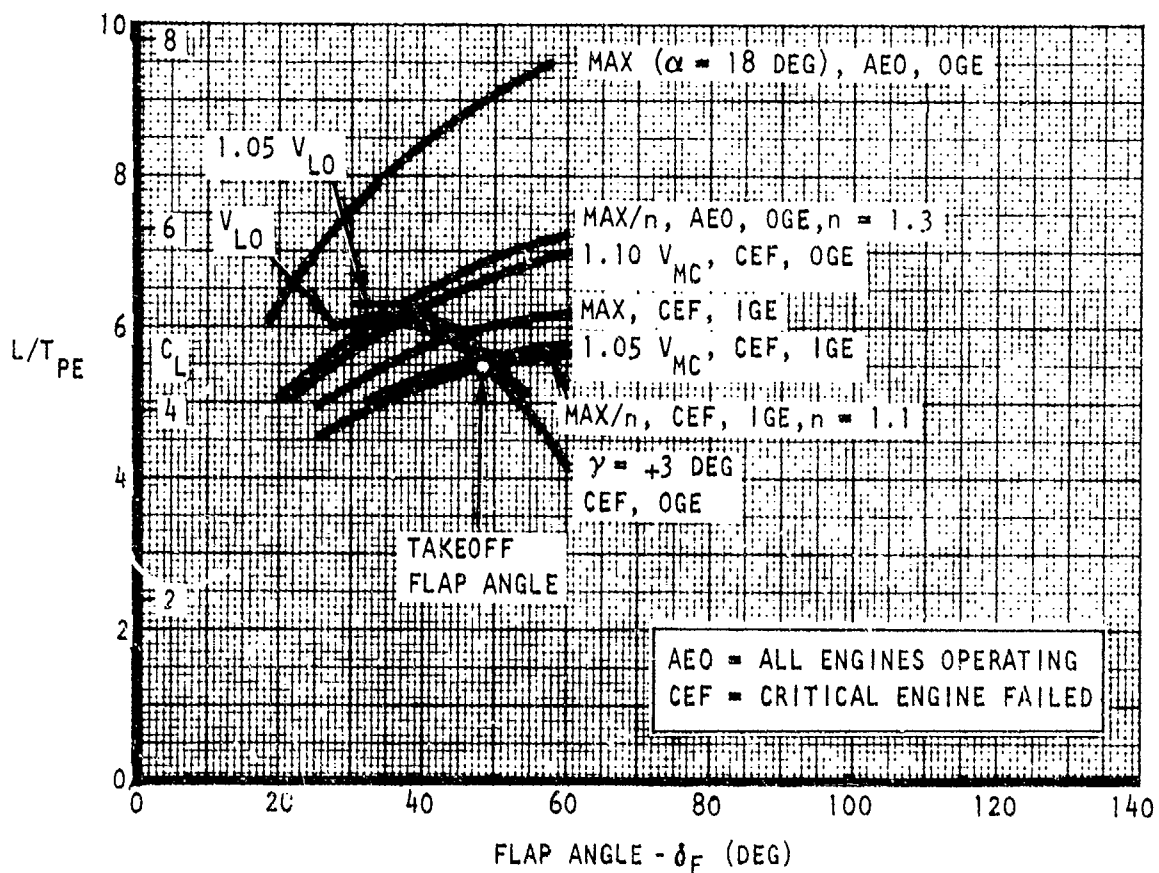
Figure 39.   Determination of Takeoff Flap Angle, $C_{\mu_{PE}} = 0.825$

NO BLC - DOUBLE-SLOTTED FLAPS

$$C_{\mu_{PE}} = 0.5$$

MAX (α = 18 DEG) AEO, OGE

MAX/n, AEO, OGE, n = 1.3

1.10 V_{MC}, CEF, OGE

MAX, CEF, IGE

1.05 V_{MC}, CEF, IGE

MAX/n, CEF, IGE, n = 1.1

γ = 3 DEG, CEF, OGE

V_{CO} = 1.05 V_{LO}

V_{CO} = V_{LO}

TAKEOFF
FLAP ANGLE

L/T_{PE}

C_L

TRIMMED CONDITIONS (0.25% MAC)
NO SPOILER DEFLECTION FOR DLC
FIRST FLAP SEGMENT 25 DEG

FLAP ANGLE, δ_F - DEG

Figure 40. Determination of Takeoff Flap Angle, $C_{\mu_{PE}}$ = 0.500

70

of attack in ground effect used in the present document is presented in Figure 41. It reflects a significant decrease in the angle. The effect is computed from equations existing for conventional aerodynamics because no reliable test data are published for this decrease at this time. The lift change used for the second step is presented in Figure 42 and extracted from test data published in Reference (11).

Decreasing the lift due to engine failure, trimming in yaw, roll, and pitch, and applying the ground effect results in the maximum lift shown in the previous Figures 39 and 40 (labeled MAX, CEF, IGE).

The various safety margins are now applied to the maximum lift data as shown in these figures as a function of flap angle. Speed margins are easily applied as illustrated in Figure 43.

It is seen that the lifting capability with the margins increases with flap angle. However the drag level of the flaps also increases. The maximum angle that can be used for takeoff is determined by climb considerations. In the present study, a 3-degree climb path requirement with one engine failed is used to limit the flap angle. The maximum flap angle at which this requirement is met is also indicated in the figures. An example of how the lift is determined at which this climb angle can be maintained at a given blowing coefficient and a given flap angle is shown in Figure 44. This figure shows the relation between the lift and drag characteristics when the angle of attack varies. The i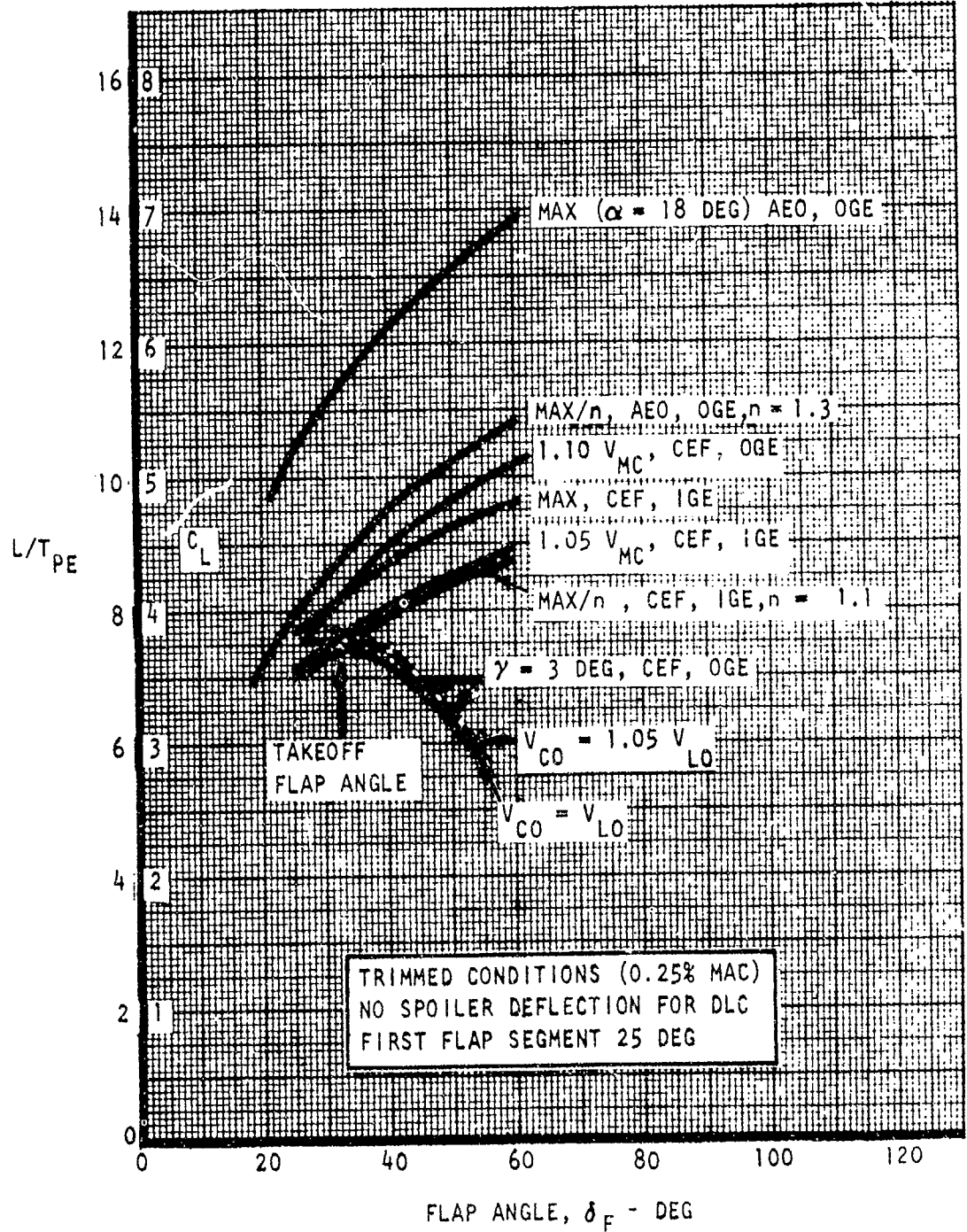ntersection of such a relation (lowest line for the critical engine inoperative) with the condition $C_D = -C_L \tan\delta$ yields the lift that meets the minimum climb limit.

The optimum flap angles to be used are those that meet the critical safety margins as well as the climb requirements. These are indicated in the above Figures 39 and 40 and labeled there as "Takeoff Flap Angle."

It should be noted that the climb curves shown pertain strictly to the blowing coefficients indicated in these figures. However, when the aircraft happens to liftoff at a blowing coefficient indicated, the speed will have increased by the time the climbout equilibrium has been obtained. At this increased speed a higher climb angle capability exists. Thus, in order not to exceed unnecessarily the required climb angle during the climbout, a somewhat higher flap angle may be used already at liftoff in anticipation of this speed increase. Assuming that the percentage speed increase is known, for example 5 percent, the higher flap angle can be determined as follows.
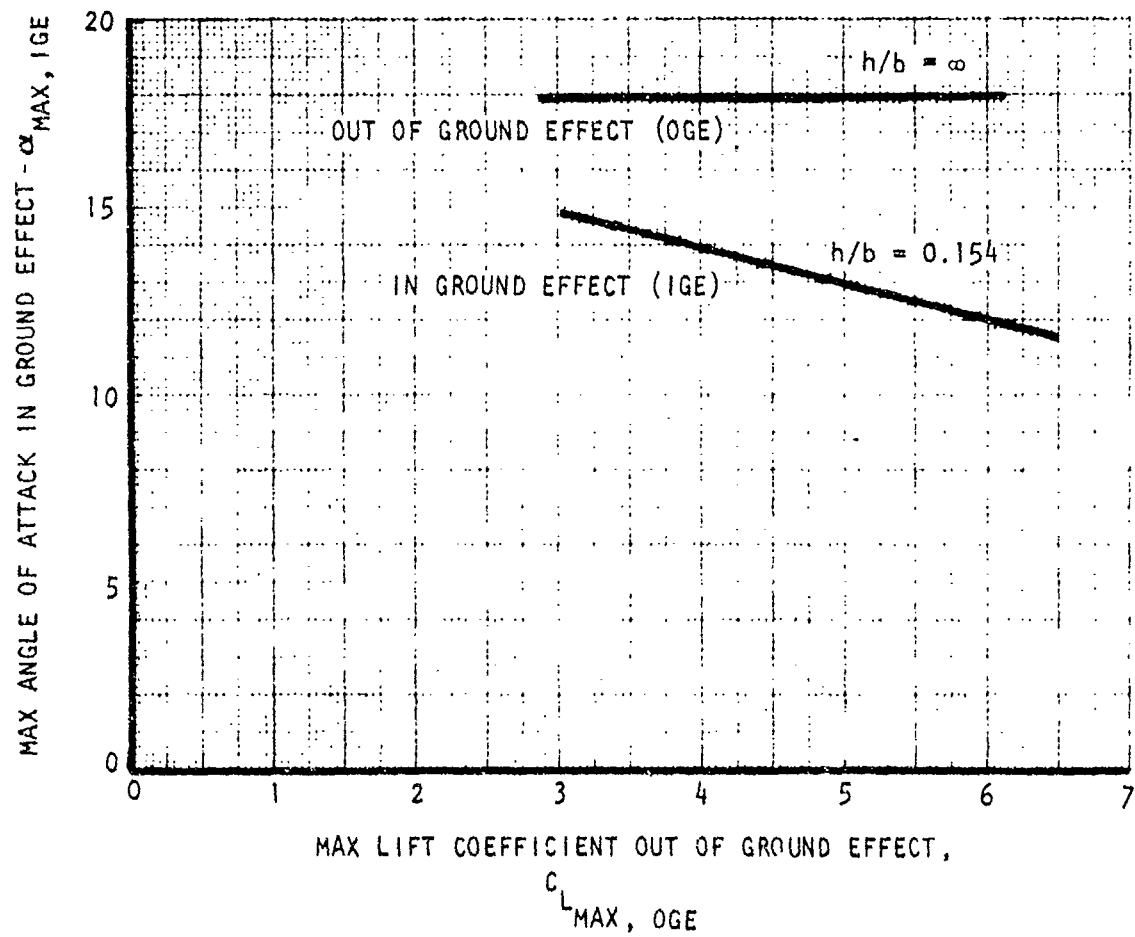
71

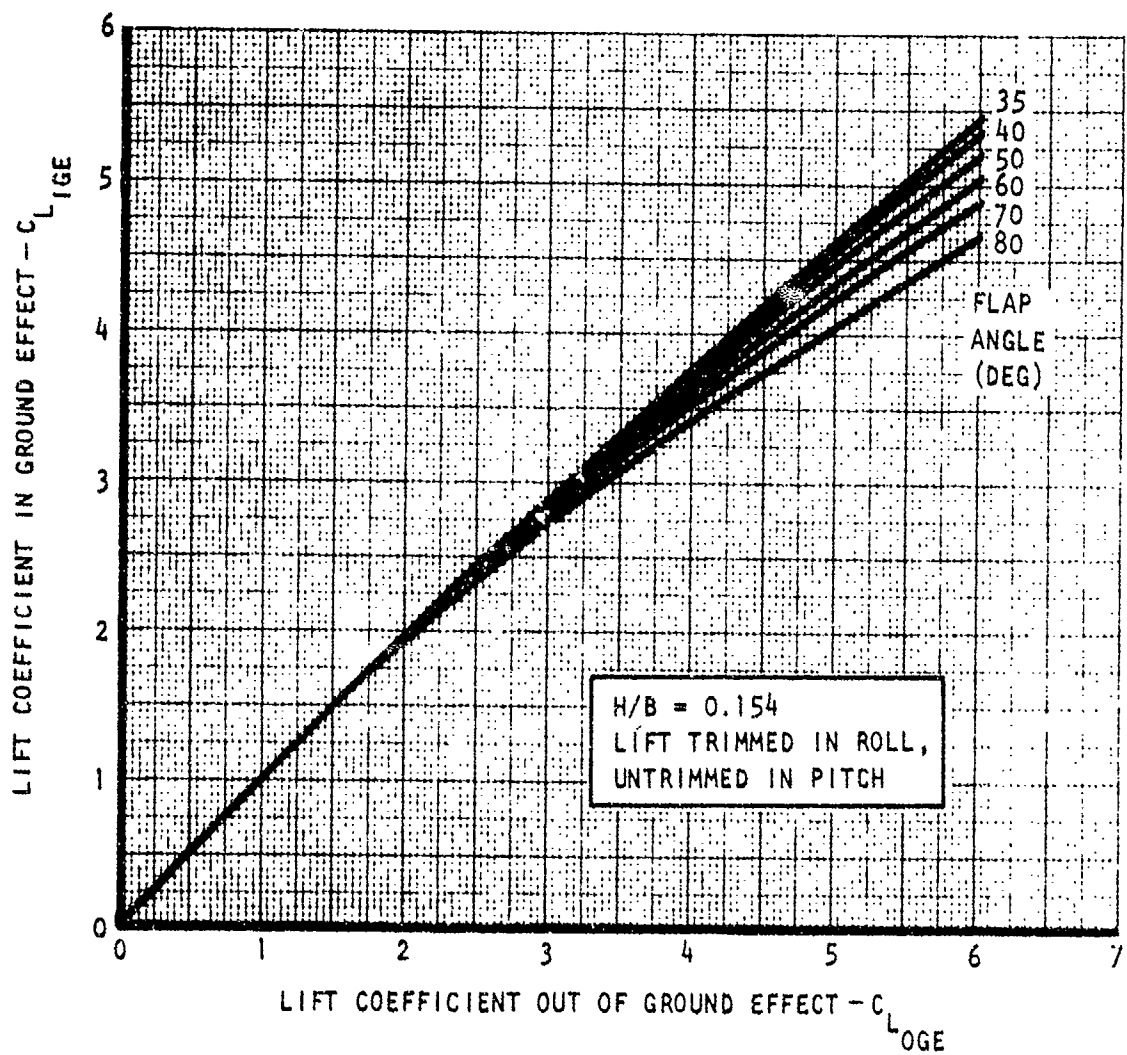Figure 41. Effect of Ground Proximity On Stall Angle of Attack

72

Figure 42. Effect of Ground Proximity on Lift

CEF
OGE
δ_F = 50 DEG
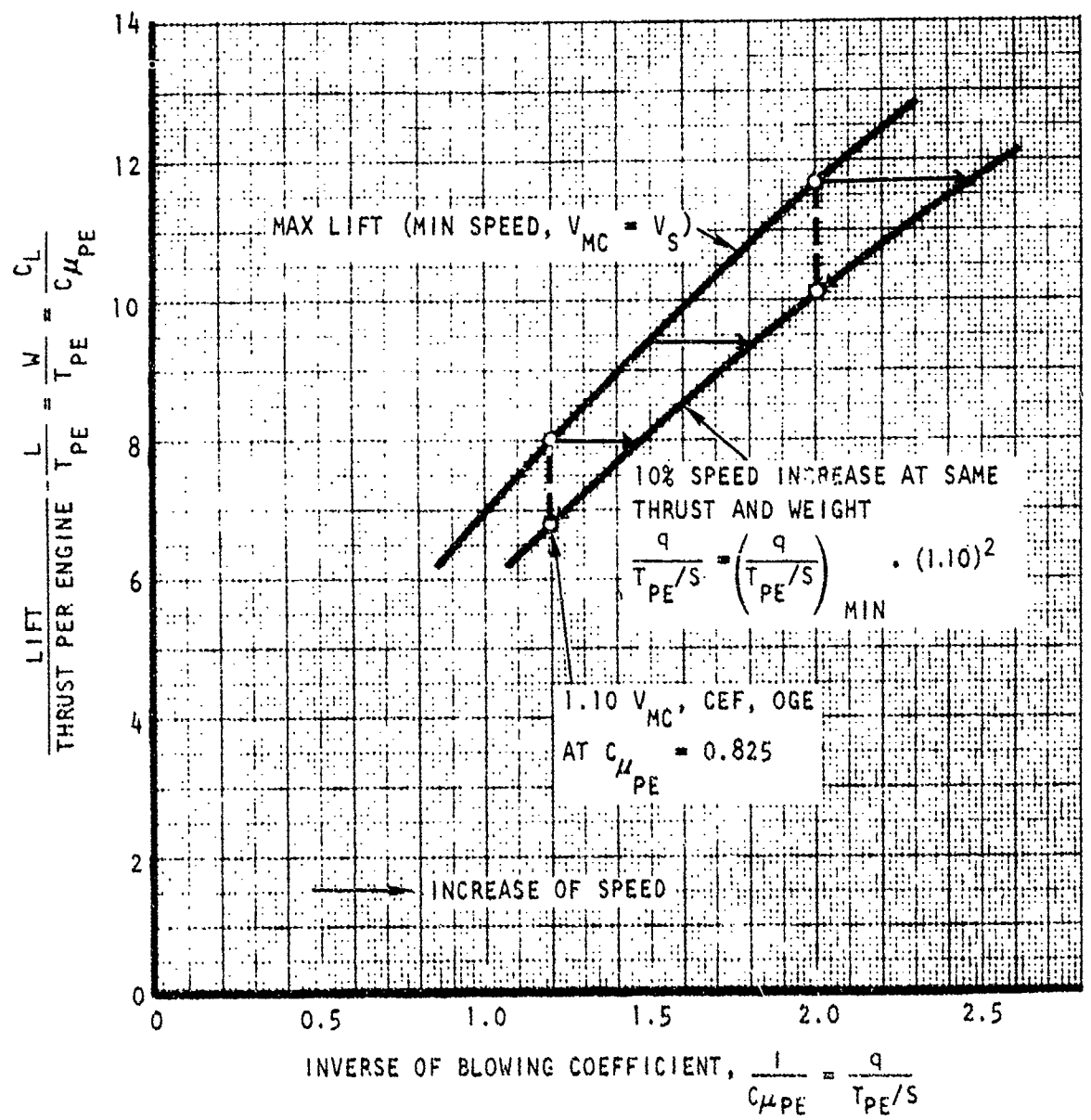
Figure 43. Determination of Lift for a Given Speed Margin

74
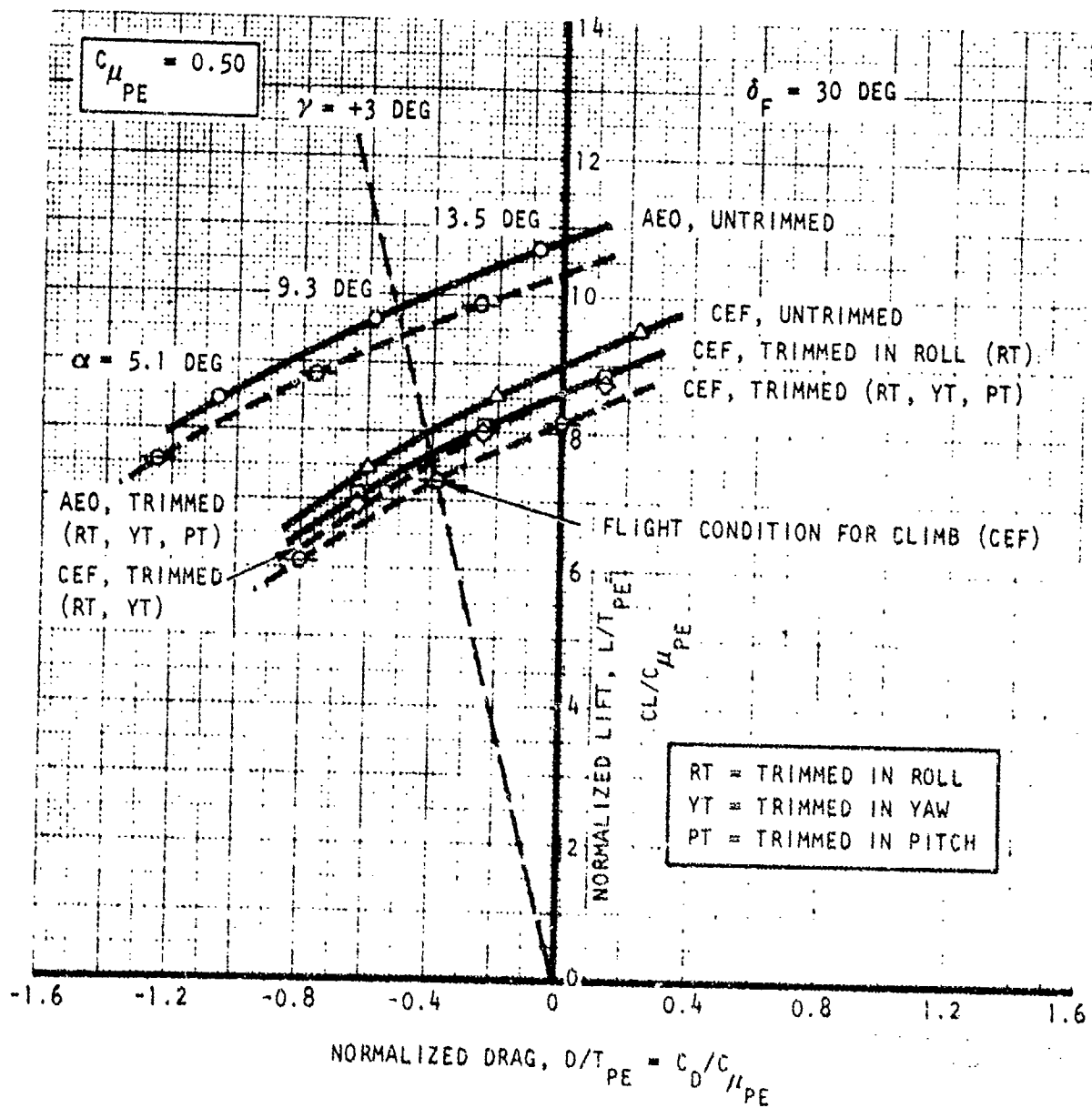
Figure 44. Drag Polar for Full-Span Double-Slotted Flaps

75

Figure 45 shows a repeat of the curves at which a climb angle of 3 degrees can be attained, each for a given blowing coefficient. With the two blowing coefficients indicated, new curves can be interpolated where the speed is a **percentage** larger. The blowing coefficient for the higher speeds are computed from

$$\left(\frac{1}{C_{\mu PE}}\right)_{CO} = \frac{q_{CO}}{T_{PE}/S} = \frac{q_{LO}}{T_{PE}/S}\left(\frac{V_{CO}}{V_{LO}}\right)^2 = \left(\frac{1}{C_{\mu PE}}\right)_{LO}(1.05)^2$$

Curves for these blowing coefficients are indicated as dashed lines. They are then transcribed into Figures 39 and 40, where new intersections with the safety margins can be found. These intersections then yield the corrected flap angles where this limitation is met. Since the increase in speed percentage is a variable depending on pilot technique, the lift off condition intersections were selected for analysis in the present study.

In any event, it is seen that at each blowing coefficient a C_L value or a value of $C_L/C_{\mu PE}$ can be obtained that represents the optimum lifting capability consistent with the ground rules and the aerodynamic characteristics of the aircraft. This C_L or $(C_L/C_{\mu PE})$ value can be plotted versus $C_{\mu PE}$ (or $1/C_{\mu PE}$), and the latter relation is chosen in Figure 46. This relation is preferred in this report because of the direct dependence on the T/W ratio which is of immediate importance in preliminary design

$$\frac{C_L}{C_{\mu PE}} = \frac{L/qS}{T_{PE}/qS} = \frac{L}{T/4} = \frac{4}{T/W}$$

This relation enters directly in the upper portion of the nomogram in Figure 37. The lower portion is only a multiplication of $1/C_{\mu PE}$ or $q/(T_{PE}/S)$ by $(1/4)(T/S)$ to obtain q. If the aerodynamic characteristics change, or if other safety or performance ground rules are used, such as climb angle, only this upper portion of the nomogram will be affected quantitatively. The type of the nomogram will be unchanged for different aerodynamic characteristics or even lift/propulsion concepts as long as C_L (or $C_L/C_{\mu PE}$) can be expressed in terms of $C_{\mu PE}$ (or $1/C_{\mu PE}$).
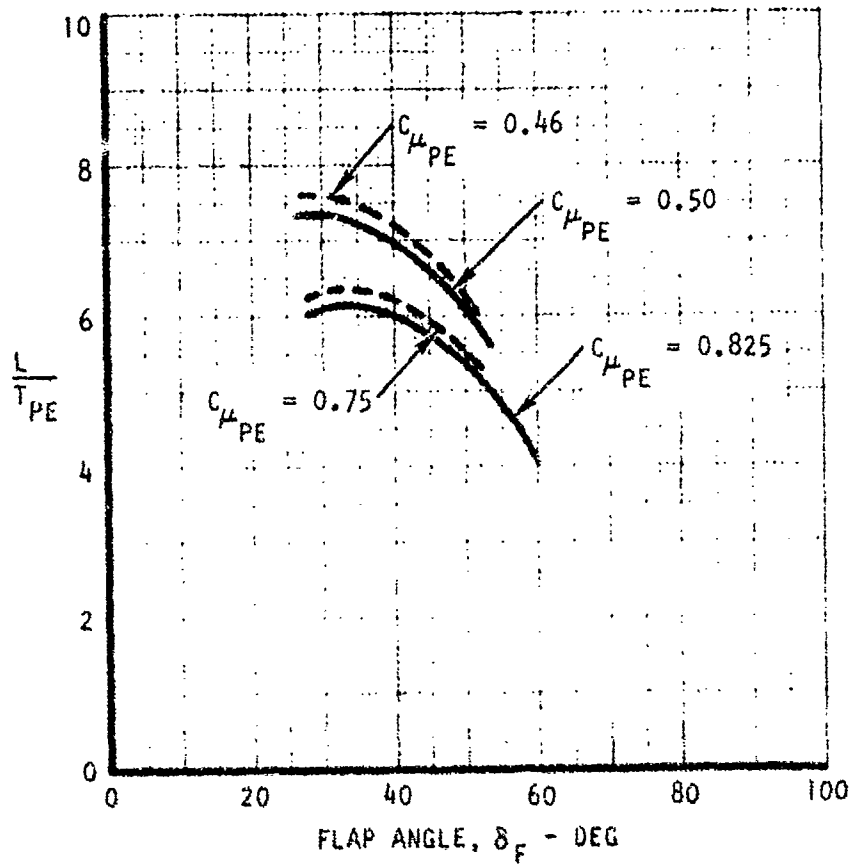
Figure 45. Effect of Speed Increase on Lift at a Constant Climb Angle = 3°

77
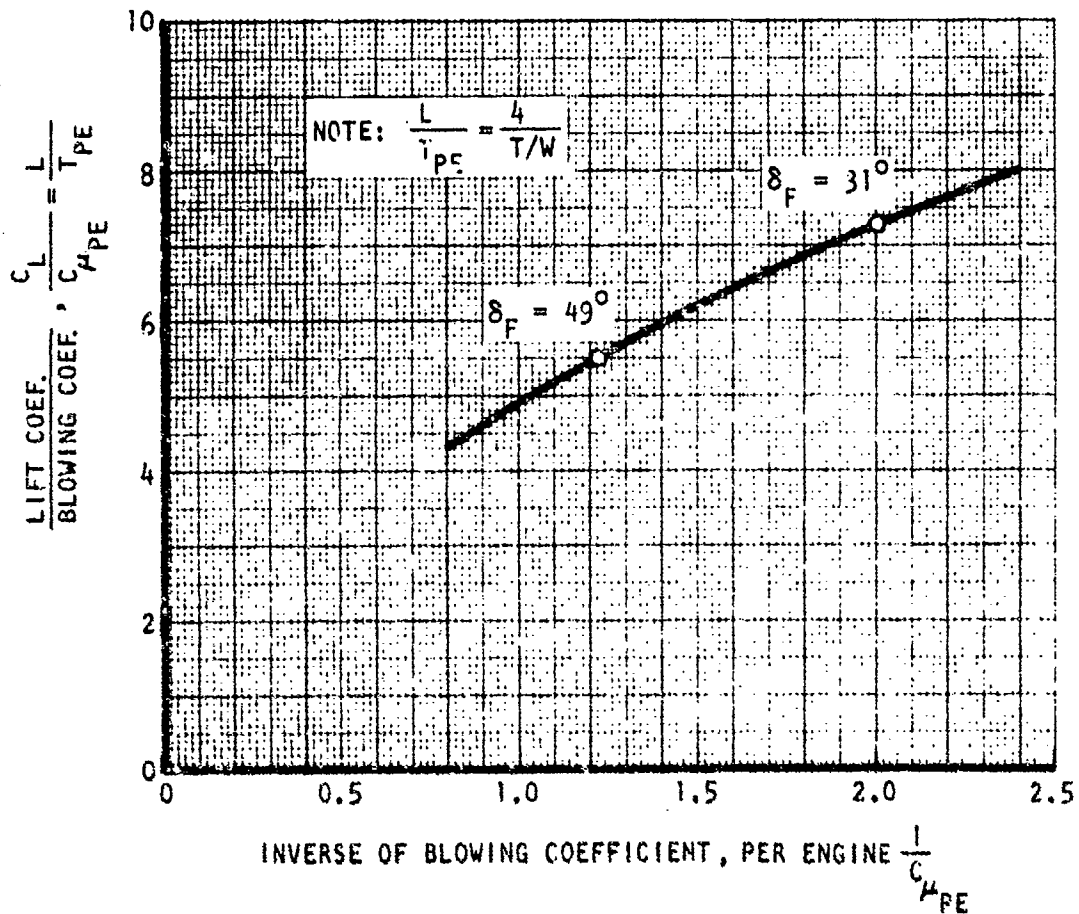
Figure 46. Takeoff Lift Versus Inverse of Blowing Coefficient
Critical Engine Failed $\gamma = + 3^{\circ}$

To facilitate changing the nomogram for different climb require-
ments, or for aerodynamic data, and for different lift/propulsion concepts
the axis system of the upper portion of the nomogram is made identical to
that of Figure 46.

3.2.1 TAKEOFF DISTANCE

(a) Nomograms and Graphs

Perhaps the most useful type of graph for the determination of balanced
takeoff distances during preliminary design stages is presented in
Figures 47a and 47b. The graph shows the distance as a function of the
thrust to weight ratio T/W, the wing loading W/S, as well as the atmos-
pheric density ratios as the main variables. No obstacle height is used.

Such a graph is suitable to assess the effects of variations in
wing area, installed engine thrust and aircraft weight, while keeping
other effects relatively constant such as certain force ratios related
to braking coefficients and aircraft drag/thrust ratios. These ratios,
however, do affect the magnitudes shown to some extent and should be
determined prior to preliminary design exercises. The graph is based
on ratios that were found to be suitable for the externally blown flap
concept presently under study. They are $F_3/T_{PE} = 1.8$ and $F_4/F_3 = 1.67$,
and a range of $F_4/|F_B|$ from 0.75 to 1.25. Herein, T_{PE} is the static
nozzle thrust per engine, F_3 and F_4 are average accelerating forces when
3 or 4 engines are operating, and $|F_B|$ is the average braking force.
The determination of the ratios is discussed later in this report.

Also, an experience value for the speed at which an engine fails,
V_F, needs to be used in the determination of the takeoff distance from
such a graph. Surprisingly, the distance is not very sensitive to this
speed at values of interest, so that a first order estimate of V_F may
yield an acceptable first assessment of the takeoff distance. It is
suggested, that the takeoff distance be determined first with an
estimated V_F (for example 60 knots true), that subsequently V_F be
determined as shown in the next chapter, and that finally the takeoff
distance be read again with the new V_F as a second iterative step.
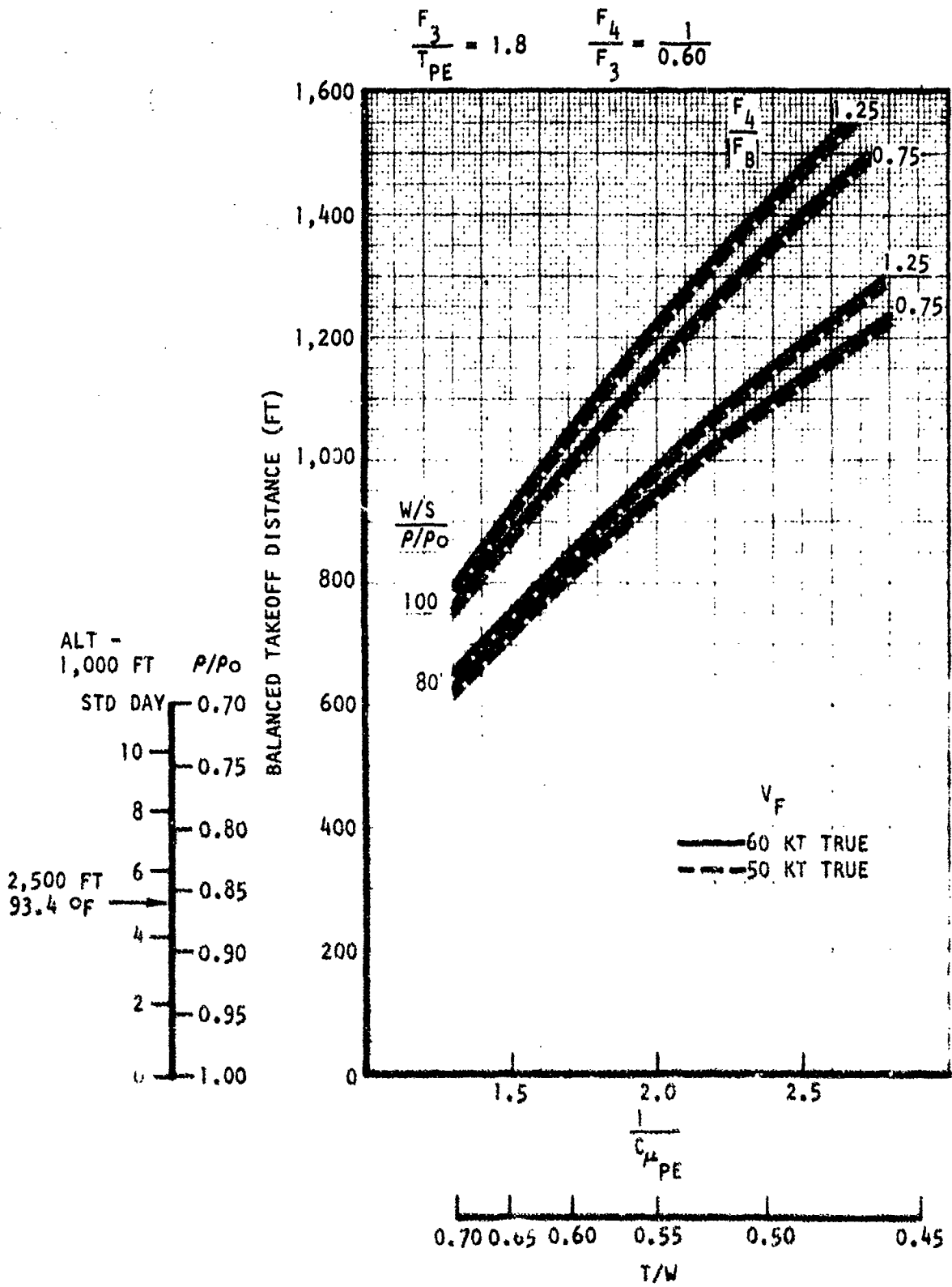
Figure 47a.   Balanced Takeoff Distance Without Obstacle Height
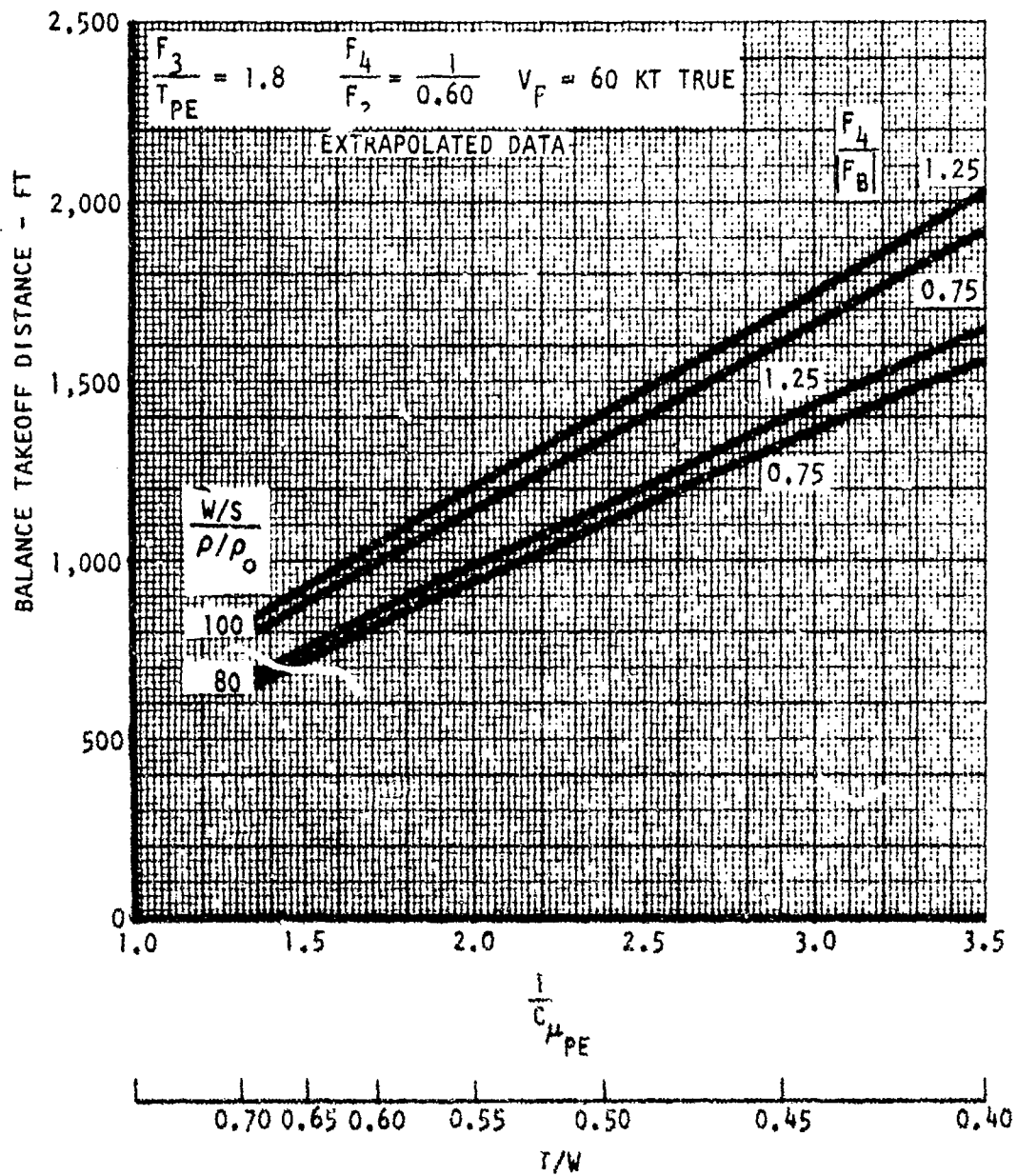
Figure 47b. Balanced Takeoff Distance Without Obstacle Height

From a graph such as given in the figure above the takeoff distance can be determined as a function of aircraft weight and field elevation for each given engine size (as expressed in T_{PE} at S.L. STD condition) and wing area, S. This is illustrated in the following example using $V_F = 60$ knots true, $F_4/1 = 1.0$, $S = 1600$ ft^2 and the above graph:

ALT	ρ/ρ_o	T (4 Eng.)	W (Lbs)	T/W	W/S	$\dfrac{W/S}{\rho/\rho_o}$	δ (Ft)
S.L. (STD)	1.0	82,200 lbs	140,000	.588	87.5	87.5	940
			150,000	.550	93.7	93.7	1115
			160,000	.515	100.0	100.0	1335
2500 Ft. (Hot)	.857	79,200 lbs	140,000	.566	87.5	102.0	1150
			150,000	.528	93.7	109.2	1375
			160,000	.495	100.0	116.7	1625

The distance of this sample computation is presented graphically in Figure 48.

Because the force ratios F_3/T_{PE} and F_4/F_3 may deviate somewhat from the values used in the above figures it is of interest to assess the sensitivity of the takeoff distance to a variation of these ratios. This sensitivity is shown by the curves in Figure 49. The curves are accurate to within 0.5 percent of the takeoff distance for all T/W and $(W/S)/(\rho/\rho_o)$ values shown in Figure 47. Using these sensitivity curves for correction factors, the takeoff distance may be approximately expressed by:

$$\delta = (\delta)_{\substack{F_3/T_{PE} = 1.80 \\ F_4/T_{PE} = 1.67}} \cdot \frac{\delta}{(\delta)}_{F_3/T_{PE} = 1.80} \cdot \frac{\delta}{(\delta)}_{F_4/T_{PE} = 1.67}$$

A nomogram has also been developed that gives the balanced takeoff distance directly, without factorization, and with varying values for the above described ratios, see Figure 50. This nomogram forms the basis of the graphs presented above. It is recommended to use this graph if the force ratios are significantly different from the values used above. The derivation of this nomogram is presented in the appendix.
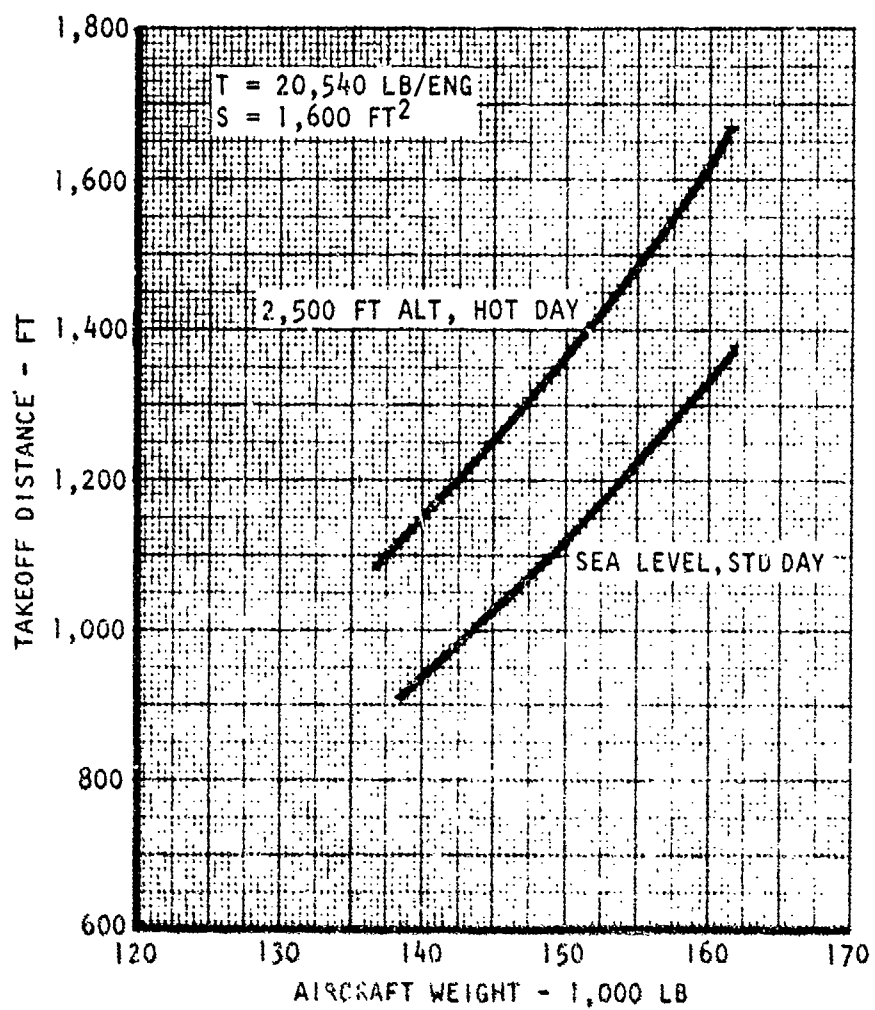
Figure 48. Sample Takeoff Distance Versus Weight

83

$$\frac{F_4}{|F_B|} = 1.0$$

$$\boxed{\frac{F_4}{F_3} = 1.67 = \frac{1}{060}}$$

$$\frac{s}{(s)} \text{ FOR } F_3/T_{PE} = 1.8$$

RATIO F_3/T_{PE}
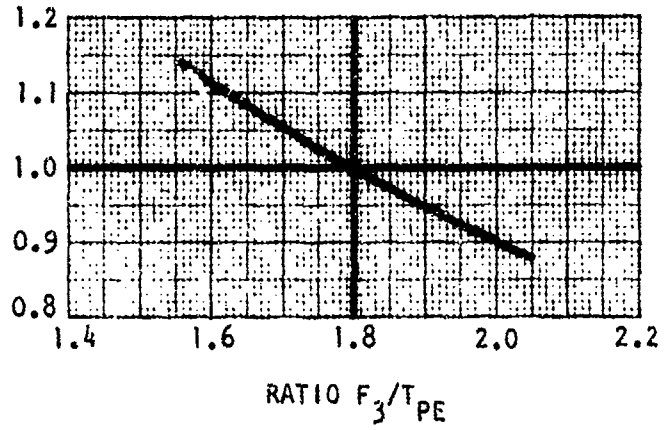
$$\boxed{\frac{F_3}{F_{PE}} = 1.8}$$

$$\frac{s}{(s)} \text{ FOR } F_4/F_3 = 1.67$$

RATIO F_4/F_3
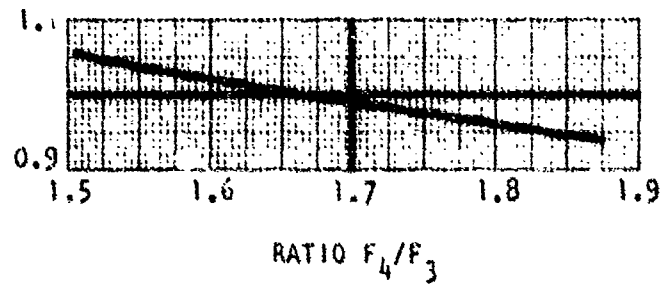
Figure 49.   Effect of Acceleration and Deceleration
Ratios on Balanced Takeoff Distance

Figure 50. Nomogram for Balanced Takeoff Distance Without Obstacle Height

(b) Ground Rules and Aerodynamic Limitations

The above graphs and nomograms for the determination of the takeoff distance are based on balanced distances without an obstacle height, see Figure 51. This means that the ground roll of a continued takeoff after engine failure is equal to the ground roll when the takeoff is aborted after the engine failure.

Equal distances are obtained by determining an aircraft speed on the ground at which proper action must be taken either to continue to takeoff or to brake after engine failure. If the speed at which the engine fails, V_F, is high, then the distance required to continue the takeoff is relatively short and the distance required to stop is relatively long. Vice versa, a low V_F results in a long takeoff distance and a short distance to bring the aircraft to a stop. Thus, the above graphs and nomograms require the determination of the value of V_F for which the ground rolls are equal.

Inherent with the use of this balanced distance, it is assumed that V_F can be determined unrestricted by other limitations, such that V_1 does not need to be increased on the basis of controllability problems during engine failure on the ground.

Assumed also is that, if an engine fails at V_F, one second elapses before the pilot recognizes the failure and comes to a decision of either to continue the takeoff or to brake. If he decides to brake, it is assumed that it will take an additional two seconds before all braking devices such as thrust reversers and wheel brakes are fully effective. During the first second before initiation of the braking, the aircraft increases speed because of the three-engine acceleration force. During the two seconds after initiation of the braking the aircraft first still continues to increase speed, but subsequently decreases speed near the end of the two-second period. For the purpose of establishing methods to determine takeoff distances, an average constant speed is assumed during the total three second period. This is equally as arbitrary as the assumption of a one-second recognition time and a two-second brake deployment time. Thus the rolling distance between start of engine failure and beginning of full braking effect is assumed to be, using the true speed for V_F:

$$\Delta \mathcal{S} = 3 \, V_F \qquad \text{(units in feet and seconds)}$$

86

CLIMBOUT
WITH CRITICAL
ENGINE FAILED

3°

4 ENG ACCEL — 3 ENG ACCEL

4 ENG ACCEL — BRAKING

3 SEC AT $\ddot{X}_{AVG} = 0$

(1 SEC RECOGNITION OF ENG FAILURE & DECISION)
(2 SEC FULL DEPLOYMENT OF FLAPS)

TOTAL TAKEOFF DISTANCE
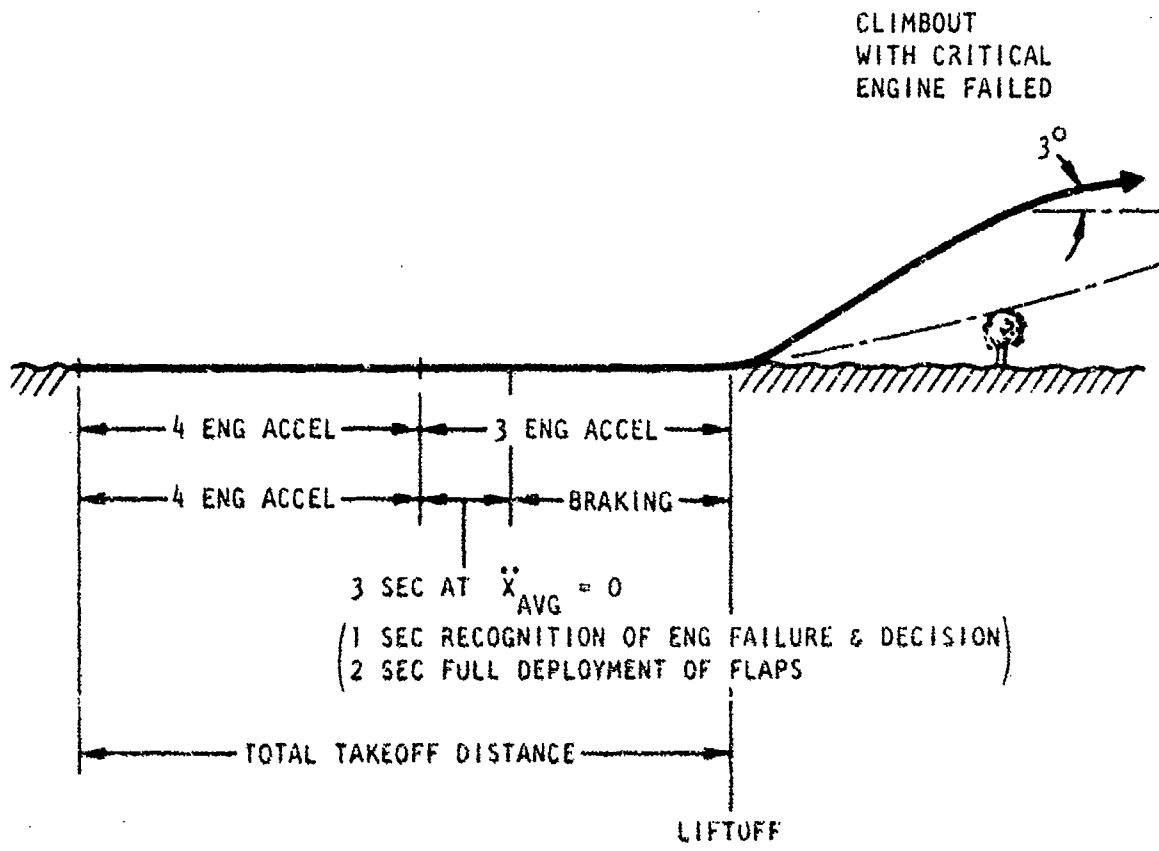
LIFTOFF

Figure 51. Takeoff Profile

87

If the pilot decides to continue the takeoff after engine failure at V_F, the takeoff distance is continued to a flight speed that meets all flight safety and climb requirements. The liftoff speed is the same as that described in the previous section and thus consistent with the ground rules stated there.

This speed is reflected in the lower portion of the vertical axis of the nomogram in Figure 50. If the aircraft aerodynamics change, or if the safety margins or climb requirements change, a different relation between T/W and $(1/C_{\mu PE})_{LO}$ needs to be substituted at this part of the nomogram as discussed in the section for liftoff speed. For this reason a scale of $(1/C_{\mu PE})_{LO}$ is included in the nomogram. This scale remains unchanged during this manipulation, and only the T/W values need to be revised.

Furthermore the ground rules used in this nomogram do not include a portion of the runway length needed to taxi the aircraft onto the runway, and to provide a surface for the nose gear to rest upon after an aborted takeoff. To provide this capability, a distance needs to be added equal to:

$$\Delta \delta = R_g + l_N$$

Where R_g is the taxi radius to the outer gear, and l_N is the distance between the nose gear and the main gear, see Figure 52.

(c) Supporting Information

Failure Speed V_F

A nomogram for the determination of the failure speed V_F is presented in Figure 53. It is based on the same force ratios F_3/T_{PE} as the nomogram for the takeoff distance in Figure 47.

The failure speed needs to be known for the accurate determination of the takeoff distance in the above mentioned section. However, conversely, the determination of V_F depends here on the takeoff distance. It is suggested to first determine the takeoff distance with an assumed V_F, subsequently to determine with this distance a new V_F from the present
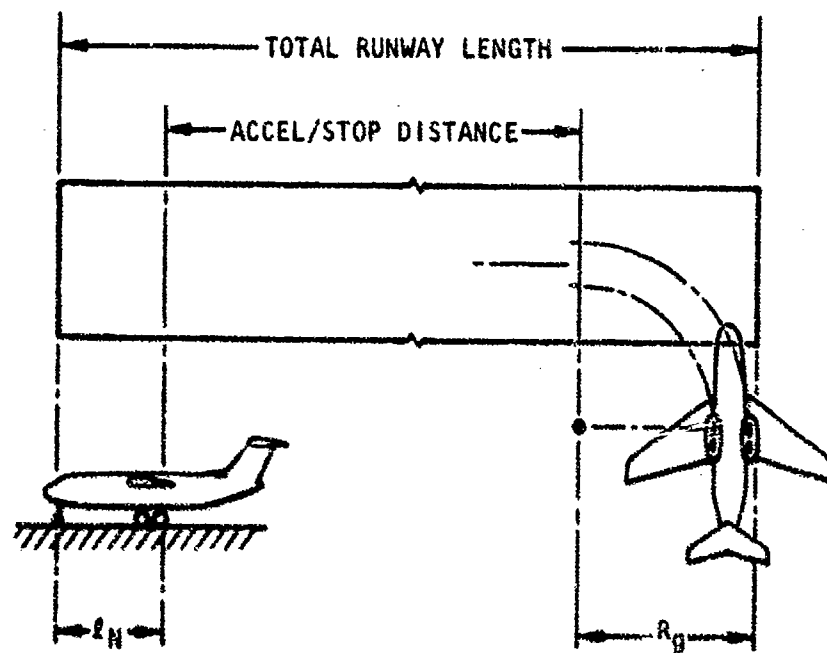
Figure 52. Definition of Total Runway Length
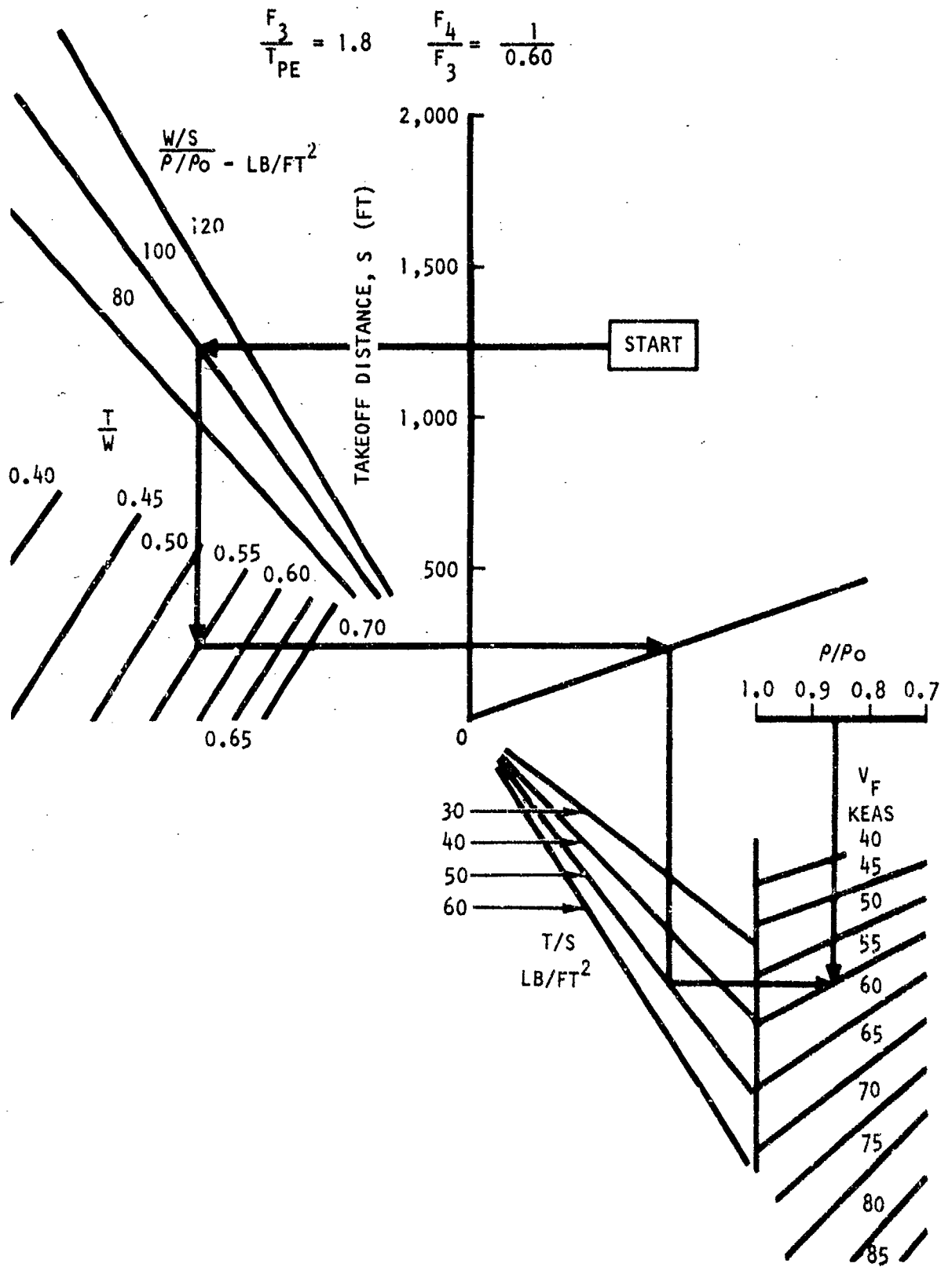
Figure 53. Nomogram for Failure Speed V_F

90

Figure 53 and then to determine a refined takeoff distance, etc., in an iterative procedure. This iteration is rapidly converging, and mostly only one corrective step is needed.

The aerodynamic data used in this nomogram, as well as the flight safety margins and climb requirements that enter into the determination of V_F are the same as for the takeoff distance nomogram. If other aerodynamic data or ground rules or force ratios F_3/T_{PE} and F_4/F_3 need to be used, a more detailed nomogram should be taken that is derived in the appendix. From this more detailed nomogram a new simplified version may be derived as of the type shown above in Figure 53, but with changed ground rules or changed aerodynamic data as necessary.

Thrust and Drag During Ground Roll

In this section nomograms for the determination of the following force ratios are presented for use in takeoff distance nomograms:

$$\frac{F_4}{F_3} = \frac{\text{Average accelerating force with 4 engines}}{\text{Average accelerating force with 3 engines}}$$

$$\frac{F_3}{T_{PE}} = \frac{\text{Average accelerating force with 3 engines}}{\text{static engine thrust at exhaust (per engine)}}$$

$$\frac{F_4}{|F_B|} = \frac{\text{Average accelerating force with 4 engines}}{\text{Average decelerating force while braking}}$$

These ratios need to be obtained only a relatively few times after selection of a lift/propulsion system whereafter probably experience values can be used.

Nomograms for F_4/T_{PE} and F_3/T_{PE} are presented in Figures 54 and 55 respectively. The ratio F_4/F_3 is then obtained from

$$\frac{F_4}{F_3} = \frac{F_4 / T_{PE}}{F_3 / T_{PE}}$$

91

Figure 54. Nomogram for Four-Engine Accelerating Force

Figure 55. Nomogram for Three-Engine Accelerating Force

93

The two nomograms are based on a ground roll during which the flaps are not blown. It is assumed that the thrust nozzles are rotated only immediately prior to liftoff to a blowing position. (Nozzle positioning may become a standard operational proc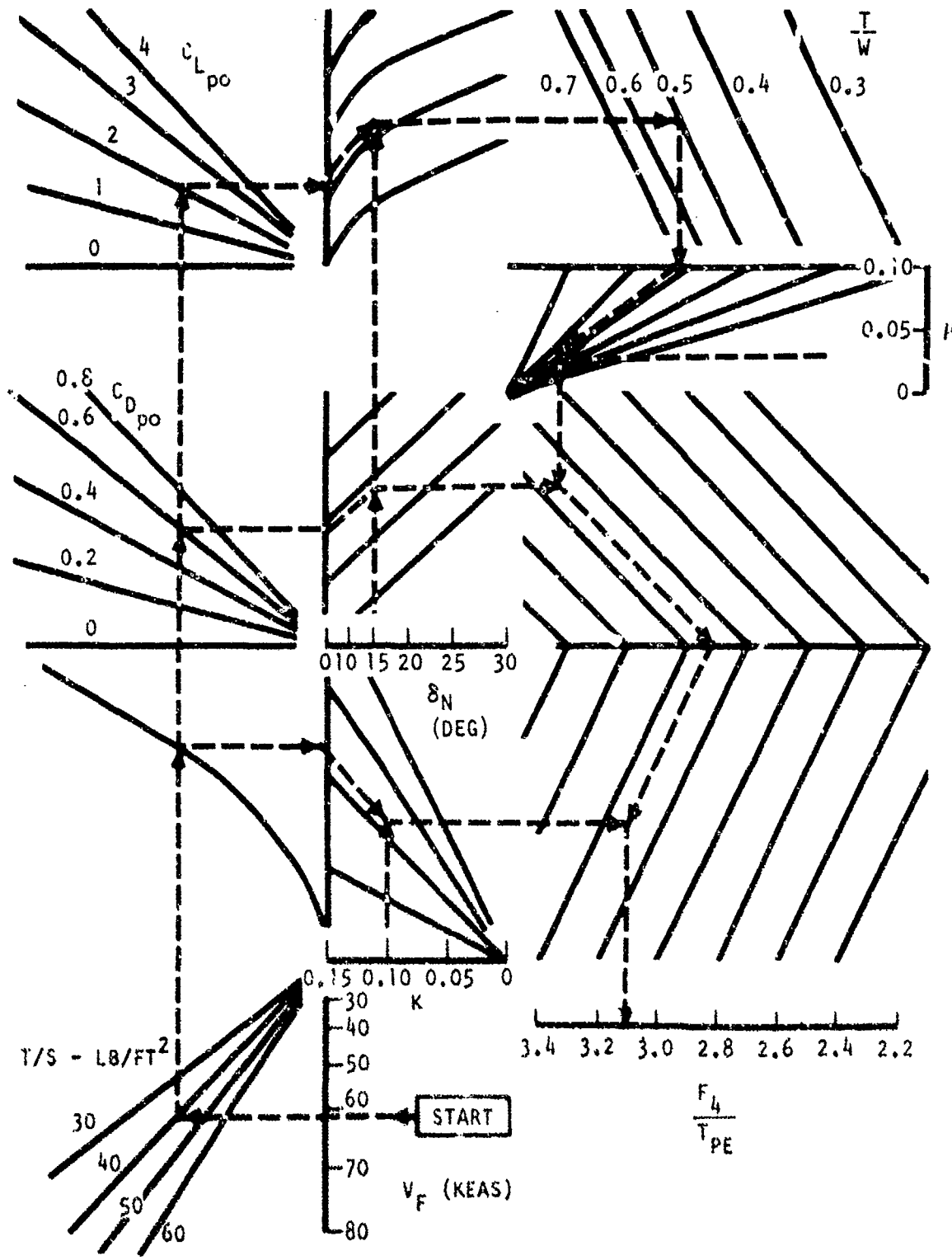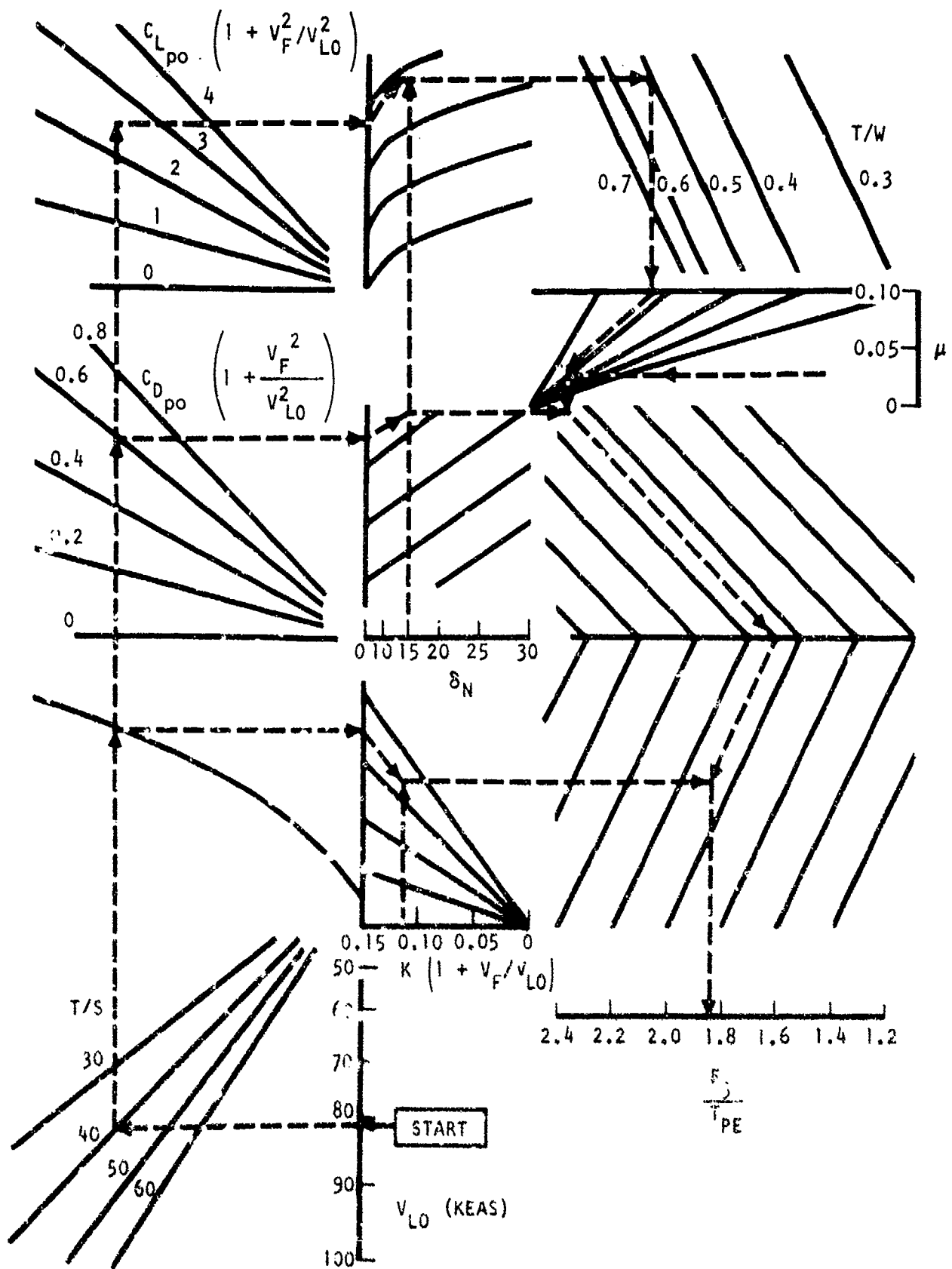edure for this type of vehicle during STOL mode employment. Its use is analogous to a collective pitch lever in helicopters, and its operation would become of secondary nature to the pilot.) Most of the ground run is thus carried out with the nozzles deflected downward by a small angle δ_N so that the exhaust is not obstructed by the flaps. This results in a relatively high forward thrust component $4T_{PE} \cos \delta_N$ in the acceleration phase. Under these circumstances aerodynamic drag and lift is generated exactly as in conventional aerodynamics, i.e., $L_{aero} = C_{LPO} q S$ and $D_{aero} = C_{DPO} q S$, where the subscript PO denotes power-off aerodynamics. Power effects are added from the thrust components without aerodynamic interference. The aerodynamic derivatives should include ground effect.

A nomogram for $|F_B|/T_{PE}$ is presented in Figure 56 on a similar basis, except that two engines out of four are assumed operating with thrust reversers, and that the remaining two engines are inoperative because one of them is assumed failed, and the other shut down to preserve thrust symmetry. No vertical thrust components are considered from the engine exhaust system with the reversers actuated. A derivation of the equations used in the nomogram are presented in the appendix.

The above nomograms include a decrease of the net engine thrust with speed increase. This decrease is primarily due to the intake momentum drag. The remainder is due to a change in the nozzle exhaust force. The equation used here for the total change with speed is

$$\frac{\Delta D_i}{T_{PE}} = \frac{NK}{\sqrt{C_{\mu PE}}}$$

where N is the number of engines operating and where K is a factor that varies only slightly with speed and power conditions.

To use the above nomograms, only the factor K needs to be determined. An example of its determination is given in Figure 57. It is suggested to determine the value of K only once for a given engine/aircraft layout because the main change with speed and power is approximated adequately by the variation in $\sqrt{C_{\mu PE}}$.

Use of the figure requires the knowledge of A_{iPE}, which is the intake area inside the inlet per engine, as well as the bypass ratio B and wing reference area S. Note that

$$A_{iPE} B / S = \pi A B / 4 (b/D_{PE})^2$$

where A is the wing aspect ratio, and D_{PE} is the diameter of the inlet throat of each engine.

Background information of the thrust change with speed is presented in the appendix.

94
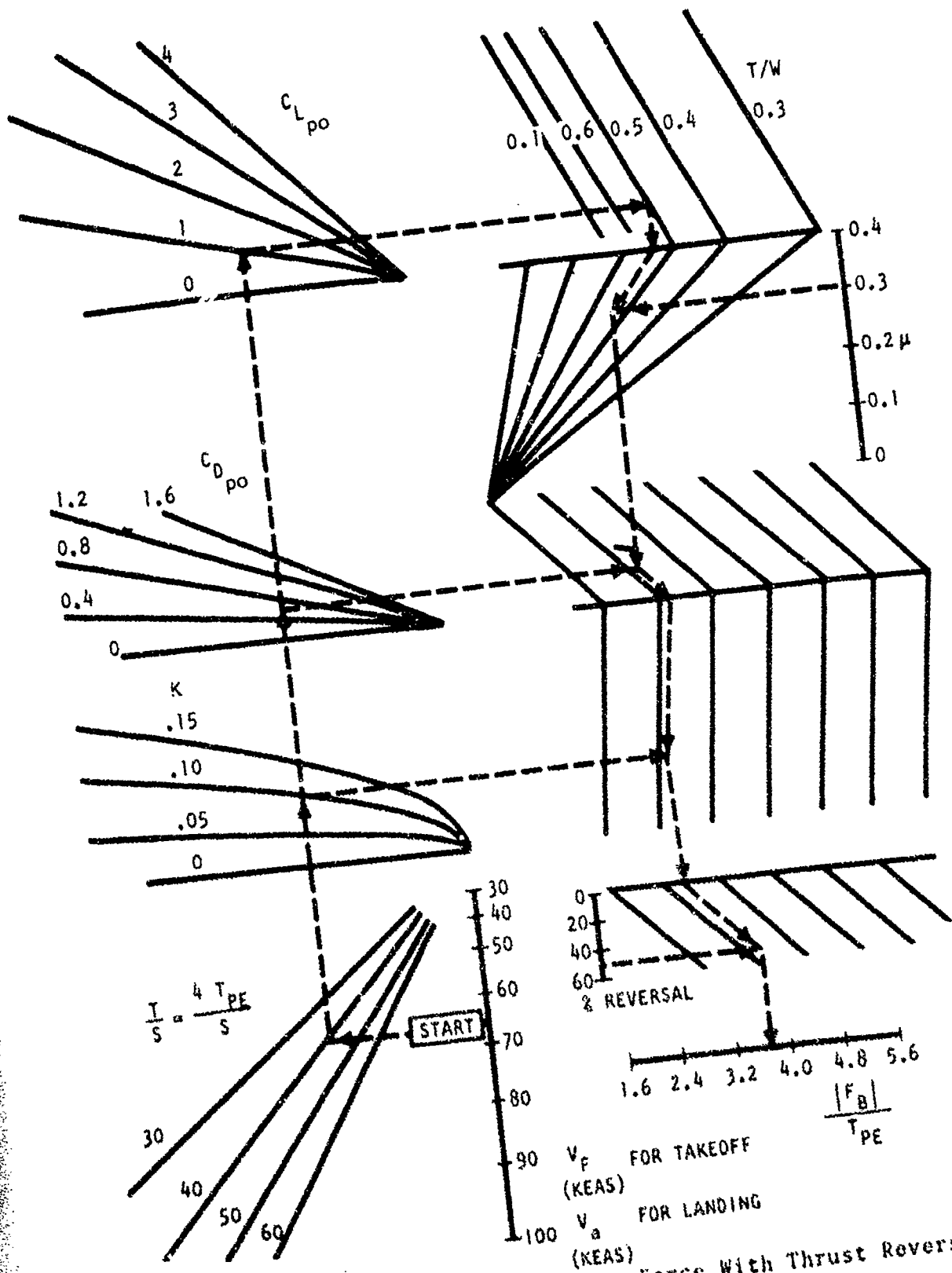
Figure 56. Nomogram for Decelerating Force With Thrust Reversal on Two Engines

95

3.1.3 SAMPLE COMPUTATIONS AND SAMPLE DATA

The takeoff distance, liftoff speed, and failure speed may be determined as follows:

First Step

Obtain a first order approximation of the takeoff distance with an assumed value for $V_F \approx 100$ ft/second true (60 KTAS) from Figure 47 using appropriate values for T/W, W/S, and ρ / ρ_o :

$\dfrac{T}{W}$	$\dfrac{W}{S}$	$\dfrac{\rho}{\rho_o}$	$\dfrac{W/S}{\rho/\rho_o}$	δ
0.50	100	0.856	117	1600

Obtain a first order approximation of the failure speed, using Figure 53.

$\dfrac{T}{W}$	$\dfrac{W/S}{\rho/\rho_o}$	$\dfrac{T}{S} = \dfrac{T}{W} \cdot \dfrac{W}{S}$	V_F KEAS	KTAS	FT/S TRUE
0.50	117	50	70.0	75.8	128

Second Step

Determine V_F/V_{LO} using Figure 37 for V_{LO}:

$\dfrac{T}{W}$	$\dfrac{T}{S}$	V_{LO} KEAS	$\dfrac{V_F}{V_{LO}}$	$1 + \dfrac{V_F}{V_{LO}}$	$1 + \dfrac{V_F^2}{V_{LO}^2}$
0.50	50	94.0	0.745	1.74	1.55

Obtain factor K for the intake momentum drag from Figure 57, using appropriate values for A_{ipe}/S and the engine bypass ratio B. In the present sample

$$\frac{A_{ipe}}{S} \quad B = 0.08$$

96

$A_{i_{PE}}$ INLET THROAT AREA PER ENGINE

S REF. WING AREA

B BYPASS RATIO OF ENGINE

Figure 57.   Nomogram for Factor k for Engine Net Thrust Decrease With Speed

97

$\dfrac{T}{W}$	$\dfrac{T}{S}$	V_{LO} KEAS	K
0.50	50	94.0	0.080

Determine force ratios involving F_4, F_3, and $|F_B|$ from Figures 54, 55, and 56. Appropriate values need to be taken for the lift and drag coefficient, thrust nozzle deflection (downward), friction coefficient and thrust reversal. If $C_{L_{po}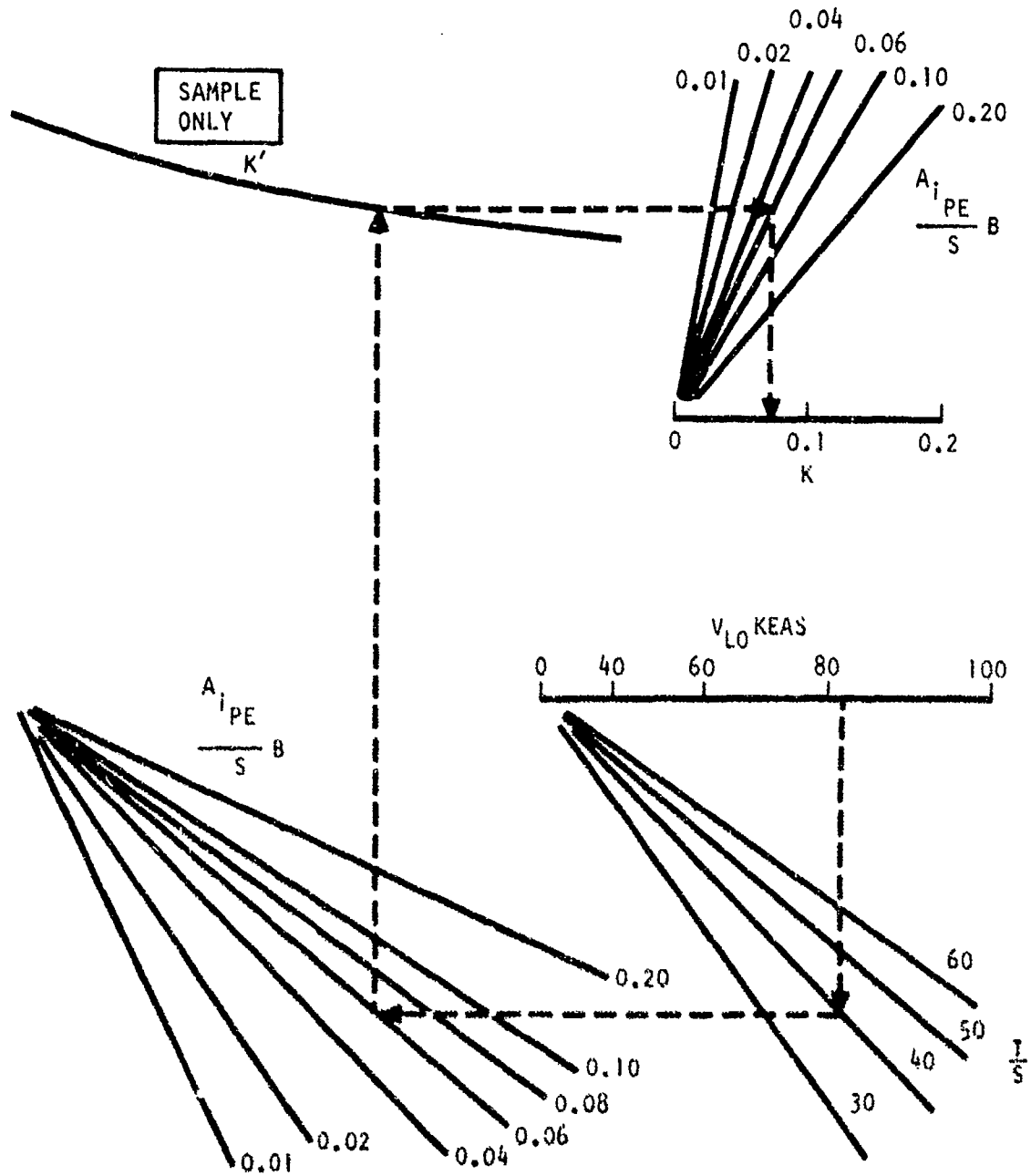} = 1.7$, $C_{D_{po}} = 0.27$, $\delta_N = 15°$, $\mu = 0.10$, and if the thrust reversal is 50 percent (on two engines) then:

$\dfrac{T}{W}$	$\dfrac{T}{S}$	V_F KEAS	$\dfrac{F_4}{T_{PE}}$	$K\left(1+\dfrac{V_F}{V_{LO}}\right)$	$C_{D_{po}}\left(1+\dfrac{V_F^2}{V_{LO}^2}\right)$	$C_{L_{po}}\left(1+\dfrac{V_F^2}{V_{LO}^2}\right)$	$\dfrac{F_3}{T_{PE}}$	$\dfrac{F_B}{T_{PE}}$	$\dfrac{F_4}{|F_B|}$	$\dfrac{F_4}{F_3}$
0.50	50	70	2.91	0.14	0.42	2.54	1.67	3.4	0.855	1.7

The takeoff distance is then determined from Figure 50:

$\dfrac{T}{W}$	$\dfrac{W/S}{\rho/\rho_o}$	$3\,V_F$ FT/S TRUE	δ
0.50	117	384	1640

The failure speed for a balanced takeoff becomes, using Figure 76 in the appendix

$\dfrac{T}{W}$	δ	$\dfrac{W/S}{\rho/\rho_o}$	$\dfrac{F_3}{T_{PE}}$	$\dfrac{F_4}{T_{PE}}$	$\dfrac{T}{S}$	V KEAS	$\dfrac{\rho}{\rho_o}$	V KTAS
.50	1640	117	1.67	0.855	50	67.0	0.856	70.5

The takeoff distance may also be determined, though less accurate, from Figures 47 and 49 with V_F from the first approximation:

$\dfrac{T}{W}$	$\dfrac{F_4}{|F_B|}$	$\dfrac{W/S}{\rho/\rho_o}$	$F_3/T_{PE}=180$, $F_4/F_3=167$ ①	$\dfrac{F_3}{T_{PE}}$	δ ②	$\dfrac{F_4}{F_3}$	δ ③	δ ①②③
0.50	0.855	117	1570	1.67	1.07	1.74	.98	1650

Further Iterative Steps

Iterative steps may be continued with the failure speed from the second approximation, but in general the accuracy of the nomograms does not warrant a further iteration.

The above procedure using Figure 50 and the above sample aircraft characteristics have been used in generating the results shown in Figures 58 and 59 which show some trends of the effect of T/W on the takeoff distance and the force ratios F_3/T_{PE}, F_4/F_3, and F_4/F_B.
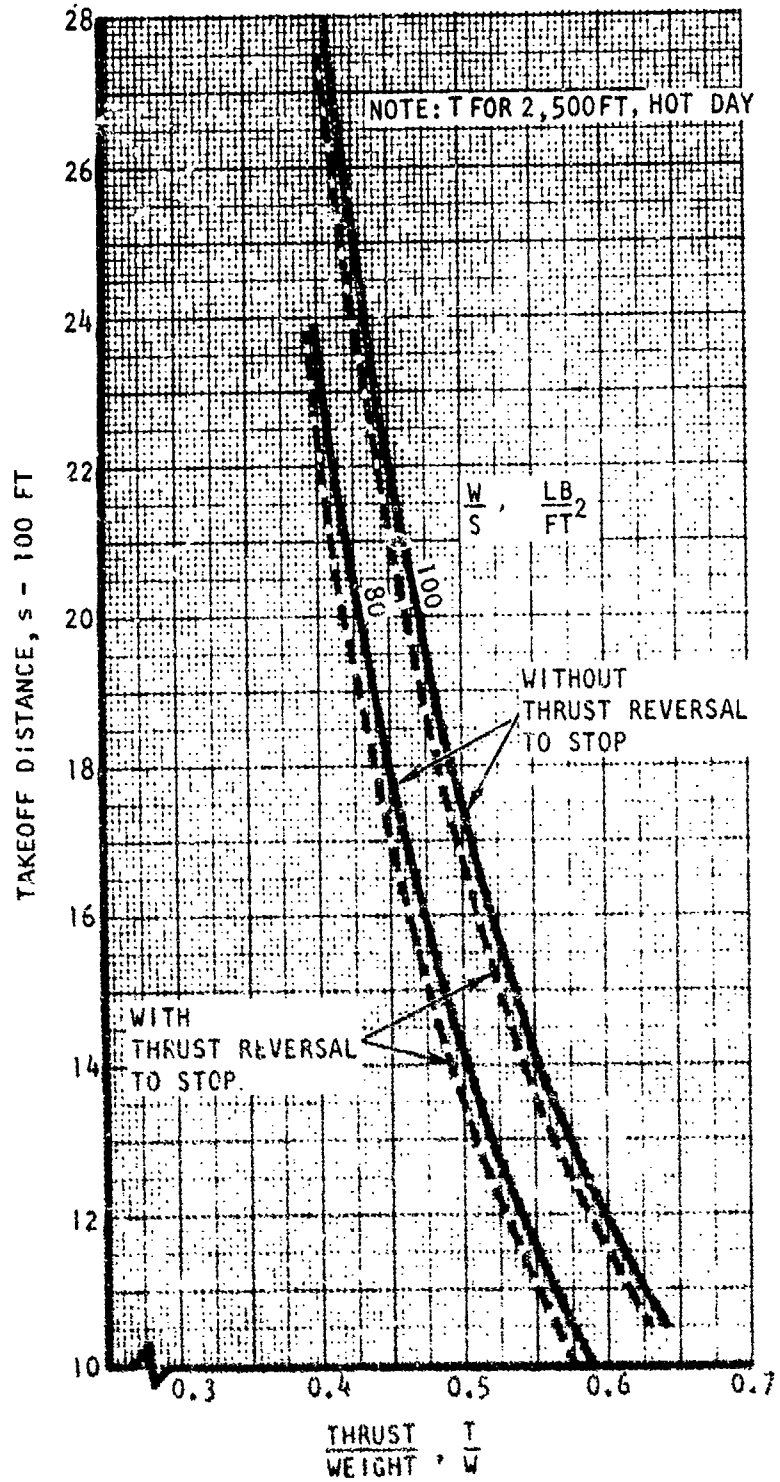
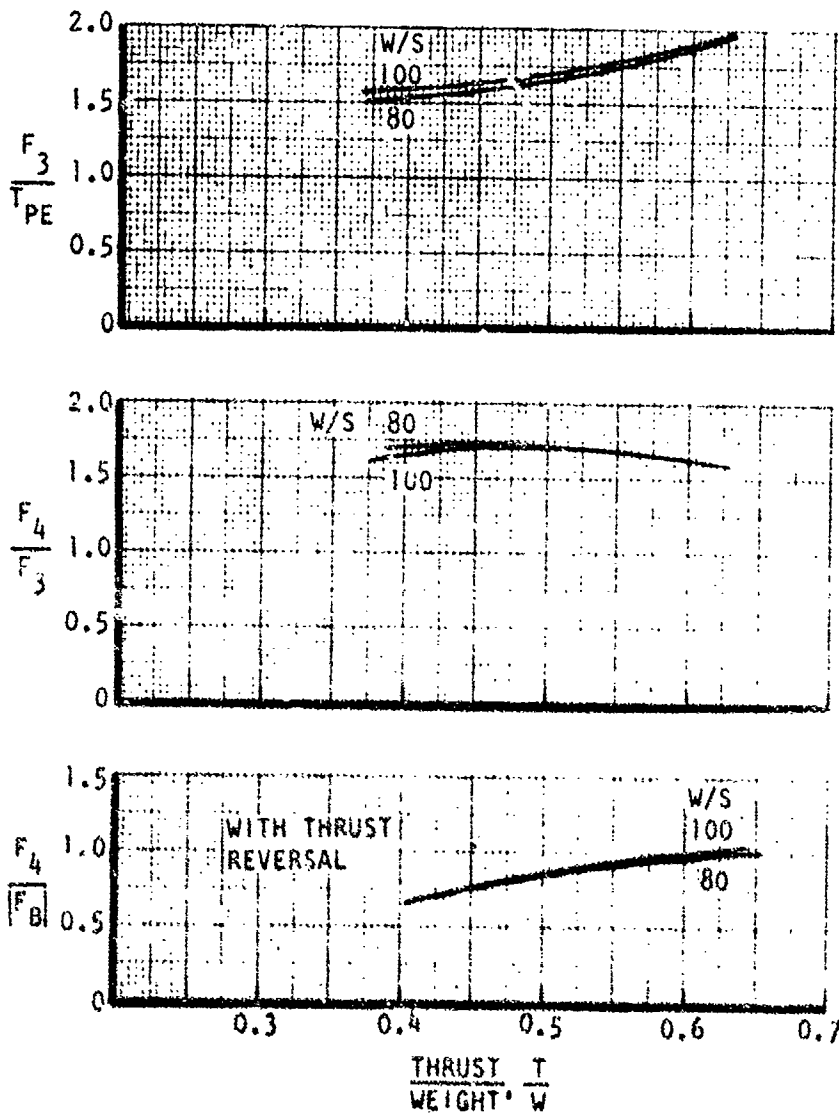Figure 58.   Sample Takeoff Distance at 2,500 Foot Altitude
Hot Day

100

Figure 59. Sample Force Ratios for Takeoff Distance
Determination

3.2 STOL LANDING PERFORMANCE

3.2.1 APPROACH SPEED

(a) A Nomogram for Approach Speed

A type of nomogram from which the approach speed can readily be determined is shown in Figure 60. Similar to the nomogram for the takeoff speed, also this nomogram is of a type that can be used for a great variety of lift/propulsion concepts as long as C_L values for approach can be expressed in terms of a blowing coefficient $C_{\mu PE}$.

(b) Ground Rules Used

In the above nomogram, the following flight safety considerations in terms of speed and maneuver margins are used:

$$V_a \geq 1.10 \, V_{mtd} \quad (CEF, \, IGE)$$

$$at \; V_a: \quad n \geq 1.15 \quad (CEF, \, IGE)$$

$$at \; V_a: \quad n \geq 1.3 \quad (CEF, \, OGE)$$

Herein, V_{mtd} is used synonomous to the stall speed in ground effect. It is assumed that the ground angle is not limited by the fuselage.

Also, the assumption is made that no significant decrease in speed occurs between the approach condition and the instant of touch down. Furthermore, it is assumed that the approach is made with a four-degree descent flight path angle which, at approach speeds of interest, results in a sink rate of about 10 ft/second.

In addition, the requirement is imposed that it be possible to waveoff with the earlier stated takeoff safety margins and with a climb angle of $\gamma = 3^\circ$ in the event that one engine is failed and that the waveoff is initiated at an altitude of 100 feet above the runway. Herein, partial flap retraction is used.
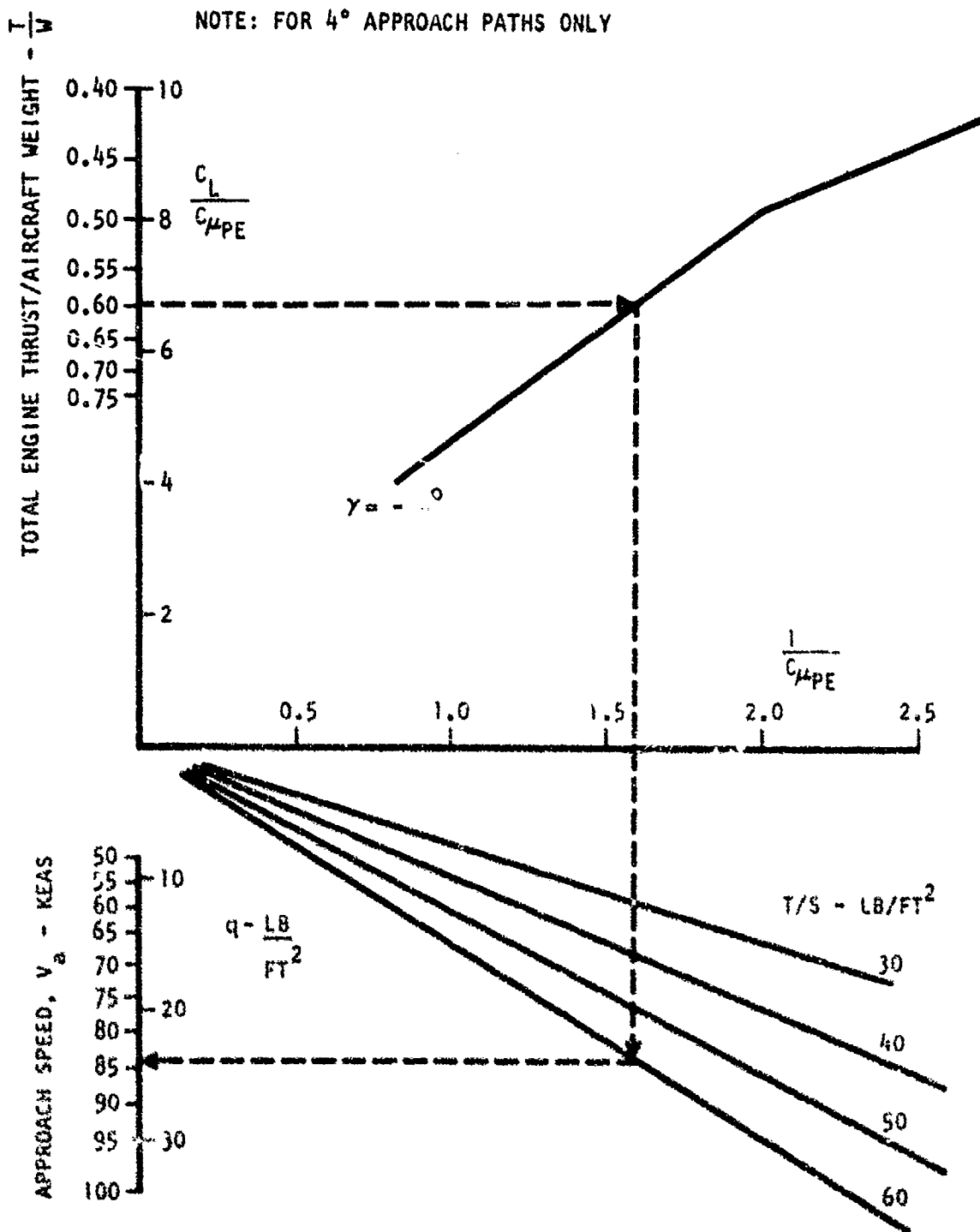
Figure 60. Nomogram for Approach Speed

103

(c) Aerodynamic Limitations

The speed margins and maneuver margins for approach are applied to the maximum lifting capability of the aircraft in a similar fashion as described in the section of aerodynamic limitations for takeoff. The same basic maximum lift data are used here, which is based on the angle of attack limit for which adequate roll control exists in case of engine failure ($\alpha = 18°$). Also the same data for ground effect on lift is used here.

The effect of the various margins on the useable lift for approach is shown in Figures 61 and 62 for two different values of the blowing coefficient. All curves are trimmed in pitch, roll, and yaw. All curves pertain to the critical engine failed (CEF), and spoilers are extended asymmetrically only on one side of the wing for rolling moment equilibrium. No spoiler deflection for DLC is used in these figures. The figures also indicate the relation between the flap angle and the lift coefficient where an approach flight path of $\gamma = -4°$ is obtained. This relation is determined in a very similar way as that for $\gamma = +3°$ in takeoff in Figure 44.

The highest lift where this flight path requirement as well as the most stringent safety margin is satisfied represents the highest useable lift for approach. This occurs at the intersection of the respective lift lines. The lift of the intersections is now plotted versus the inverse of the blowing coefficient in Figure 63. Such a figure yields the minimum approach speed for any given value of the thrust T_{PE}. At any given T_{PE} and $W = L$, a condition to the right of the line has safety margins greater than those stated above. Conditions to the left represent speeds that are lower than that at which the safety margins can be met.

The curve in Figure 63 is included in the nomogram in Figure 60 for values of $1/C_{\mu PE}$ lower than 2.0 (see next chapter for values greater than 2.0). The upper portion of the vertical axis in this nomogram represents $C_L/C_{\mu PE}$ which is readily expressed in T/W by

$$\frac{C_L}{C_{\mu PE}} = \frac{L}{T_{PE}} = \frac{W}{T/4} = \frac{4}{T/W}$$

The horizontal axes in both figures are also identical. This axis system has been used in the nomogram to facilitate changes in the relation between $C_L/C_{\mu PE}$ versus $1/C_{\mu PE}$ when the aerodynamics change or when the safety requirements or the descent rate are altered. The relation shown is valid for the externally blown flap lift/propulsion concept with

104

NO BLC
DOUBLE-SLOTTED FLAPS

$$\boxed{C_{\mu_{PE}} = 0.825}$$

TRIMMED CONDITIONS (25% MAC)
NO SPOILER DEFLECTION FOR DLC
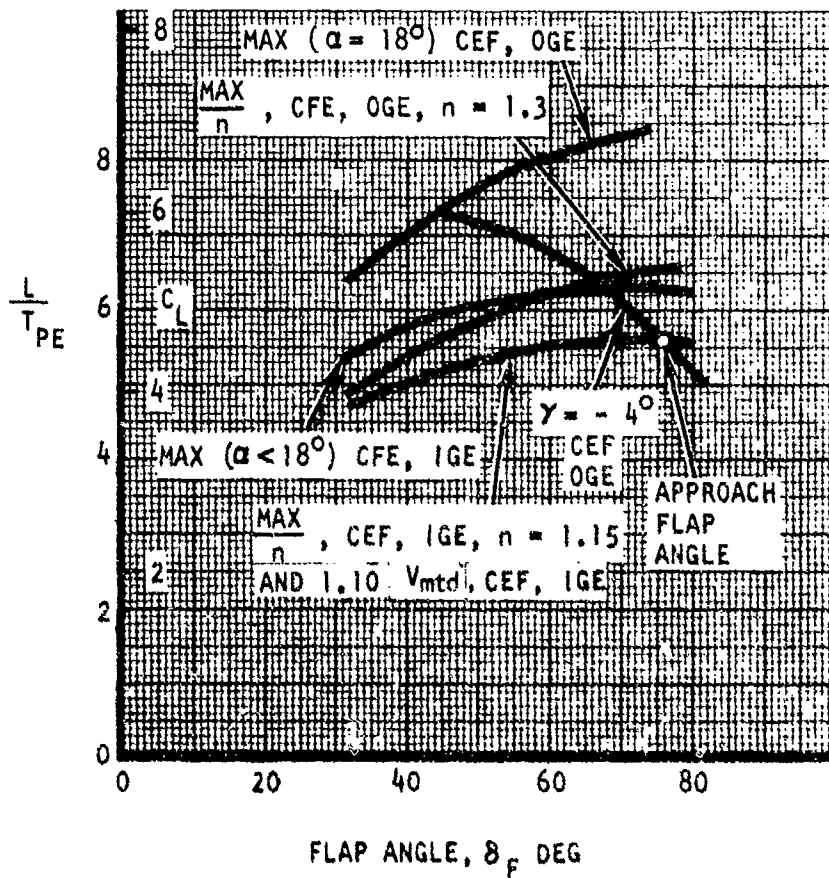FIRST FLAP SEGMENT 25°

Figure 61. Determination of Approach Flap Angle

NO BLC
DOUBLE-SLOTTED FLAPS

$$C_{\mu_{PE}} = 0.50$$

TRIMMED CONDITIONS (25% MAC)
NO SPOILER DEFLECTION FOR DLC
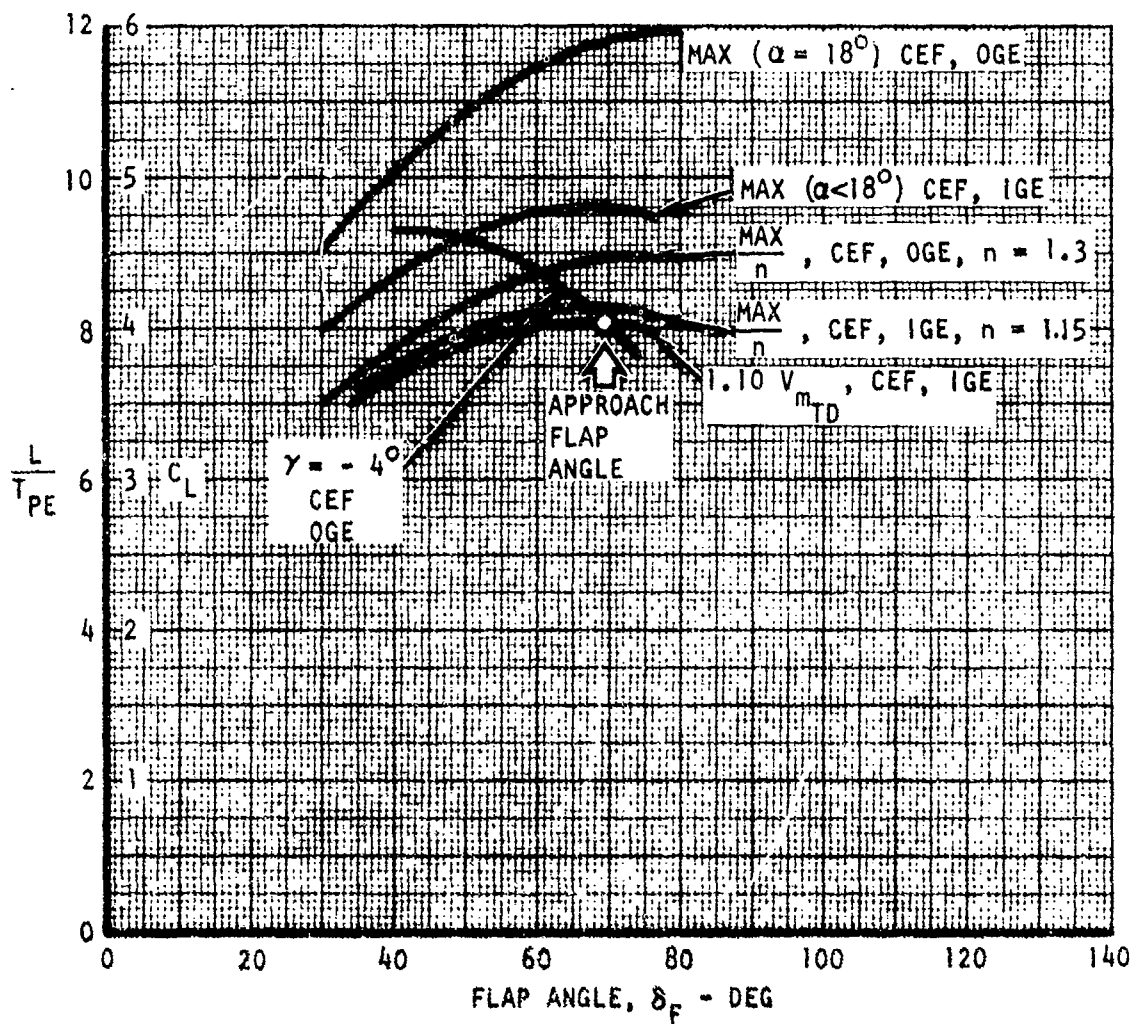FIRST FLAP SEGMENT 25°

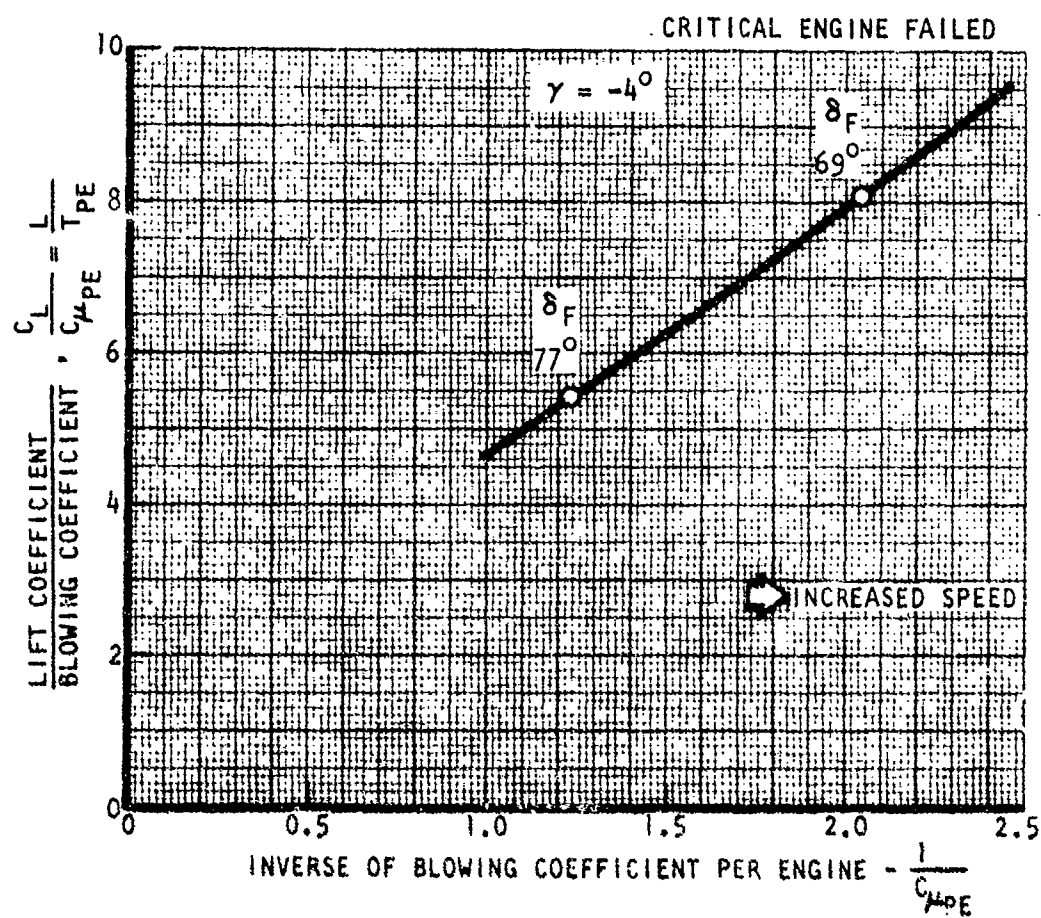Figure 62. Determination of Approach Flap Angle

Figure 63. Lift Versus Inverse of Blowing Coefficient for
Approach Without Waveoff Consideration

aerodynamic characteristics based on a certain wind tunnel test. However, again this type of nomogram can be used for many different lift/propulsion concepts as long as C_L can be expressed in terms of a coefficient such as $C_{\mu PE}$.

One safety requirement not included thus far and which can change the relation in Figure 63 pertains to the waveoff capability. This capability is discussed in the following section.

(d)   Waveoff Constraints

Waveoff considerations become important whenever the speed after a pullup from the approach is less than the speed for takeoff with one engine failed. It is assumed here that the speed for waveoff is at least equal to that for takeoff so that at least equal safety margins and climb capabilities exist as after the takeoff.

To compare these speeds, first a comparison between the relation of L/T_{PE} versus $1/C_{\mu PE}$ for approach and takeoff is made, as shown in Figure 64. The relation for approach is taken from the above Figure 63, while the relation for takeoff or waveoff is found from Figure 46.

It is seen that the inverse of the blowing coefficient is lower for approach than for landing at L/T_{PE} values of interest. This inverse of the coefficient is indicative of the dynamic pressure or speed at given values of T_{PE} because

$$9 = \frac{1}{C_{\mu_{PE}}}(T_{PE}/S)$$

This means the approach speed is lower than the takeoff speed at equal values of the thrust T_{PE}. Generally it may be assumed that the thrusts are indeed the same and equal to the maximum because the thrust of three engines is advanced fully after failure of one engine in order to obtain a minimum landing distance with three engines operating. Thus, it is seen that with the safety margins for approach and takeoff presently used, the waveoff requirements may indeed become the most stringent safety requirement for the landing approach.
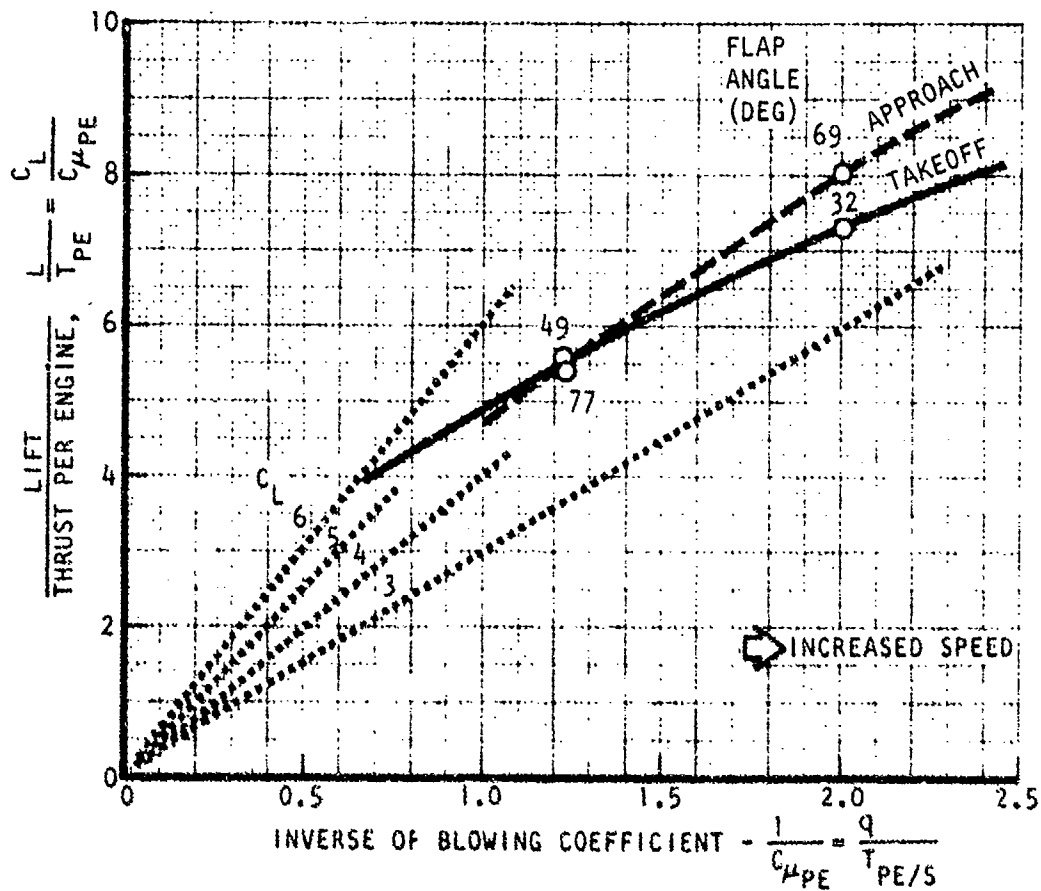
Figure 64. Lift Versus Inverse of Blowing Coefficient For Takeoff and Approach Speeds With the Critical Engine Failed

One way to insure adequate climb capability after waveoff is to use the same relation of $C_L/C_{\mu PE}$ versus $1/C_{\mu PE}$ for approach as for takeoff, and to disregard the relation for approach derived in the previous section. This results in an increased approach speed and thus increased landing distance.

Another procedure would be to change the thrust level. However, this would necessitate the use of less than maximum thrust during the three engine approach, and this results in a greater landing distance in normal operation. Both these procedures are not used in the present report.

However, it is also possible that the speed increases while the pullup and a flap reduction is carried out, especially when the flap angle can be reduced fairly rapidly and when the pullup is not severe. In that case the approach speed can indeed be lower than the climbout speed. To investigate this possibility the drag characteristics of the aircraft are analyzed here and related to the maneuver requirements and flap retraction rate.

The pullup should be the minimum possible within safety constraints. One of these constraints is posed by the loss of altitude after waveoff initiation. It can be shown that the altitude loss is

$$\Delta H = -\frac{1}{2} \frac{V_z^2}{\Delta n g}$$

where

V_z = rate of sink in ft/second

Δn = normal acceleration due to pullup

Assuming that the waveoff is initiated at an altitude of 100 feet above the runway with one engine inoperative, and that only 80 percent of this altitude may be consumed for clearance, the required normal acceleration for V_z = -10 ft/second becomes:

$$\Delta n = \frac{-\frac{1}{2} \cdot 10^2}{-80(32.2)} = 0.0194$$

110

Another constraint is the assumed requirement that the flight path is curved upward at the end of the runway in such a way that the flight path angle is equal to the design takeoff flight path angle with one engine inoperative. It can be shown that the distance, δ, travelled to change the flight path from the approach angle, γ_a, to the takeoff climb angle, $\dot\gamma_c$, is:

$$\delta = (\gamma_c - \gamma_a)\frac{V^2}{\Delta n g}$$

where the angles are in radians, and V is the aircraft flight velocity in ft/second. Assuming that $\gamma_a = -4°/57.3$, $\gamma_c = +3°/57.3$, V = 135 ft/second or 80 knots, and that δ = 2000 feet, this equation yields:

$$\Delta n = \left(\frac{3+4}{57.3}\right)\frac{135^2}{2000 \cdot g} = 0.0346 \approx 0.035$$

Using this latter amount for the required normal acceleration, a first order assessment is made of the speed increase as shown somewhat schematically in Figure 65.

In this sample the normal acceleration is reached after one second of waveoff initiation, and the flap is reduced from 69° to 32° in three seconds. It is assumed that a double slotted flap is used, and that only the setting of the last segment needs to be changed. The external aerodynamic forces on the flap probably can be made to keep the power requirements for the flap actuation mechanism to a reasonably low value. In the present sample, the first flap segment is kept unchanged between approach and waveoff at 25°.

The average acceleration obtained from this figure is $\ddot x = 0.032g$, and the speed increases during the waveoff by 15 ft/second or 11 percent.

This means that the approach in this sample can be made with a speed that is only 90 percent of the takeoff climb speed because during the waveoff maneuver the speed can be increased to the 100 percent level of the takeoff climb speed. Applying the 90 percent value to the relation of $C_L/C_{\mu PE}$ versus $1/C_{\mu PE}$ of the takeoff condition, results in values that can be used to satisfy the waveoff climb condition, see Figure 66.

The final relation of $C_L/C_{\mu PE}$ versus $1/C_{\mu PE}$ to be used for approach must be either the one for the waveoff consideration from the above figure, or the one satisfying the approach safety margins in the descent flight flight path from Figure 63, whichever is critical. This final relation is shown in Figure 67 and forms the basis of the upper portion of the approach speed nomogram in Figure 60.
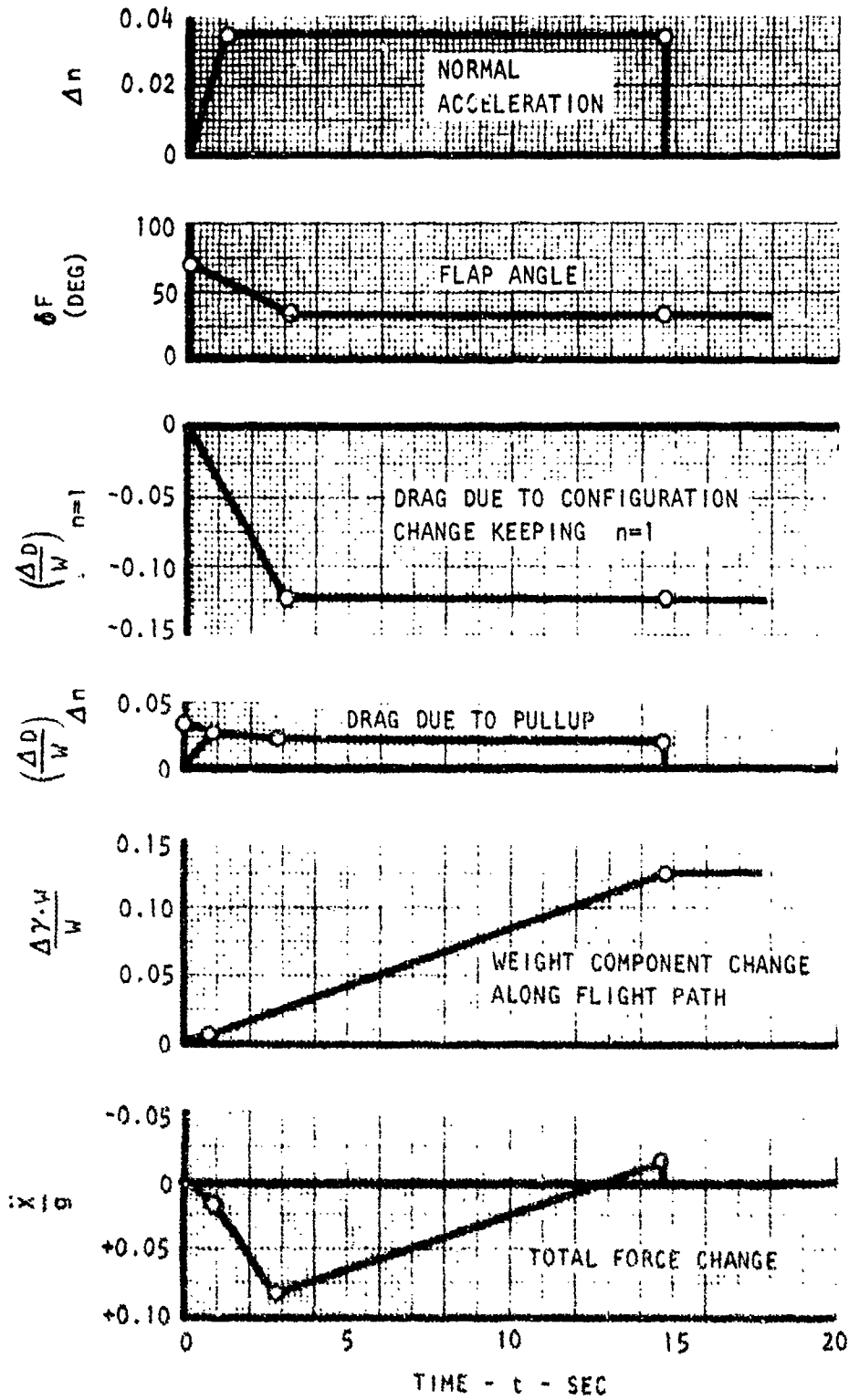
Figure 65. Drag and Acceleration Characteristics During Waveoff
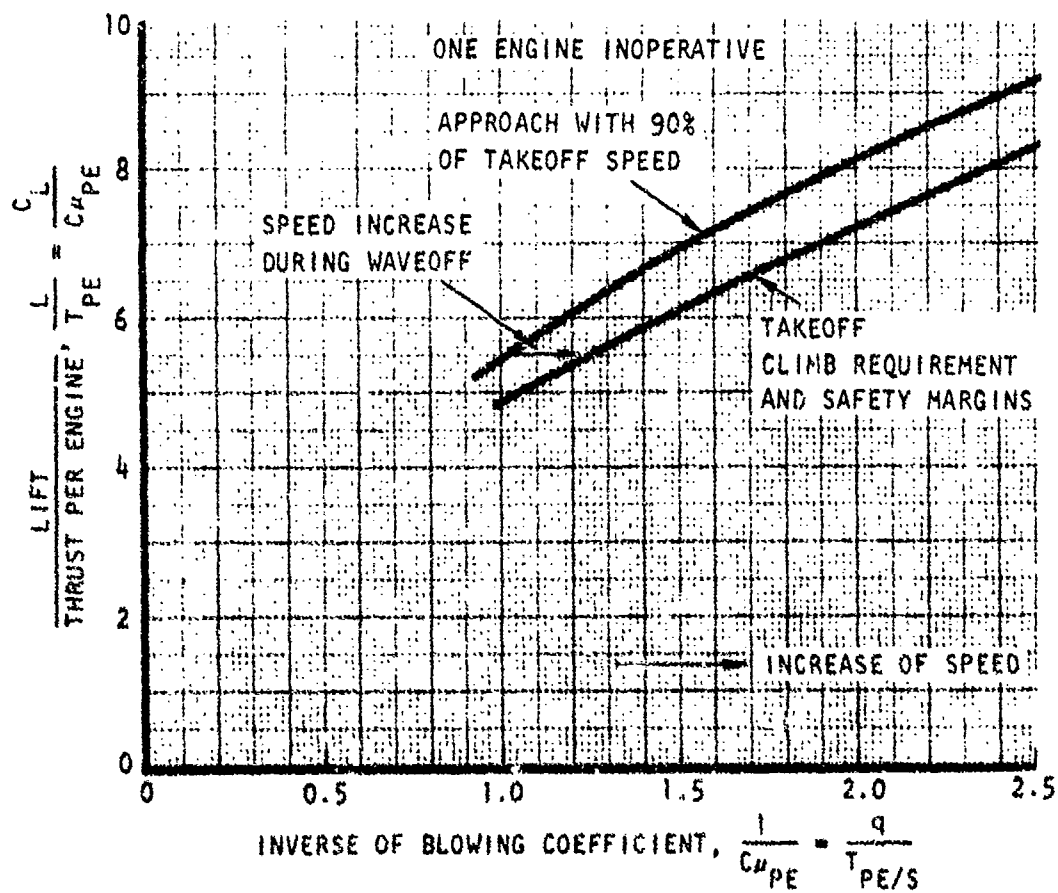
112

Figure 66. Lift Versus Inverse of Blowing Coefficient For Waveoff Capability During Approach
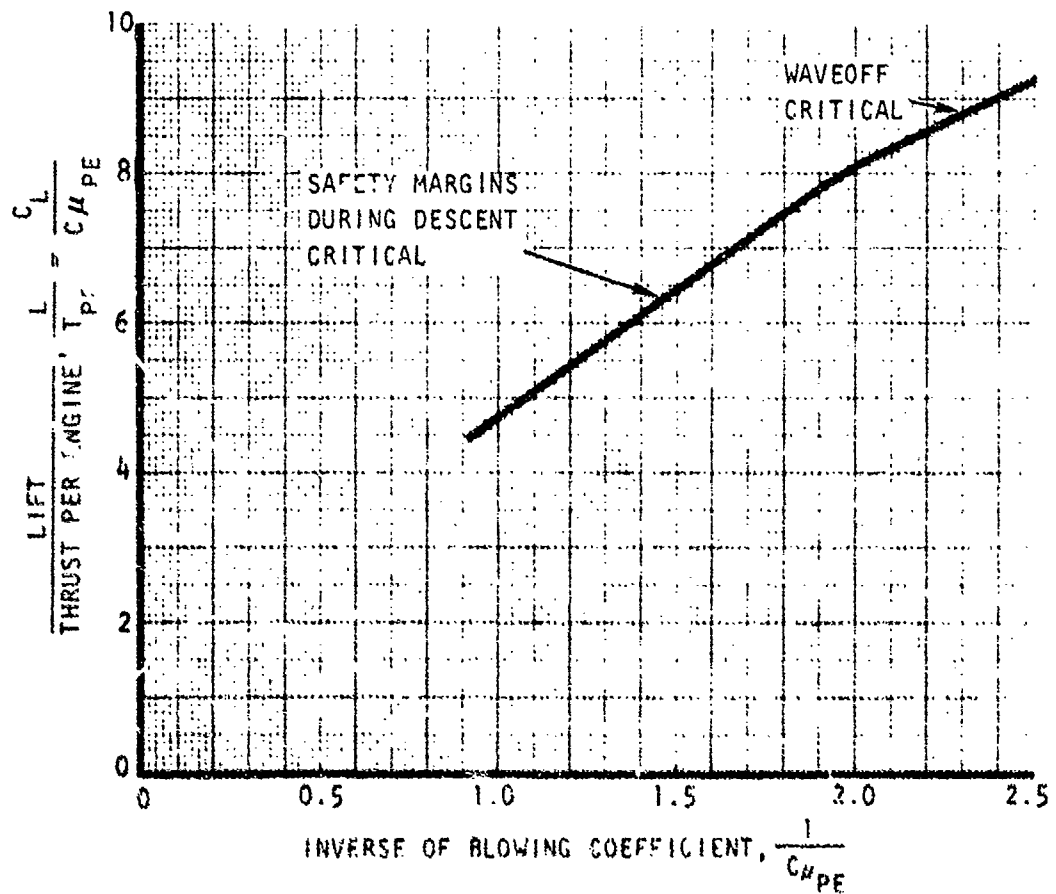
ONE ENGINE INOPERATIVE

Figure 67. Lift Versus Inverse of Blowing Coefficient for Waveoff
Capability During Approach

114

3.2.2 LANDING DISTANCE

(a) Nomograms for Landing Distance

A nomogram for the determination of the landing distance with an aircraft height of 50 feet at the threshold and a sink rate of 10 ft/second is presented in Figure 68. The nomogram is determined from

$$ \delta = \left(\frac{H}{-V_Z} + 2 \right) V_a + \frac{V_a^2}{2g\,(\ddot{x}/g)} $$

where

H = height at threshold, 50 feet

$-V_Z$ = rate of sink, (ft/second)

V_a = true approach velocity, (ft/second)

$$ \frac{\ddot{x}}{g} = \frac{|F_B|}{W} = \frac{|F_B|}{T_{PE}} \cdot \frac{T/W}{4} $$

The value of the braking force, $|F_B|$, can be determined from Figure 56.

Another nomogram where the height above the ground and the approach glide path is a variable is presented in Figure 69. The total deceleration is:

$$ \frac{\ddot{x}}{g} = \mu + \left(\frac{T_R}{T} \right)_{PE} \frac{N_R T}{W} + \frac{D_{AV}}{W} = \frac{|F_B|}{W} $$

where

$\left(\frac{T_R}{T} \right)_{PE}$ = Thrust reversal ratio of each engine used during reversal

$\left(\frac{T_R}{T} \right)_{PE} \cdot 100$ = "percent thrust reversal"

N_R = Number of engines used for reversal, $N_R = 2$

T = Four engine static nozzle thrust

Note that in the second nomogram the true speed must be entered.

115

AT APPROACH SINK RATE = 10 FT/SEC

$$\frac{\ddot{X}}{G} = \left|\frac{F_B}{W}\right| = \left|\frac{F_B}{T_{PE}}\right| \frac{1}{4} \frac{T}{W}$$
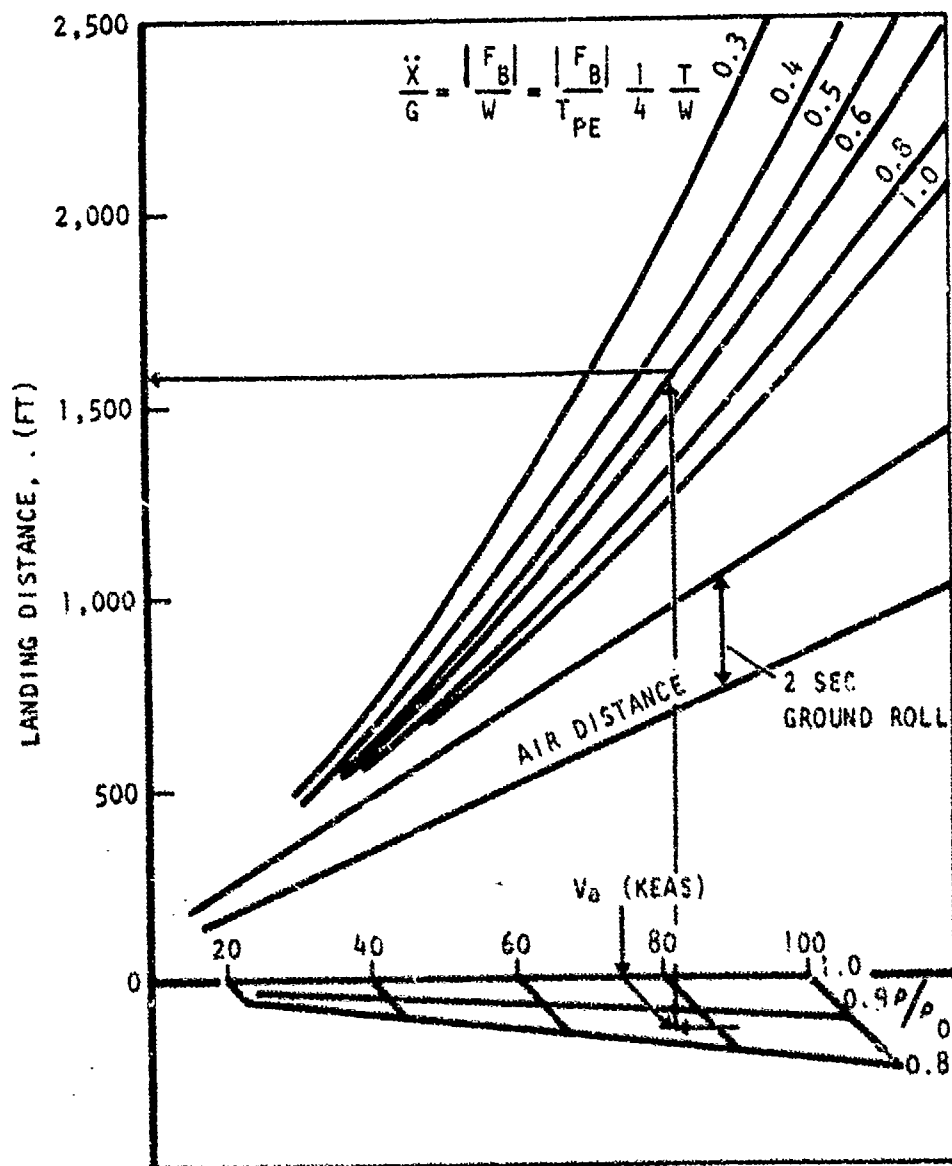
Figure 68. Landing Distance With 50-Ft Height at Threshold
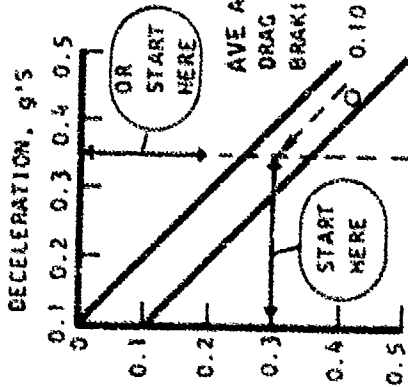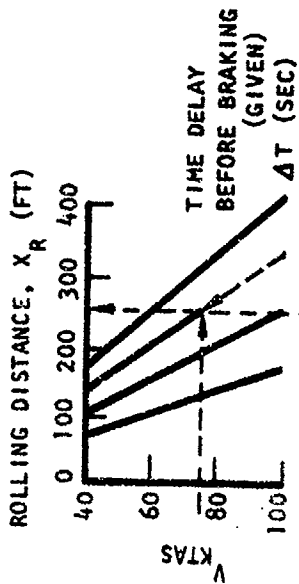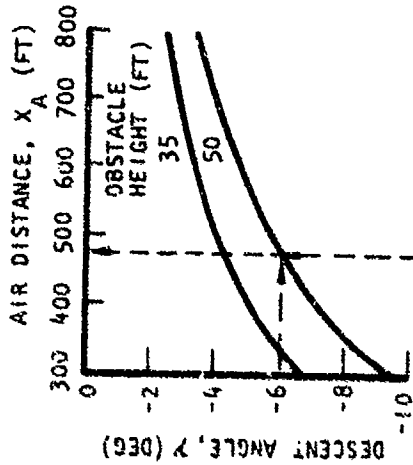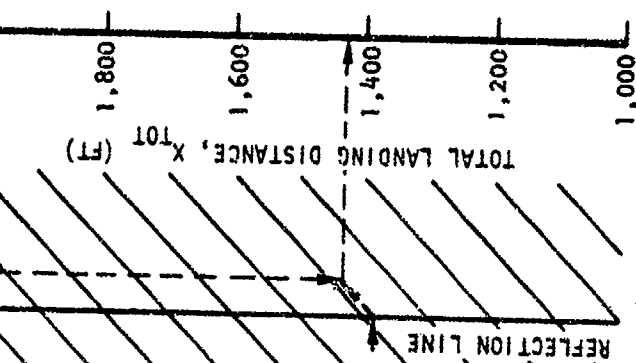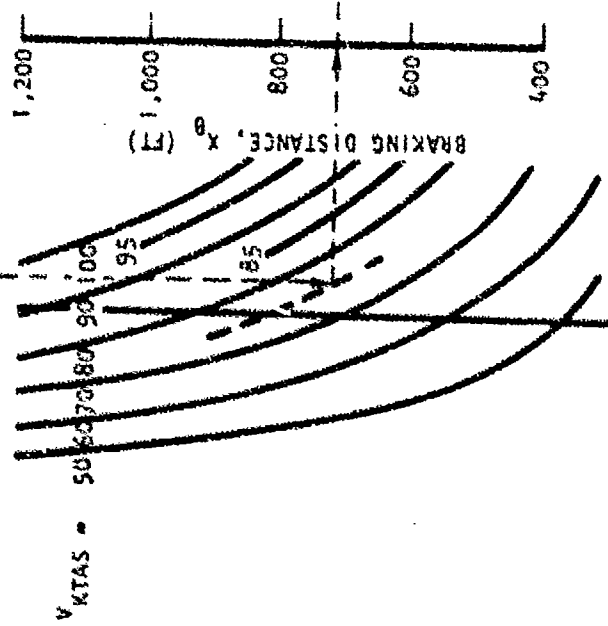
Figure 69. Landing Field Length for Given V and γ

117

(b) Ground Rules Used

The ground rules on which the nomogram in Figure 68 is based are
(see also sketch in Figure 70):

Height at threshold: 50 feet above runway

Above threshold: Aircraft speed satisfies flight safety margins
                  stated in 3.2.1
                  Sink rate, $-V_Z = 10$ ft/second

No landing flare

Two seconds ground roll without deceleration

Full deceleration two seconds after touchdown

Deceleration with:

$\mu = 0.30$
    50 percent thrust reversal on two engines
    Spoilers fully deflected

3.2.3 SAMPLE COMPUTATIONS

The landing distance with a height of 50 feet at the threshold is
determined as follows.

Obtain the approach speed, V_a, from Figure 60 for given values of
T/W and W/S, for example:

$\frac{T}{W}$	$\frac{W}{S}$	$\frac{T}{S} = \frac{T}{W} \cdot \frac{W}{S}$	V_a KEAS
0.50	80	40.0	76.5

118
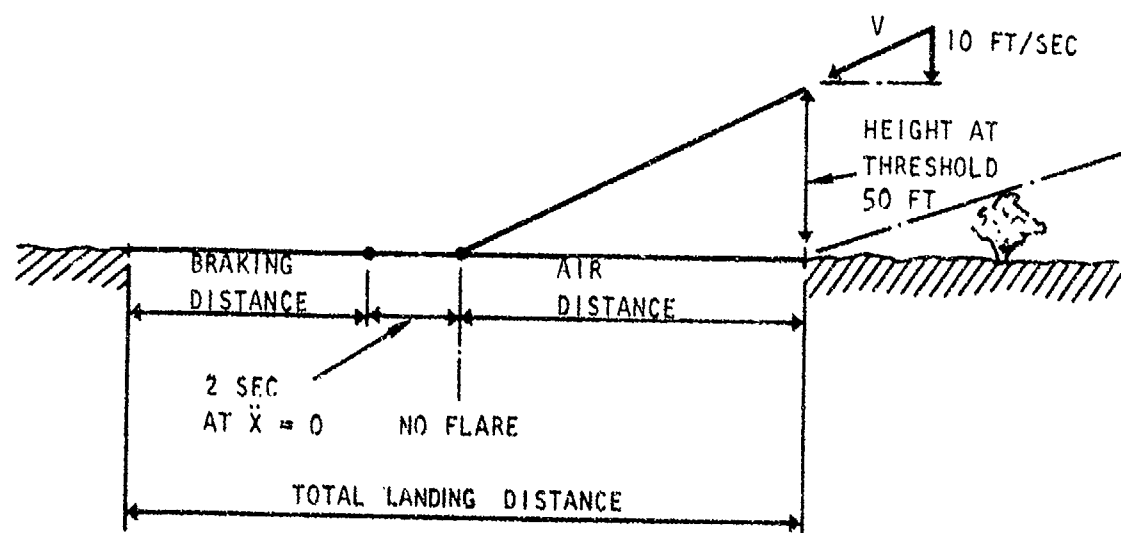
Figure 70. Landing Profile

119

Determine $|F_B|/T_{PE}$ from Figure 56, for example using $C_{D_{po}}$ = 0.50, $C_{L_{po}}$ = 0 with spoilers opened, K = .11 (from Figure 57) or experience value), μ = .030, 50 percent thrust reversal on two engines:

$\dfrac{T}{W}$	V_a KEAS	$\dfrac{T}{S}$	$\dfrac{|F_B|}{T_{PE}}$
.50	76.5	40.0	4.0

Determine the landing distance from Figure 68, using ρ/ρ_o = .857 as a sample value

$\dfrac{T}{W}$	$\dfrac{1}{4} \dfrac{|F_B|}{T_{PE}} \cdot \dfrac{T}{W}$	V_a KEAS	$\dfrac{\rho}{\rho_o}$	δ FT
.50	.50	76.5	.857	1580

An example of landing distances as a function of T/W and W/S with the above constants is presented in Figure 71.
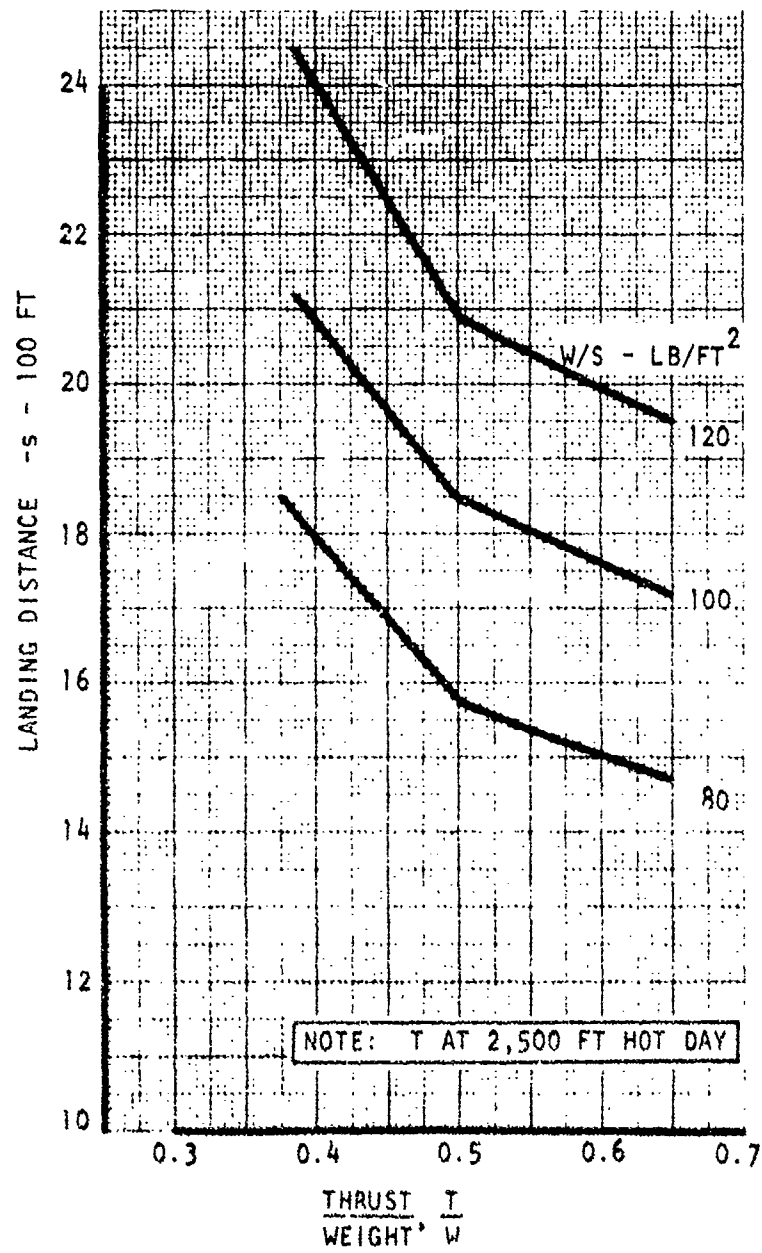
Figure 71. Landing Distance at 2,500-Foot Altitude, Hot Day

(The reverse side of this page is blank.)

Section IV

CONCLUSIONS AND RECOMMENDATIONS

Ground rules for takeoff and landing have been recommended for use in a supplement to MIL-C-5011A, "Military Specification; Charts, Standard Aircraft Characteristics and Performance, Piloted Aircraft". Also methods and nomograms for the determination of the field performance were presented on the basis of these recommended ground rules. The ground rules were derived on the basis of safe speed margins, reasonable maneuver characteristics, and controllability after engine failure or severe gust. The performance methods and ground rules are sufficiently general to be applicable to a variety of lift/propulsion concepts for STOL aircraft.

Numerous assumptions were made with regard to pilot reaction to engine failure and gust, in particular, recognition time and total time needed to control the aircraft. These still must be verified with test data or simulator data. An assessment of ground rules was made with these assumed pilot techniques, primarily to show what the safety require ments possibly could be, to describe a frame of aircraft characteristics within which the pilot has to operate, and to build a technical or theoretical background that might aid in the planning and conducting of more meaningful test setups.

With this frame of recommended criteria as a reference, it is suggested to obtain information with regard to airport gust and the pilot response mechanism. Included should be down draft to determine the vertical clearance to obstacles or the best height above the threshold. Also, included should be the effect of rear gusts, and in particular the pilot response to it and whether thrust increases can be carried out timely.

Similarly, pilot response to engine failure near touchdown, and his reaction to a rebounce should be determined, as well as requirements with respect to the maximum rate of lift control that should be made available to him for proper control. A relation between required magnitude of control should be established as a function of maximum rate of lift control.

Assault landings were not proposed without one engine-out safety. Alternatives should be studied in conjunction with a military operations analysis which is beyond the scope of the present study.

APPENDIX

(The reverse side of this page is blank.)

A.1 TAKEOFF DISTANCE AND FAILURE SPEED

Equations are derived for the balanced field length for takeoff without consideration of an obstacle; the ground roll distance to liftoff is made equal to the accelerate and stop distance in case of an engine failure.

The distance for the takeoff ground roll, $\mathscr{S}$, is basically computed from

$$\mathscr{S} = \int V\, dt = \int \left(V \frac{dt}{dV} \right) dV = \int \frac{V}{\left(\frac{dV}{dt} \right)}\, dV$$

Herein, the acceleration dV/dt varies with the aircraft speed. It is generally the highest at the beginning of the takeoff (v = 0), and less at liftoff. For the purpose of simplifying the takeoff computation, the ground run is split in two sections, and over each of the two sections the acceleration will be taken constant. The first section will cover the acceleration with four engines operating, and the second section will pertain to the condition with one engine failed. Thus

$$\mathscr{S} = \frac{1}{\left(\frac{dV}{dt} \right)_4} \int_0^{V_F} V\, dV + \frac{1}{\left(\frac{dV}{dt} \right)_3} \int_{V_F}^{V_{LO}} V\, dV$$

where $\left(\dfrac{dV}{dt} \right)_4$ = average acceleration with four engines

$\left(\dfrac{dV}{dt} \right)_3$ = average acceleration with three engines

V_F = speed at which one engine fails

V_{LO} = speed at which the aircraft lifts off the ground

An average acceleration is sometimes used as an approximation for conventional aircraft. In the case of STOL aircraft, the acceleration is usually larger than for conventional aircraft, which means that the percentage change of the acceleration with speed is generally less for

STOL aircraft. Thus, it appears, that the use of average accelerations is appropriate for the present report.

The accelerations are now related to average net forward forces, F, as follows:

$$\frac{W}{g}\left(\frac{dV}{dt}\right)_{AV} = F_{AV}$$

or

$$\left(\frac{dV}{dt}\right)_4 = \frac{g}{W}\,F_4$$

$$\left(\frac{dV}{dt}\right)_3 = \frac{g}{W}\,F_3$$

where the subscripts 3 and 4 denote average forces in the 3 and 4-engine operation. This yields

$$\mathcal{S} = \frac{1}{(g/W)}\left[\frac{\frac{1}{2}V_F^2}{F_4} + \frac{\frac{1}{2}V_{LO}^2 - \frac{1}{2}V_F^2}{F_3}\right]$$

or

$$\mathcal{S}\Big/\left(\frac{W}{g\rho}\right) = \frac{q_F}{F_4} + \frac{q_{LO} - q_F}{F_3}$$

In order to present nomograms with the wing loading W/S as a variable, the wing area S is introduced. Also, because F_3 and F_4 are directly related to the engine thrust, the thrust is used to nondimensionalize F_3 and F_4. The static value of it is used for the reference thrust in order to avoid confusion related to net thrust changes with speed. These changes are caused by intake momentum effects and gross thrust changes. Thrust values of a single nozzle, i.e., the thrust per engine, T_{PE}, is used so that no change in reference thrust needs to be

128

made in going from a normal operating condition to a case with an engine failed. The above equation becomes:

$$\frac{\delta}{\left(\frac{W/S}{\rho g}\right)} = \frac{\left(\frac{q_F S}{T_{PE}}\right)}{\left(\frac{F_4}{T_{PE}}\right)} + \frac{\left(\frac{q_{LO} S}{T_{PE}}\right) - \left(\frac{q_F S}{T_{PE}}\right)}{\left(\frac{F_3}{T_{PE}}\right)}$$

or

$$\frac{\delta}{\left(\frac{W/S}{\rho g}\right)} = \frac{\left(\frac{1}{C_{\mu PE}}\right)_{LO}}{\left(\frac{F_3}{T_{PE}}\right)} - \frac{\left(\frac{1}{C_{\mu PE}}\right)_F}{\left(\frac{F_4}{T_{PE}}\right)} \left[\frac{\left(\frac{F_4}{T_{PE}}\right)}{\left(\frac{F_3}{T_{PE}}\right)} - 1\right] = \frac{\left(\frac{1}{C_{\mu PE}}\right)_{LO}}{\left(\frac{F_3}{T_{PE}}\right)} - \frac{\left(\frac{1}{C_{\mu PE}}\right)_F}{\left(\frac{F_4}{T_{PE}}\right)} \left[\frac{F_4}{F_3} - 1\right]$$

in which, by definition

$$C_{\mu PE} = \frac{T_{PE}}{q S}$$

This equation is presented graphically as "curve Ⓐ" in Figure 72. The takeoff distance is plotted to the left and nondimensionalized by $(W/S)/\rho g$. At the bottom of the curve is the takeoff distance when the engine fails immediately after brake release, i.e., when $(1/C_{\mu PE})_F = 0$. Increased values on the vertical axis represent an increase in forward speed at which the engine fails. At such increased forward speeds, the takeoff distance becomes shorter because some acceleration is obtained with four engines. The shortening of this distance is indicated by the slope of "curve Ⓐ".

The above takeoff distance to liftoff must be compared to the accelerate and stop distance in the event the takeoff is aborted. The accelerate-stop-distance is computed from

$$\delta = \frac{1}{\left(\frac{dV}{dt}\right)_4} \int_0^{V_F} V \, dV + \Delta \delta + \frac{1}{\left(\frac{dV}{dt}\right)_B} \int_{V_F}^0 V \, dV$$

SLOPE OF CURVE Ⓐ

$$
\frac{d \dfrac{s}{\left(\dfrac{W/S}{\rho g}\right)}}{d \dfrac{\left(c\dfrac{1}{\mu_{PE}}\right)_F}{\left(F_4/T_{PE}\right)}} = -\left[\frac{F_4/T_{PE}}{F_3/T_{PE}} - 1\right] = -\left[\frac{F_4}{F_3} - 1\right]
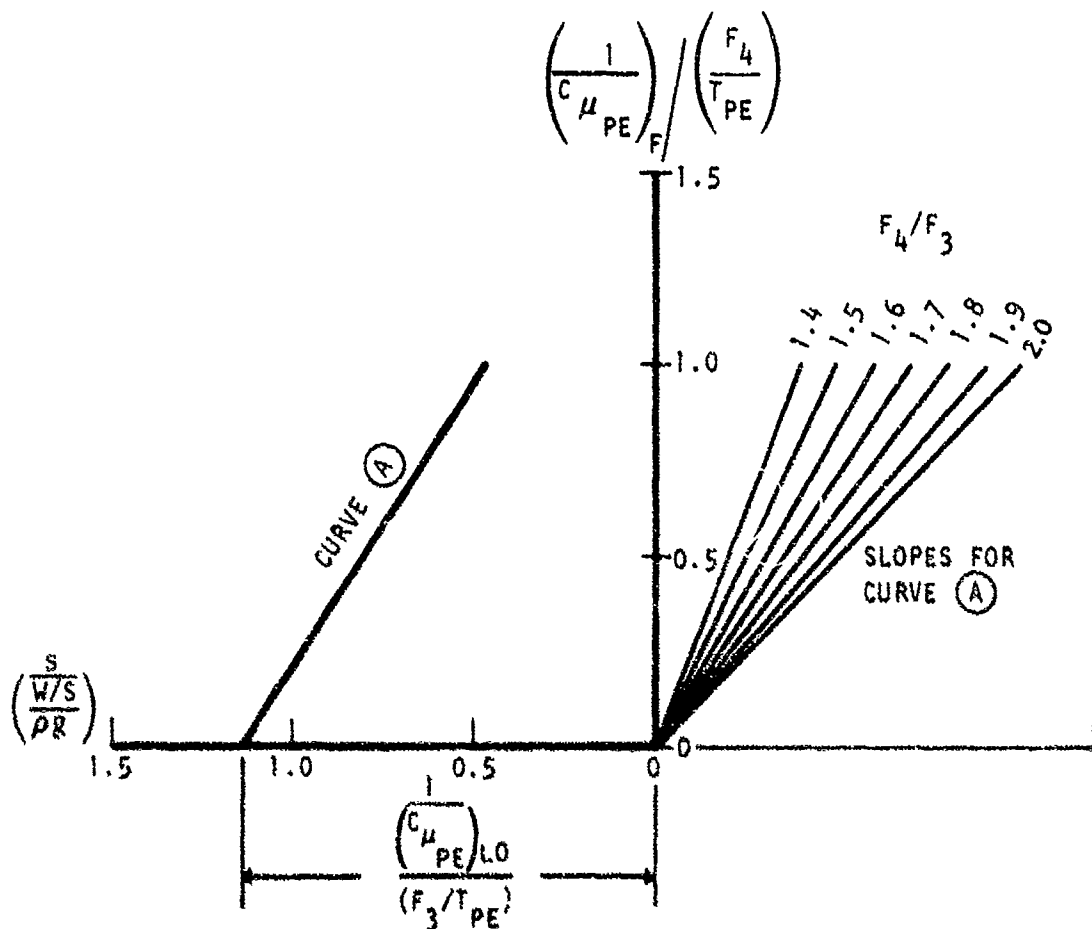$$

Figure 72. Portion of Nomogram for Takeoff Distance Continued Takeoff After Engine Failure

130

where $(dV/dt)_B$ is the deceleration of the aircraft, and $\Delta\delta$ an increase of the distance for any reason, such as the distance traveled after engine failure and before 100 percent braking is achieved.

Using

$$\left(\frac{dV}{dt}\right)_4 = \frac{q}{W} F_4$$

$$\left|\frac{dV}{dt}\right|_B = \frac{q}{W} |F_B|$$

the above equation becomes

$$\delta = \frac{\frac{1}{2} V_F^2}{\frac{q}{W} F_4} + \Delta\delta + \frac{\frac{1}{2} V_B^2}{\frac{q}{W} |F_B|}$$

This yields:

$$\frac{\delta}{\left(\frac{W/S}{\rho g}\right)} = \frac{\left(\frac{q_F S}{T_{PE}}\right)}{\left(\frac{F_4}{T_{PE}}\right)} + \frac{\Delta\delta}{\left(\frac{W/S}{\rho g}\right)} + \frac{\left(\frac{q_B S}{T_{PE}}\right)}{\left(\frac{F_B}{T_{PE}}\right)}$$

or

$$\frac{\delta}{\left(\frac{W/S}{\rho g}\right)} = \frac{\Delta\delta}{\left(\frac{W/S}{\rho g}\right)} + \frac{\left(\frac{1}{C_{LPE}}\right)_F}{\left(\frac{F_4}{T_{PE}}\right)} \left[1 + \frac{q_B}{q_F} \frac{F_4}{|F_B|}\right]$$

This equation can be presented graphically as shown by "curve Ⓑ" in Figure 73. At the intersection of this curve with the horizontal axis the distance $\Delta\delta$ is shown in the nondimensional form. At this axis, the aircraft speed is zero at the moment of engine failure. This is expressed by $(1/C_\mu)_F = 0$. Then the distance to accelerate is zero and also the distance to stop is zero, leaving only the effect of $\Delta\delta$. With increase of the forward speed at which the engine fails also the accelerate/stop distance increases which is expressed by the slope of "curve Ⓑ".

To convert a given distance $\Delta\delta$ into the above nondimensionalized form $\Delta\delta/(W/S\rho g)$ a small nomogram is included in the figure to the right. This conversion is based on

$$\frac{\Delta\delta}{\left(\frac{W/S}{\rho g}\right)} = \Delta\delta \cdot \frac{1}{\left(\frac{W/S}{\rho \cdot g}\right)\frac{1}{\rho/\rho_0}} = \Delta\delta \frac{\rho \cdot g}{\left(\frac{W/S}{\rho/\rho_0}\right)} = \Delta\delta \frac{.0766 \ lbs/FT^3}{\left(\frac{W/S}{\rho/\rho_0}\right)}$$

The accelerate and stop distance presented in the above form is expresssed in the same coordinate system as the distance of a continued takeoff after engine failure. This facilitates a direct comparison. This comparison is needed to make the accelerate/stop distance equal to the continued takeoff distance, which is the condition for the takeoff distance to be balanced. The graphical solution for obtaining this balance is illustrated in the lower left of Figure 74 by the intersection of curves Ⓐ and Ⓑ.

Going vertically from this intersection, the balanced field length can be found. The conversion from the nondimensional field length to the actual field length is shown at the top of the figure, using

$$\delta = \frac{\delta}{\left(\frac{W/S}{\rho g}\right)} \cdot \frac{\left(\frac{W/S}{\rho/\rho_0}\right)}{.0766 \ lbs/FT^3} \qquad (FT)$$

Going horizontally from the intersection in this figure yields the inverse of the blowing coefficient existing at the speed at which the engine fails in the balanced case. From

$$\frac{1}{(C_{\mu PE})_F} = \frac{q_F}{T_{PE}/S} = \frac{\frac{1}{2}\rho V_r^2}{T_{PE}/S}$$

132

SLOPE OF CURVE Ⓑ:

$$\frac{-d\left(\dfrac{s}{\frac{W/S}{\rho q}}\right)}{d\left(\dfrac{\left(\frac{1}{C}\mu_{PE}\right)_F}{\left(F_4/T_{PE}\right)}\right)} = 1 + \frac{F_4}{|F_3|}$$

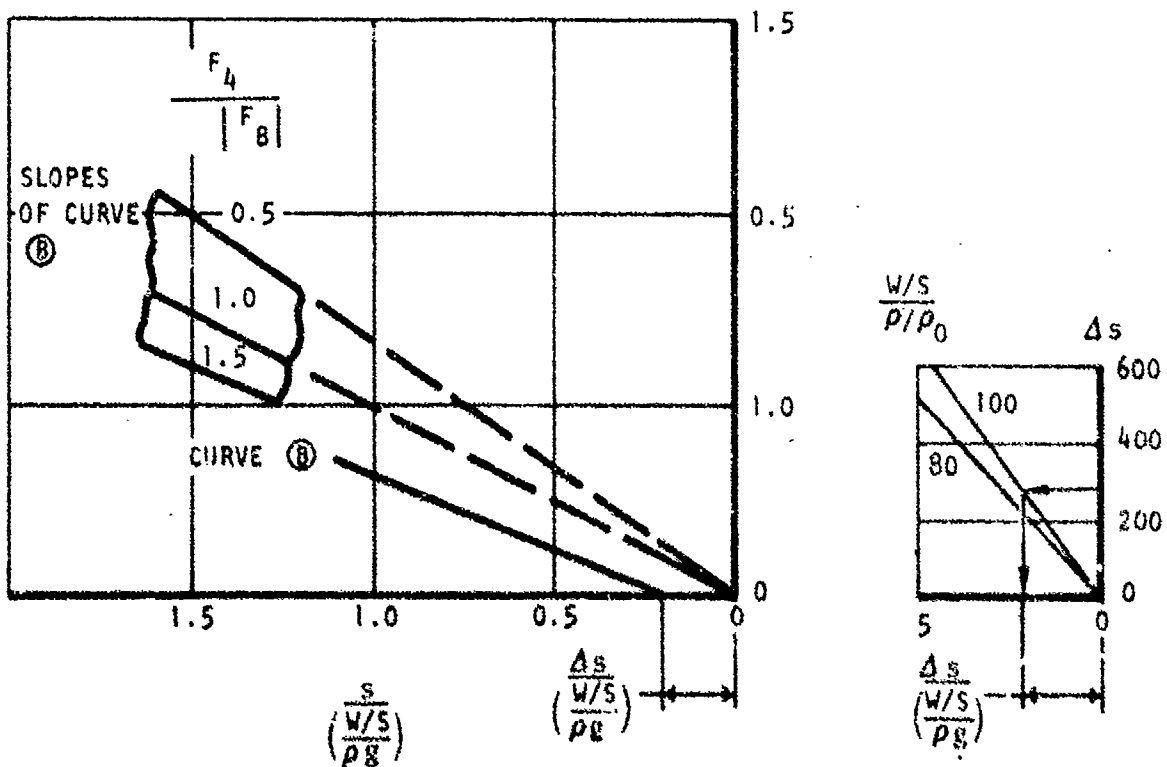$$\left(\frac{1}{C}\mu_{PE}\right)_F \bigg/ \left(\frac{F_4}{T_{PE}}\right)$$

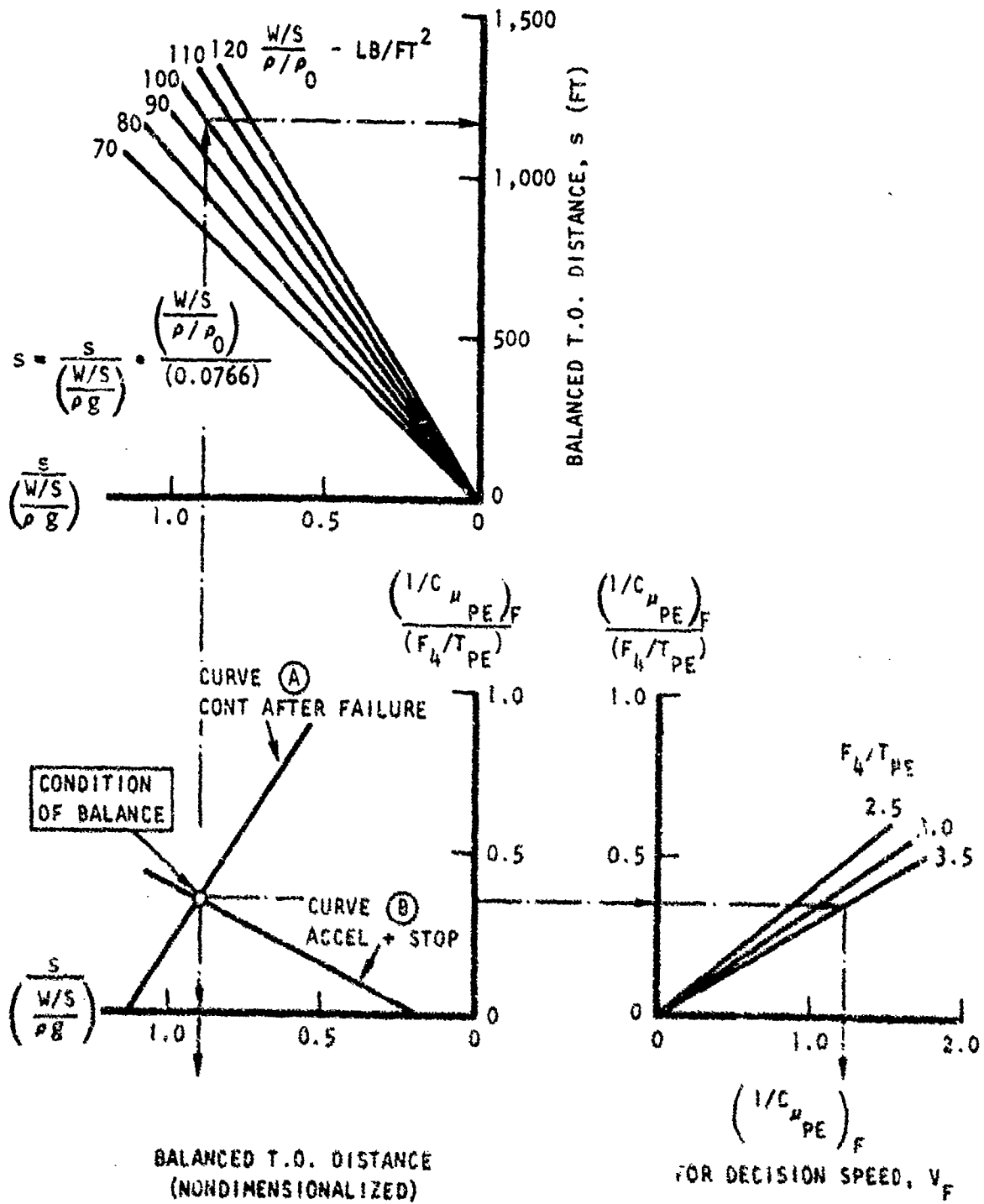Figure 73. Portion of Nomogram for Takeoff Distance Acceleration and Stop Distance

133

Figure 74. Graphical Presentation of Balancing of the Takeoff Distance

134

This speed can be determined when the thrust level T_{PE} and the atmospheric density is known. In this balanced condition, the failure speed V_F is equal to the decision speed by definition.

The above described portions of the nomograms pertaining to the balanced takeoff distance are now combined into the single nomogram shown in Figure 75.

A nomogram for the determination of the failure speed is given in Figure 76 based on the same principles, except assuming that the takeoff distance is known from a previous iterative step.

A.2   ACCELERATING FORCE

The average force in the forward direction when all engines are operating can be expressed as

$$F_4 = T_{AV} - D_{AV} - \mu\left(W - L_{AV}\right)$$

where

T_{AV} = average engine thrust component

D_{AV} = average aerodynamic drag

L_{AV} = average aerodynamic lift and vertical thrust component

The respective average forces are expressed as follows using T_{PE} as the definition of the static nozzle thrust per engine:

$$T_{AV} = 4\,T_{PE}\,\cos\delta_N - \tfrac{1}{2}\,4K\,T_{PE}\,/\sqrt{(C_{L,PE})_F}$$

$$D_{AV} = \tfrac{1}{2}\,q_F\,C_{D_{PE}}\,S$$

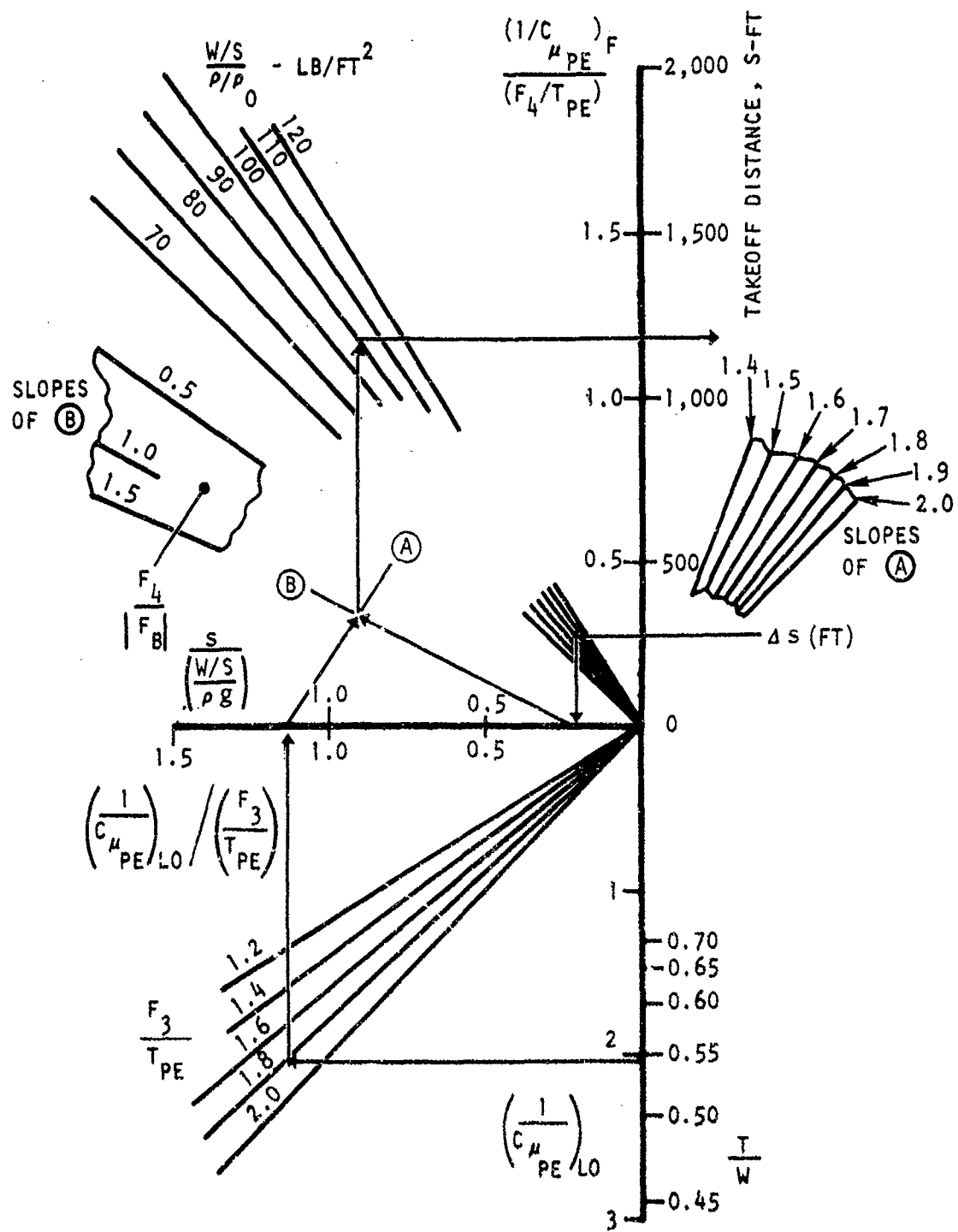$$L_{AV} = \tfrac{1}{2}\,q_F\,C_{L_{PO}}\,S + 4\,T_{PE}\,\sin\delta_N$$

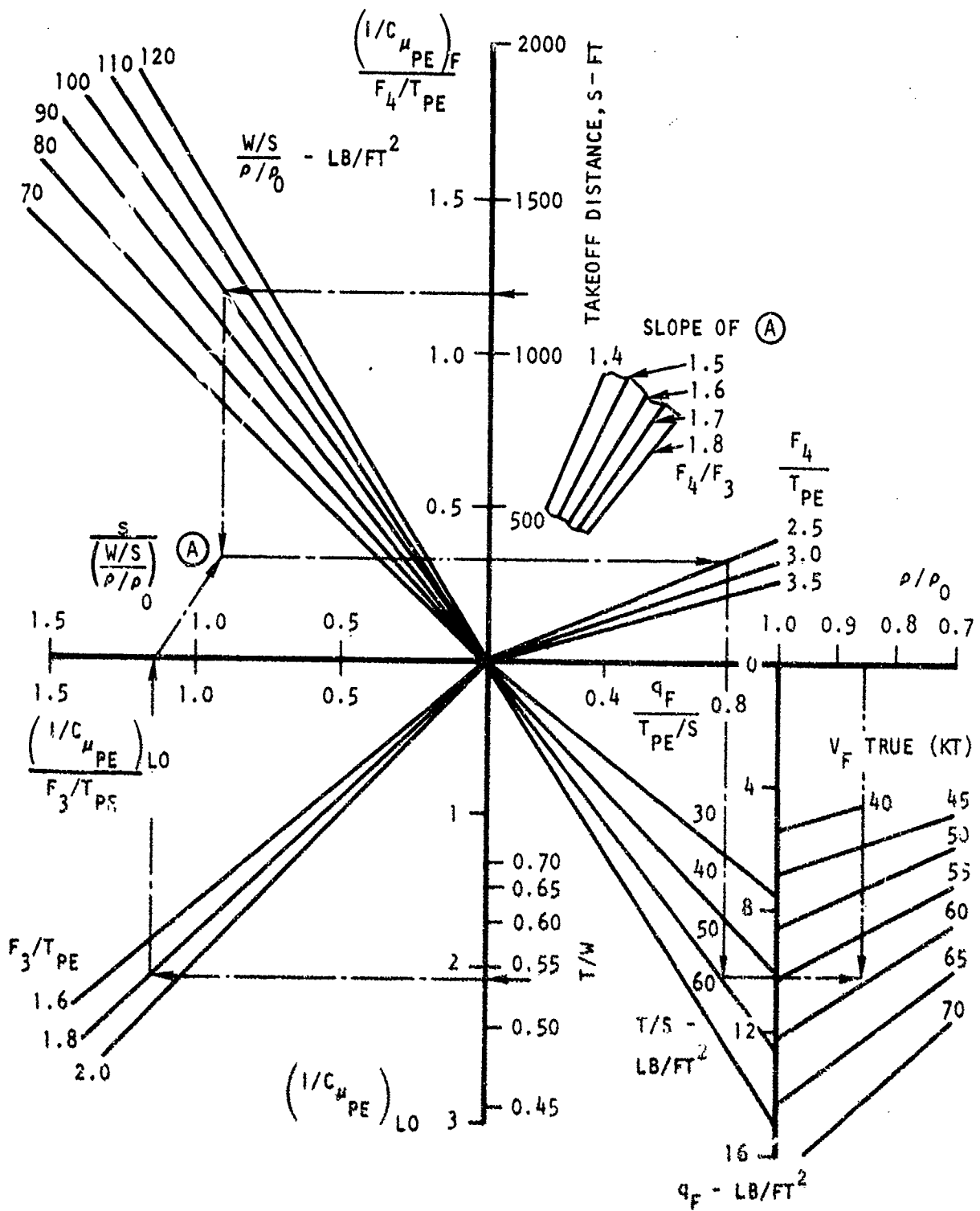Figure 75. Nomogram for Takeoff Distance With Detailed Explanation of Axis System

136

Figure 76. Nomogram for Failure Speed V_F With Detailed Explanation of Axis System

Substitution yields:

$$\frac{F_4}{T_{PE}} = 4 - 4(1-\cos\delta_N) - \frac{1}{2}\frac{4K}{\sqrt{(C_{L_{PE}})_F}} - \frac{1}{2}\frac{C_{D_{PO}}}{(C_{L_{PE}})_F} - \mu\left[\frac{W}{T_{PE}} - \frac{1}{2}\frac{C_{L_{PO}}}{(C_{L_{PE}})_F} - 4\sin\delta_N\right]$$

The nomogram based on this equation is given in Figure 54.

Similar to the accelerating force with four engines, the force for three engines operating is obtained from:

$$F_3 = T_{AV} - D_{AV} - \mu\left(W - L_{AV}\right)$$

where now:

$$T_{AV} = 3T_{PE}\cos\delta_N - \frac{1}{2}\left[\frac{3K}{\sqrt{(C_{L_{PE}})_F}} + \frac{3K}{\sqrt{(C_{L_{PE}})_{L_0}}}\right]T_{PE}$$

$$D_{AV} = \frac{1}{2}\left[q_F C_{D_{PO}} S + q_{L_0} C_{D_{PO}} S\right]$$

$$L_{AV} = \frac{1}{2}\left[q_F C_{L_{PO}} S + q_{L_0} C_{L_{PO}} S\right] + 3T_{PE}\sin\delta_N$$

or

$$T_{AV} = 3T_{PE}\cos\delta_N - \frac{3K}{2}\left[\sqrt{\frac{q_F}{T_{PE}/S}} + \sqrt{\frac{q_{L_0}}{T_{PE}/S}}\right]T_{PE}$$

$$= 3T_{PE}\cos\delta_N - \left(\frac{1+V_F/V_{L_0}}{2}\right)\left(\frac{3K}{\sqrt{(C_{L_{PE}})_{L_0}}}\right)T_{PE}$$

$$D_{AV} = \frac{1+(V_F/V_{L_0})^2}{2}q_{L_0}C_{D_{PO}}S$$

$$L_{AV} = \frac{1+(V_F/V_{L_0})^2}{2}q_{L_0}C_{L_{PO}}S + 3T_{PE}\sin\delta_N$$

138

Substitution into the equation for F_3 yields:

$$\frac{F_\Theta}{T_{PE}} = 3 - 3\left(1 - \cos S_N\right) - \frac{1}{2} \cdot \frac{3K\left(1 + V_F/V_{LO}\right)}{\sqrt{\left(C_{\mu PE}\right)_{LO}}} - \frac{1}{2} \cdot \frac{C_{DPO}\left(1 + V_F^2/V_{LO}^2\right)}{\left(C_{\mu PE}\right)_{LO}}$$
$$- \mu\left[\frac{W}{T_{PE}} - \frac{1}{2}\frac{C_{LPO}\left(1 + V_F^2/V_{LO}^2\right)}{\left(C_{\mu PE}\right)_{LO}} - 3\sin S_N\right]$$

This equation forms the basis of the nomogram in Figure 55.

A.3 DECELERATING FORCE

Using the same general approach as above, the braking force is obtained from:

$$\left| F_\mathcal{R} \right| = \frac{N_R}{4}\left(\frac{T_R}{T}\right)T + \Delta D_i + D_{AV} + \mu\left(W - L_{AV}\right)$$

where:

N_R = number of engines with reversed thrust

$\dfrac{T_R}{T}$ = ratio of thrust in reversed condition to thrust in unreversed condition, per engine ($100\ T_R/T$ = % thrust reversal)

T = sum of static nozzle thrust from four engines

$\Delta D_i = (1/2)N_R \dfrac{K}{\sqrt{\left(C_{\mu PE}\right)}} \cdot T_{PE}$ = average reduction of net thrust due to speed increase, primarily intake momentum drag

$D_{AV} = (1/2)q\ C_{D_{po}}\ S$

$L_{AV} = (1/2)q\ C_{L_{po}}\ S$

Substitution and dividing by T_{PE} yields:

$$\frac{|F_\Theta|}{T_{PE}} = \frac{N_R}{4}\left(\frac{T_R}{T}\right)\frac{T}{T_{RE}} + \frac{1}{2}N_R\frac{K}{\sqrt{C_{\mu PE}}} + \frac{1}{2}\frac{C_{DPO}}{C_{\mu PE}} + \mu\left(\frac{W}{T_{PE}} - \frac{1}{2}\frac{C_{LPO}}{C_{\mu PE}}\right)$$

or, using $N_R = 2$ for the nomogram in Figure 56:

$$\frac{|F_\Theta|}{T_{PE}} = 2\frac{T_R}{T} + \frac{K}{\sqrt{C_{\mu PE}}} + \frac{1}{2}\frac{C_{DPO}}{C_{\mu PE}} + \mu\left(\frac{4}{T/W} - \frac{1}{2}\frac{C_{LPO}}{C_{\mu PE}}\right)$$

A.4 ENGINE NET THRUST DECREASE WITH SPEED

The engine net thrust decrease that occurs when the speed increases can be expressed as a drag increment per engine as follows:

$$\frac{\Delta D_i}{\Delta T_{PE}} = K\sqrt{\frac{q}{T_{PE}/S}}$$

The factor K is also a function of q and T_{PE}, and depends on the engines used (but only to a relatively minor extent except for the bypass ratio). The equation is rewritten into:

$$\frac{\Delta D_i}{\Delta T_{PE}} = \left[\frac{\Delta D_i/T_{PE}}{\sqrt{\frac{q}{T_{PE}/A_{jPE}}}\,\beta}\right]\cdot\sqrt{\frac{q}{T_{PE}/A_{jPE}}}\,\beta$$

140

or

$$\frac{\Delta D_i}{T_{PE}} = \left[\frac{\Delta D_i / T_{PE}}{\sqrt{\frac{q}{T_{PE}/A_{iPE}}}\, B}\right] \cdot \sqrt{\frac{A_{iPE}}{S}\, B} \cdot \sqrt{\frac{q}{T_{PE}/S}}$$

where

A_{iPE} = inlet throat area per engine

B = engine bypass ratio

and where

$$K = \left[\frac{\Delta D_i / T_{PE}}{\sqrt{\frac{q}{T_{PE}/A_{iPE}}}\, B}\right] \cdot \sqrt{\frac{A_{iPE}}{S}\, B}$$

It has been found that $\Delta D_i / T_{PE}$ deviates only slightly from a linear variation with

with $\sqrt{\frac{q}{T_{PE}/A_{iPE}}}\, B$

Use of the bypass ratio in this form resulted in an empirical relation where data from different engines and bypass ratios very nearly collapsed into a single relation. An example of this is shown in Figure 77. This means, that in a limited region of interest

$$\frac{\Delta D_i / T_{PE}}{\sqrt{\frac{q}{T_{PE}/A_{iPE}}}\, B} \approx \text{Constant}$$

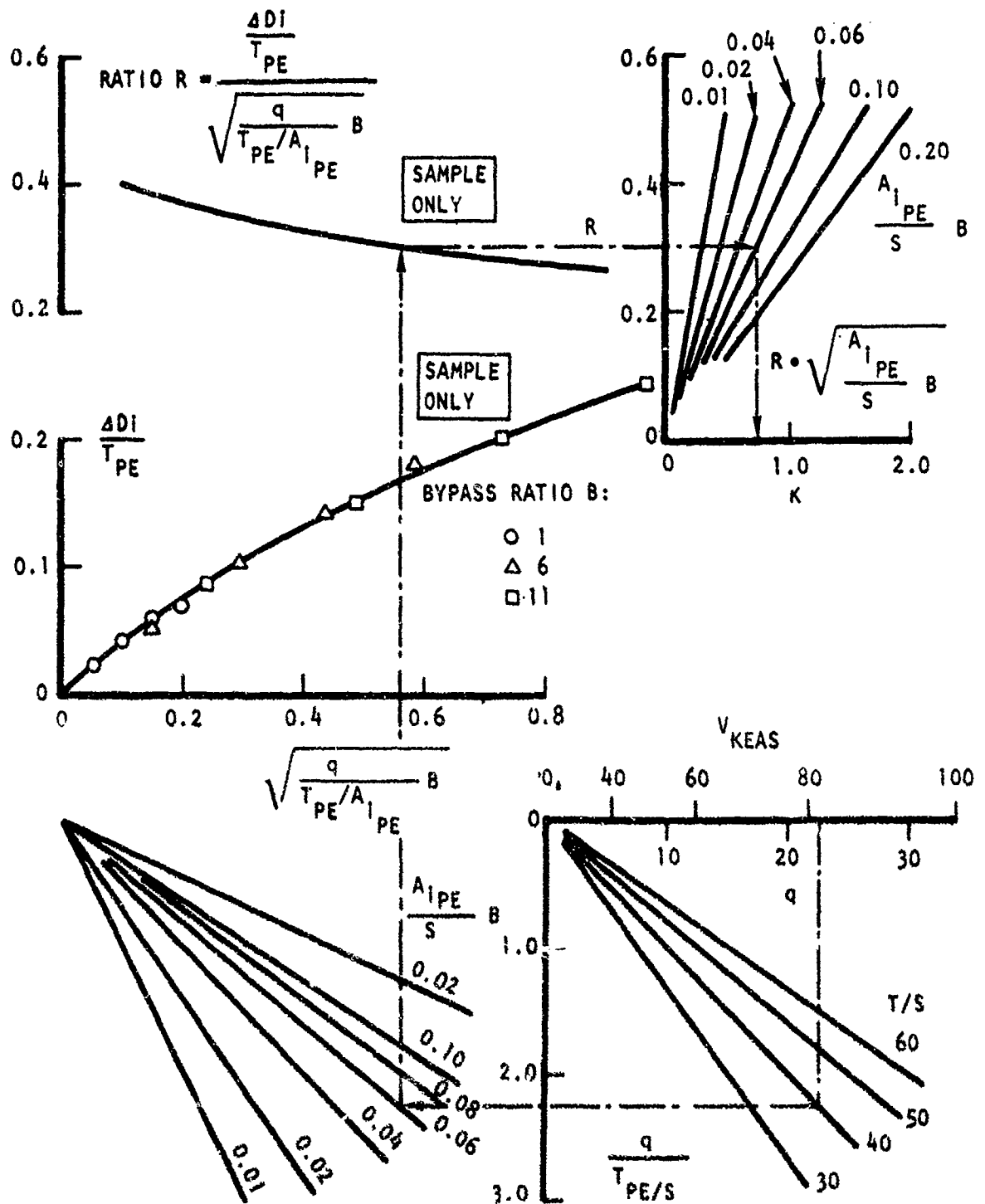and for given values of A_{iPE} and B also $K \approx$ constant.

141

Figure 77. Nomogram for Factor K With Detailed Explanation of Axis System

142

The determination of the value K is shown in the nomograms in this figure. The engine data used therein are only samples. Before determining the factor K for a particular engine/aircraft layout, the engine data should be plotted as shown in the nomogram for verification of detailed explanation of the variables involved.

A.5 GUST RESPONSE

To derive a differential equation for the determination of the vehicle's angle of attack excursion in response to a discrete vertical gust, the summation of the response and forcing function forces can be written as;

$$m(\Delta \ddot{z}) = C_{L_\alpha} \Delta\alpha \, qS + C_{L_{\dot\alpha}} \cdot \dot\alpha \, qS + C_{L_\alpha}\left(\frac{V_g}{V}\right) qS .$$

Since, $\Delta\ddot{z} = (\dot\theta - \dot\alpha)V$, rearranging and solving for $\dot\theta$;

$$\dot\theta = \dot\alpha\left[1 + C_{L_{\dot\alpha}}\frac{qS}{mV}\right] + C_{L_\alpha}\frac{qS}{mV}\left[\Delta\alpha + \left(\frac{V_g}{V}\right)\right] \text{ differentiating,}$$

$$\ddot\theta = \ddot\alpha\left[1 + C_{L_{\dot\alpha}}\frac{qS}{mV}\right] + \dot\alpha C_{L_\alpha}\frac{qS}{mV} + \left(\frac{V_g}{V}\right)' C_{L_\alpha}\frac{qS}{mV} .$$

From $I\ddot\theta = M$, $\ddot\theta$ is shown to be;

$$\ddot\theta = C_{M_\alpha}\Delta\alpha \, qS\bar{c}/I + C_{M_{\dot\alpha}}\dot\alpha \, qS\bar{c}/I + C_{M_q}\dot\theta \, qS\bar{c}/I + C_{M_\alpha}\left(\frac{V_g}{V}\right) qS\bar{c}/I .$$

Setting like expressions equal and separating the α and (V_g/V) terms;

$$\ddot\alpha\left[1 + C_{L_{\dot\alpha}}\frac{qS}{mV}\right] + \dot\alpha\left[C_{L_\alpha}\frac{qS}{mV} - C_{M_{\dot\alpha}}\frac{qS\bar{c}}{I} - C_{M_q}\frac{qS\bar{c}}{I} - C_{M_q}\frac{qS\bar{c}}{I}C_{L_{\dot\alpha}}\frac{qS}{mV}\right]$$

$$+ \Delta\alpha\left[-C_{M_\alpha}\frac{qS\bar{c}}{I} - C_{M_q}\frac{qS\bar{c}}{I}C_{L_\alpha}\frac{qS}{mV}\right] = \left(\frac{V_g}{V}\right)\left[C_{M_q}\frac{qS\bar{c}}{I}C_{L_\alpha}\frac{qS}{mV} + C_{M_\alpha}\frac{qS\bar{c}}{I}\right]$$

$$- \left(\frac{V_g}{V}\right)'\left[C_{L_\alpha}\frac{qS}{mV}\right]$$

143

Expressing as a second-order system differential equation, where $\ddot{\alpha} + 2\omega_n \dot{\alpha} + \omega_n^2 \Delta\alpha = f\left(\frac{Vg}{V}\right)$ when critical damping is assumed ($\zeta = 1$);

$$\ddot{\alpha} + 2\omega_n\dot{\alpha} + \omega_n^2\Delta\alpha = -\omega_n^2\left(\frac{Vg}{V}\right) - C_{L_\alpha}\frac{qS}{mV}\left[\frac{\frac{d}{dt}(Vg/V)}{1 + C_{L_{\dot{\alpha}}}\frac{qS}{mV}}\right]$$

$$\text{and} \quad \omega_n^2 = -\frac{qS\bar{c}}{I}\left(C_{m_\alpha} + C_{M_q}C_{L_\alpha}\frac{qS}{mV}\right) \ .$$

144

REFERENCES

1. MIL-C-5011A, "Military Specification - Charts; Standard Aircraft Characteristics and Performance, Piloted Aircraft," Navy - Bureau of Wright Air Development Center, Wright Patterson AFB, Dayton, Ohio, dated 5 November 1951

2. R. C. Innis, C. A. Holzhauser, and H. C. Quigley, NASA TND 5594, "Airworthiness Considerations for STOL Aircraft," NASA/Ames Research Center, Moffett Field, California; dated January 1970

3. MIL-F-83300, "Military Specification - Flying Qualities of Piloted V/STOL Aircraft", USAF, dated 31 December 1970

4. R. C. Innis, C. A. Holzhauser, and R. P. Gallant, NASA TND 4939, "Flight Tests Under IFR with STOL Transport Aircraft," dated December 1968

5. M. D. Marks and D. O. Carpenter, AIAA 70-1332, "Low Speed Handling Characteristics of the STOL Aircraft," American Institute of Aeronautics and Astronautics, dated 19-22 October 1970

6. R. H. Sawyer and P. Peterson, Paper No. 20 NASA STOL Technology Conference, "Integration of STOL Aircraft into the ATC System," NASA/Ames Research Center, 17-19 October 1972

7. T. Pecsvaradi and E. Erzberger, Paper No. 21, NASA STOL Technology Conference, "4-D Guidance of STOL Aircraft in Terminal Area," NASA/Ames Research Center, 17-19 October 1972

8. J. L. Hassell and J. H. Judd, Paper No. 14, NASA STOL Technology Conference, "Study of Ground Proximity Effects on Powered Lift STOL Landing Performance," NASA/Ames Research Center, 17-19 October 1972

9. MIL-F-8785B(ASG), "Military Specification - Flying Qualities of Piloted Airplanes", WAF, 7 August 1969, Amendment 3, March 1971

10. MIL-M-007700B(USAF), "Military Specification - Manuals, Flight", WAF, 16 February 1971

11. "Ch. C. Smith, Jr., A. E. Phelps, and R. L. Henderson,NASA Preliminary Data, "Effect of Ground Proximity on the Aerodynamic Characteristics of an Externally Blown Jet Flap VTOL Aircraft Corporation, 13 September 1971 (LWP 987).